UCA Universidad de Cádiz

IN·MAR
Instituto universitario de investigación marina

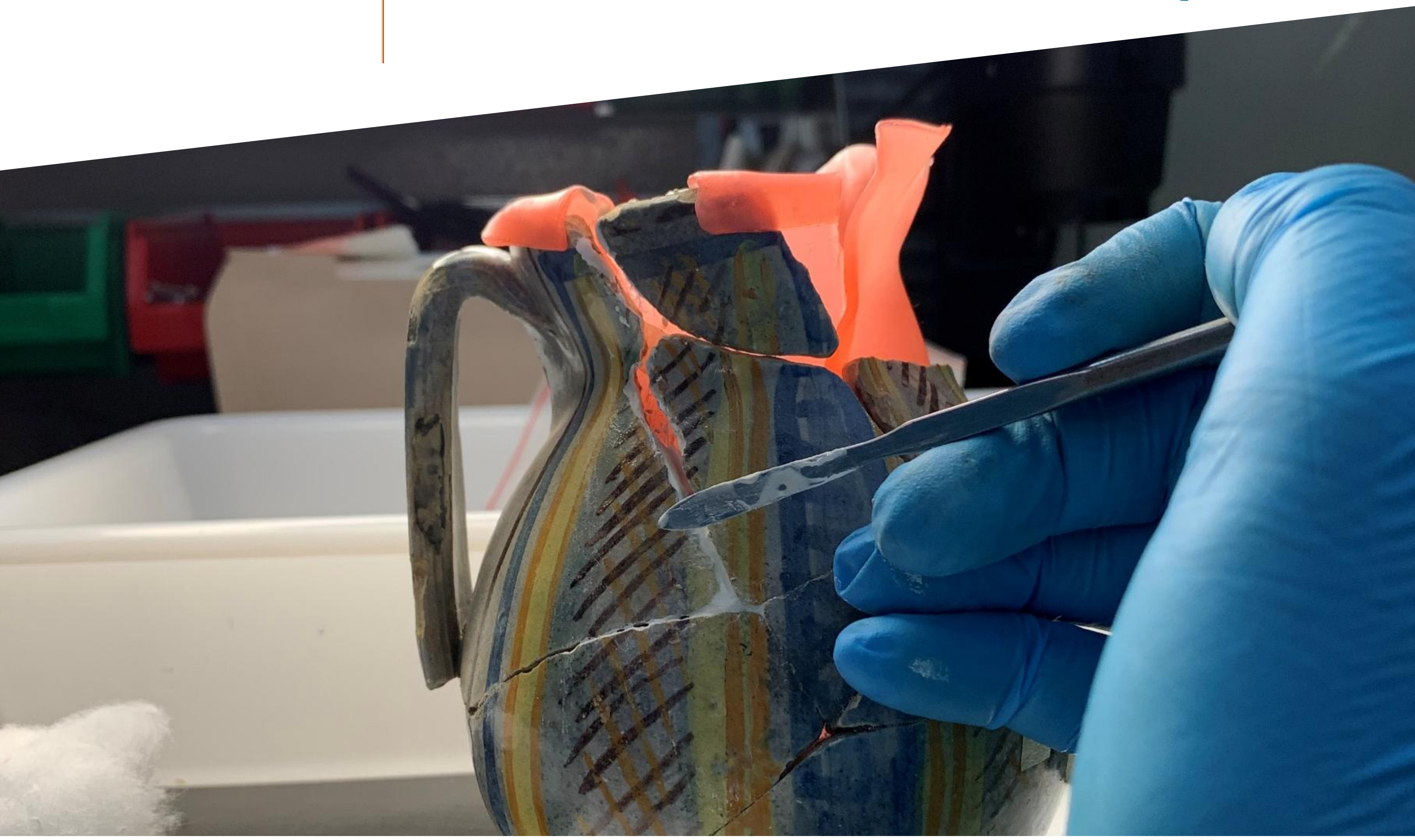

LEC-PH
Laboratorio de Estudios y Conservación del Patrimonio Histórico

# MEMORIA ANUAL
# 2024

# ÍNDICE

Laboratorio de Conservación y Restauración
Aulario Simón Bolívar,
Avda. Duque de Nájera, 16- 11002 Cádiz
Laboratorio de Estudio de Materiales
Centro Andaluz Superior de Estudios Marinos
Avda. de la Universidad, s/n-11510 Puerto Real
Correo electrónico: **laboratorio.lecph@uca.es**

## 1. EL LEC-PH

La función principal del LEC-PH es ofrecer a los investigadores y profesionales, pertenecientes a la UCA y otras instituciones de investigación y empresas, una serie de servicios que comprenden desde la realización de estudios y análisis del patrimonio hasta la ejecución de proyectos de conservación y restauración del material cultural, histórico y arqueológico, contribuyendo a consolidar el área de especialización de "*El Valor Cultural del Mar*" del Campus de Excelencia Internacional del Mar (CEIMAR).

El LEC-PH, Servicio Periférico de Instituto de Investigación Marina (INMAR), distribuye su trabajo en dos grandes secciones temáticas, absolutamente complementarias y necesitadas la una de la otra, que definen la denominación del laboratorio: el Laboratorio de Estudio de Materiales, situado en el Centro Andaluz Superior de Estudios Marinos (CASEM) y el Laboratorio de Conservación y Restauración de Materiales, emplazado en el Edificio Simón Bolívar.

## 2. MOTIVACIÓN DE LA MEMORIA

El objetivo de las memorias de actividades anuales, en esta ocasión la del año 2024, es alienar al LEC-PH con los compromisos de transparencia de la UCA, con la finalidad de facilitar a todas las personas interesadas, miembros o no de nuestra comunidad universitaria, el acceso libre, de forma clara y resumida, a la información más relevante de nuestras actividades de investigación, transferencia, divulgación y formación, como garantía de una correcta gestión de los fondos públicos y rendición de cuentas a la sociedad.

Estas memorias son accesibles a través de la página web de LEC-PH (https://lec-ph.uca.es/).

## 3. PERSONAL

Durante 2024 el LEC-PH contó con tres profesionales, uno de plantilla y dos contratadas por distintos programas:

Manuel Bethencourt Núñez. Investigador responsable del LEC-PH. Es Catedrático de Universidad en el Departamento de Ciencia de los Materiales e Ingeniería Metalúrgica y Química Inorgánica de la Universidad de Cádiz y miembro del grupo del PAIDI TEP-231. Contrato: funcionario de carrea. Contacto: manuel.bethencourt@uca.es.

Marina Goñalons Lapiedra. Contratada por Capítulo VI a cargo del proyecto Port-SUB, "Patrimonio Cultural Subacuático en espacios portuarios de Andalucía. Hacia la investigación, protección y gestión inteligente y sostenible en el marco de la economía azul." Graduada en Conservación y Restauración de Bienes Culturales (UPV-EHU). Máster en Arqueología Náutica y Subacuática (UCA). Contrato UCA: laboral, desde el 10/06/24 hasta el 24/11/24. Contacto: marina.gonalons@uca.es.

Elisa Fernández Tutela. Graduada en Conservación y Restauración de Bienes Culturales (UGR), Máster en Diagnóstico del Estado de Conservación del Patrimonio Histórico (UPO), Máster en Arqueología Náutica y Subacuática (UCA). Actualmente es doctoranda del programa Historia Arqueología Marítima

Hasta octubre de 2023 es Personal Técnico de Apoyo, logrando en esas fechas la plaza de coordinadora del Departamento de Conservación del Centro de Arqueología Subacuática del Institutito Andaluz del Patrimonio Histórico. Contrato UCA: laboral, desde 28/04/21 hasta 22/10/23. Contacto: elisa.fernandez.tudela@juntadeandalucia.es.

Por otro lado, el LEC-PH colabora con numerosos investigadores y grupos de investigación, nacionales y extranjeros. Durante el año 2024 han realizado estancias en el laboratorio el Dr. Nicolás C. Ciarlo, investigador adjunto del Consejo Nacional de Investigaciones Científicas y Técnicas (Argentina), la Dra. Diana Arano Robles, conservadora-restauradora del Instituto Nacional de Antropología e Historia (México), y D. Jaime Mújica, docente y conservador en la Universidad Federal de Pelotas (Brasil). Finalmente, Dña. Elisa Fernández Tutela, responsable del Área de Conservación del Centro de Arqueología Subacuática de Andalucía, es doctoranda del programa Historia y Arqueología Marítima, desarrollando su investigación en el LEC-PH.

## 4. ACTIVIDADES

El LEC-PH da servicio a distintos grupos de investigación, administraciones públicas y empresas, y también desarrolla su propia labor de investigación, comprometiéndose con cada intervención, apostando por los criterios de adecuación, mínima intervención y mínimo impacto ecológico en sus tratamientos. También se compromete con la puesta en valor la importancia de la formación, difusión y la sensibilización de la sociedad para la preservación y estudio del patrimonio cultural; ofreciendo talleres, apoyo a estudiantes y visitas guiadas a las instalaciones. A continuación, se presentan de forma resumida las actividades llevadas a cabo durante el año 2024.

### 4.1. INVESTIGACIÓN

#### 4.1.1. Participación en Proyectos de I+D+I solicitados por grupos PAIDI

- **Participación en proyectos de arqueología subacuática**

Laboratorio de Conservación y Restauración
Aulario Simón Bolívar,
Avda. Duque de Nájera, 16- 11002 Cádiz
Laboratorio de Estudio de Materiales
Centro Andaluz Superior de Estudios Marinos
Avda. de la Universidad, s/n-11510 Puerto Real
Correo electrónico: **laboratorio.lecph@uca.es**

Arqueomallornauta (UCA). Este proyecto de colaboración entre la Universidad de Barcelona, Universidad de Cádiz, Universidad de les Illes Balears y el Consell de Mallorca tiene como objetivo analizar el tráfico marítimo en Mallorca en la Antigüedad Tardía a través de los hallazgos subacuáticos. La UCA ha asumido a lo largo de 2024 los tratamientos de conservación de los distintos materiales (Figuras 1 y 2, Anexo II). Investigador Responsable: Darío Bernal (grupo HUM-440).

Entre las columnas de Hércules, arqueología subacuática de un espacio privilegiado. La Bahía de Algeciras (HERAKLES), Programa Operativo FEDER Andalucía 2014-2020 (FEDER-UCA18-107327, Res. UCA/REC/12VPCT/2019). El Proyecto Herakles tiene como objetivo conocer el patrimonio arqueológico y subacuático en el Estrecho de Gibraltar desde la Bahía de Algeciras. Se han podido inventariar más de 150 pecios hundidos, desde el siglo V a.C. hasta la época contemporánea. Durante el 2024 se han realizado los procesos de estabilización y conservación del patrimonio arqueológico fruto del proyecto (Figuras 3 y 4, Anexo II). Investigador Responsable: Felipe Cerezo (grupo HUM-440).

Patrimonio Cultural Subacuático en espacios portuarios de Andalucía. Hacia la investigación, protección y gestión inteligente y sostenible en el marco de la economía azul. (Port-SUB), (Figura 5 Anexo II). Ayudas es la realización de proyectos de investigación de I+D+i que contribuyan a la consecución de los objetivos del Plan Complementario de Ciencias Marinas. Plan Andaluz de Investigación. De 23 de enero de 2023 al 31 de diciembre de 2025. (Investigador Responsable: Felipe Cerezo (grupo HUM-440).

Aplicación de investigación no invasiva en el asentamiento de Guardias Viejas (El Ejido, Almería): un caso innovador en el potencial *Portus Murgitanus* (CEI-JD-07), en el marco de la Convocatoria de Ayudas a Proyectos de Investigación para Jóvenes CEI·MAR 2023. Investigador Responsable: Isabel Rondan (grupo HUM-240).

- **Proyectos de arqueometría**

Vulnerability of Littoral Cultural Heritage to environmental agents: impact of Climate Change (VOLICHE). Plan Estatal, Retos, 01/01/2021-30/12/2023. Ref. PID2020-117812RB-I00. El objetivo principal de este proyecto es evaluar la vulnerabilidad del Patrimonio Cultural, tanto subacuático como emergido, las condiciones ambientales actuales y el efecto del impacto del cambio climático en su preservación in situ, estableciendo metodologías innovadoras aplicadas bajo una perspectiva holística, integrando el conocimiento de diferentes disciplinas e incluyendo la experiencia de las distintas partes interesadas y usuarios finales. Investigadores Responsables: Manuel Bethencourt (grupo TEP-231), Tomás Fernández-Montblanc (grupo RMN-205).

### 4.1.2. Participación en publicaciones (en prensa) (Anexo I)

D. Arano. N. Ciarlo, G. Carrasco, B. Barba-Meniecke, M. Bethencourt. Copper-based sheathing and fastenings for wooden ships: An archeometallurgical study of the Carron, Ancla Macuca, RMS Forth, and El Pesquero wreck sites located in the gulf of Mexico (Late 18th to Mid-19th Century). Aceptado: 30 de noviembre de 2024 (en prensa).

M. Bethencourt, N. Ciarlo. Arqueología subacuática. Casos de estudio. En: Caracterización y Diagnóstico del Patrimonio Cultural, Seminarios de la Sociedad Española de Mineralogía. Aceptado: 2 de diciembre de 2024 (en prensa).

E. Fernández-Tudela, R. Zarzuela Sánchez, M. Goñalons Lapiedra, A. Gil, D. Bernal-Casasola, M.Á. Cau-Ontiveros, E. García Riaza, J. Cardell Perelló, M. Bethencourt Núñez. Assessment of consolidants for the preservation of *Tituli Picti* on amphorae from the Ses Fontanelles Late Roman shipwreck (Mallorca, Spain): An analytical approach, Journal of Cultural Heritage, aceptado 20 diciembre 2024 (en prensa).

C. Ferrero-Martin, A. Izquierdo, M. Bethencourt, T. Fernandez-Montblanc. A Risk Assessment of Underwater Cultural Heritage for Wave-Induced Hazards: The Impact of Climate Change on Cadiz Bay. Journal of Marine Science and Engineering, aceptado: 30 de diciembre de 2024 (en prensa).

### 4.1.3. Participación en congresos (Anexo I)

E. Fernández-Tudela, M. Goñalons Lapiedra, L. C. Zambrano Valdivia, D. Bernal-Casasola, M.Á. Cau-Ontiveros, E. García Riaza, J. Cardell Perelló, M. Bethencourt Núñez, Tests for the efficacy of three consolidation methods for the organic collection of Ses Fontanelles Shipwreck (Mallorca, Balearic Islands, Spain), TechnoHeritage, 25 a 27 de septiembre de 2024, Santiago de Compostela.

E. Fernández-Tudela, R. Zarzuela Sánchez, M. Goñalons Lapiedra, A. Gil, D. Bernal-Casasola, M.Á. Cau-Ontiveros, E. García Riaza, J. Cardell Perelló, M. Bethencourt Núñez. Assessment of the effectiveness of consolidants for the preservation of *Tituli Picti* on amphorae from the Late Roman Ses Fontanelles wreck (Mallorca, Spain): An analytical approach, TechnoHeritage, 25 a 27 de septiembre de 2024, Santiago de Compostela.

O. Ortega, M. Bethencourt, N. Ciarlo, T. Fernández-Montblanc, Desaparición del Reina Regente: Posibles causas y localización. Primeros datos obtenidos. 3as Jornadas Luso Españolas de Hidrografía, 9 a 11 de octubre de 2024, Cádiz.

D. Arano, N. Ciarlo, G. Carrasco, H. Barba-Meinecke, M. Bethencourt, Historia y metalurgia de los revestimientos de cobre para el casco de embarcaciones de la

Laboratorio de Conservación y Restauración
Aulario Simón Bolívar,
Avda. Duque de Nájera, 16- 11002 Cádiz
Laboratorio de Estudio de Materiales
Centro Andaluz Superior de Estudios Marinos
Avda. de la Universidad, s/n-11510 Puerto Real
Correo electrónico: **laboratorio.lecph@uca.es**

Armada y Marina Mercante españolas (1780-1820), VIII Simposio Internacional de Historia y Arqueología Marítima: Mar adentro, mar afuera: conexiones, percepciones y vestigios en el espacio marítimo y litoral, 21 a 25 de octubre de 2024, Mérida, Yucatán (México).

## 4.2. TRANSFERENCIA

### Contratos con el exterior (art. 83 LOU)

Análisis arqueológico-histórico de una colección de artefactos del cargamento del pecio Deltebre I (1813) (OT2024/213). Financiado por: Centro de Arqueología Subacuática de Cataluña. Responsable: M. Bethencourt.

Tratamiento de conservación mediante electrolisis de ancla de procedencia subacuática y pieza de artillería de procedencia desconocida para la Autoridad Portuaria de la bahía de Algeciras. (OT2024/212). Financiado por: la Autoridad Portuaria de la bahía de Algeciras. Responsable: F. Cerezo.

## 4.3. DIVULGACIÓN

- M. Bethencourt. Influencia de las condiciones fisicoquímicas en el estado de conservación de los pecios *Fougueux* y *Bucentaure* (1805). Seminario de Procesos Bioculturales de Formación de Sitios Arqueológicos Sumergidos. 5 de julio de 2024. Instituto Colombiano de Antropología e Historia (ICANH).

- Propuesta y selección de la Universidad de Cádiz como sede del congreso MetalEspaña2025: IV Congreso de Conservación y Restauración del Patrimonio Metálico. Se trata de un evento de carácter nacional con presencia de investigadores latino americanos que busca destacar los avances en investigación aplicada, innovación tecnológica y proyectos de conservación de objetos y obras metálicas. MetalEspaña2025 será la cuarta edición de este congreso, tras las exitosas convocatorias de MetalEspaña08 (Universidad Autónoma de Madrid), MetalEspaña2015 (Casa de Moneda de Segovia) y MetalEspaña20 (Universidad Autónoma de Madrid). Esta edición marca un hito especial, ya que será la primera vez que el congreso se celebrará en la Comunidad Autónoma de Andalucía, lo que simboliza el compromiso de extender la importancia del patrimonio metálico por todo el territorio nacional.

  Durante 2024 se han cerrado las fechas (23 a 25 de noviembre de 2025), y se ha logrado la participación del Servicio de Conservación, Restauración y Estudios Científicos del Patrimonio Arqueológico (SECYR-UAM), Laboratorio de Estudios y Conservación del Patrimonio Histórico (LEC-PH, UCA), Fábrica Nacional de Moneda y Timbre-Real Casa de la Moneda (FNMT-RCM), Consejo Internacional de Museos (ICOM), Museo de Cádiz, Centro de Arqueología Subacuática de Andalucía perteneciente al Instituto Andaluz del

Laboratorio de Conservación y Restauración
Aulario Simón Bolívar,
Avda. Duque de Nájera, 16- 11002 Cádiz
Laboratorio de Estudio de Materiales
Centro Andaluz Superior de Estudios Marinos
Avda. de la Universidad, s/n-11510 Puerto Real
Correo electrónico: **laboratorio.lecph@uca.es**

Patrimonio Histórico (CAS-IAPH), Instituto Hidrográfico de la Armada (IHM), y el Campus de Excelencia Internacional del Mar (CEIMAR). Al finalizar 2024 ya se contaba con el apoyo económico de la Fundación Universidad Autónoma de Madrid (FUAM), y la empresa Titania, Ensayos y Proyectos Industriales, S.L., y se solicitó financiación a la FNMT-RCM, al Consejo Social de la UCA, al Instituto de Investigación Marina y al Vicerrectorado de Investigación y Transferencia de la UCA.

- Thinking Azul Andalucía. Zona Expositiva III, 3as Jornadas Luso Españolas de Hidrografía, 9 a 11 de octubre de 2024, Cádiz. M. Goñalons Lapiedra. (Figura 6, Anexo II).

- Blue Zone Forum - InnovAzul, 20 al 22 de noviembre de 2024. Stand: Patrimonio Cultural Sumergido. M. Goñalons Lapiedra. (Figura 7, Anexo II).

- Grabación de documental con entrevista para programa de IB3 Televisó, por la empresa Salom Estudi, en referencia a los trabajos realizados en el LEC-PH con los materiales del pecio de Ses Fontanelles (Palma de Mallorca). M. Goñalons Lapiedra.

## 4.4. FORMACIÓN

### 4.4.1. De alumnado de Doctorado y Máster

Durante el año 2024 han continuado (pendientes de defensa) la colaboración de los trabajos de investigación de las siguientes Tesis Doctorales:

- Diagnóstico de las alteraciones del plomo de procedencia subacuática y su caracterización a través de los cepos de plomo del Museo de Cádiz. Alumna: Elisa Fernández Tudela, Programa de Doctorado de Historia y Arqueología Marítimas. Directores: M. Bethencourt, L.C. Zambrano.

- Del pasado a la modernidad, formas diversas de investigar lo antaño: una perspectiva histórica desde la arqueología marítima y subacuática de la Bahía de Santa Marta, Colombia. Alumno: Deyber José Hernández Martínez. Directores: M. Bethencourt, N. Ciarlo.

Durante el año 2024 han continuado los trabajos de investigación de los siguientes Trabajos Fin de Máster del Máster de Arqueología Náutica y Subacuática. Se han defendido los siguientes:

- Comparación entre la fotogrametría digital y la batimetría obtenida con un sondador multihaz montado en un USV, como técnicas de documentación y supervisión de pecios de interés. Alumno: Juan Rengel Ortega. Tutor: M. Bethencourt, F. Cerezo.

- Caracterización y estudio arqueométrico de dos piezas de artillería de proveniencia subacuática. Alumno: Jesús Adrián Marcos San Fulgencio. Tutores: M. Bethencourt, N. Ciarlo.

Y se ha continuado con las labores de investigación (pendientes de defensa):

- Procesos de intervención en material mixto. Restauración de un saquete de metralla del siglo XVIII. Alumna: Sara Ventura Acosta. Tutores: M. Bethencourt, E. Fernández.

- Empleo de vehículos autónomos para la evaluación de los cambios morfológicos en yacimientos subacuáticos. Alumna: Sara Franceschin. Tutor: M. Bethencourt, C. Beltrame.

- Análisis arqueométrico y contextual de un calibre de artillero del siglo XVI-XVII de procedencia subacuática. Alumna: Iris Bartolomé Ortúñez. Tutores: M. Bethencourt, N. Ciarlo.

### 4.4.2. Tutorización de prácticas de empresa

Realización de prácticas curriculares del Máster de Arqueología Náutica y Subacuática (UCA). Tareas: Investigación y Conservación de objetos arqueológicos procedentes de la Bahía de Algeciras. Tratamientos de limpieza, estabilización y protección de objetos cerámicos, metálicos y orgánicos (Proyecto Herakles) en el LEC-PH. Alumna: Andrea Franco. Tutor académico; Felipe Cerezo Andreo. Tutorización laboratorio: M. Goñalons Lapiedra. Fecha de realización: 17/06/24 a 31/07/24.

Realización de prácticas curriculares del Máster de Arqueología Náutica y Subacuática (UCA). Tareas: Investigación y Conservación de objetos arqueológicos procedentes de la Bahía de Algeciras. Tratamientos de limpieza, estabilización y protección de objetos cerámicos, metálicos y orgánicos (Proyecto Herakles) en el LEC-PH. Alumna: Ilaria Vitiello. Tutor académico; Felipe Cerezo Andreo. Tutorización laboratorio: M. Goñalons Lapiedra. Fecha de realización: 23/09/24 a 18/10/24.

Los Planes de Prácticas diseñados por M. Goñalons Lapiedra para ambas alumnas se encuentran en el **Anexo III**.

# ANEXO I

## Productividad

## Participación en publicaciones

# Copper-based sheathing and fastenings for wooden ships

| | |
|---|---|
| Journal: | *Metallography, Microstructure, and Analysis* |
| Manuscript ID | MMA-24-11-1965.R1 |
| Manuscript Type: | Original Research Article |
| Date Submitted by the Author: | n/a |
| Complete List of Authors: | Arano Recio, Diana; Instituto Nacional de Antropología e Historia, Sección de Conservación - Restauración<br>Ciarlo, Nicolas; Universidad de Buenos Aires, Instituto de Arqueología \| Facultad de Filosofía y Letras; Consejo Nacional de Investigaciones Científicas y Técnicas<br>Carrasco González, Guadalupe; Universidad de Cádiz, Departamento de Historia Moderna, Contemporánea, de América y del Arte, Facultad de Filosofía y Letras<br>Meinecke, Helena; Instituto Nacional de Antropologia e Historia, Subdirección de Arqueología Subacuática, Componente Península de Yucatán<br>Bethencourt Núñez, Manuel; Universidad de Cádiz, Dpto. de Ciencia de los Materiales e Ingeniería Metalúrgica y Química Inorgánica Facultad de Ciencias del Mar y Ambientales |
| Area of Expertise/Keywords: | Archaeometallurgy, Copper Alloys, Indentation Hardness, Metallography, Scanning Electron Microscopy |
| | |

SCHOLARONE™
Manuscripts

# Copper-based sheathing and fastenings for wooden ships. An Archaeometallurgical study of the Carron, Ancla Macuca, RMS *Forth*, and El Pesquero wreck sites located in the Gulf of Mexico (late 18$^{th}$ to mid-19$^{th}$ century)

D. Arano*[1], N.C. Ciarlo[2], G. Carrasco[3], H. Barba[4], M. Bethencourt[5]

1 Sección de Conservación, Instituto Nacional de Antropología e Historia, Yucatán, México.

2 Consejo Nacional de Investigaciones Científicas y Técnicas (CONICET) – Instituto de Arqueología, Facultad de Filosofía y Letras, Universidad de Buenos Aires, Argentina.

3 Departamento de Historia Moderna, Universidad de Cádiz, España.

4 Subdirección de Arqueología Subacuática, Componente Península de Yucatán, Instituto Nacional de Antropología e Historia, México.

5 Departamento de Ciencia de los Materiales e Ingeniería Metalúrgica y Química Inorgánica, Facultad de Ciencias del Mar y Ambientales, Instituto de Investigaciones Marinas (INMAR), Universidad de Cádiz, España.



**Abstract**

One challenge in maritime archaeology is correlating historical records, archaeological findings, and material analysis data to accurately date and establish the provenance of shipwrecks. In the late 18th and early 19th centuries, European naval construction emphasized improvements to the durability of wooden ships, especially for tropical waters. The introduction of metal sheathing was a significant innovation to safeguard ship hulls against wood-boring organisms. Archaeometallurgical analysis of copper-based sheathing and fastenings provides crucial insights into shipwreck technology and construction context. This study examines copper sheathing and fastenings on wooden ships from the late 18th to mid-19th century, focusing on

wrecks in the Gulf of Mexico. Artifact analysis from these sites sheds light on evolving shipbuilding practices during the early industrial period. Additionally, archaeometallurgical analysis has provided chronological references that assist in identifying these wrecks, particularly given the absence of ship hulls, which have degraded under tropical marine conditions.

**Keywords**: archaeometallurgy, nautical technology, 18th and 19th century, shipwrecks

**Introduction**

During the late 18th and early 19th centuries, maritime activities in the Gulf of Mexico, the Antilles, and the Caribbean were diverse, and predominantly driven by commerce, resource exploitation, and military conflicts. Evidence of these activities can be found in historical records and archaeological remains, particularly shipwrecks, which offer valuable insights into the region's nautical activities. European vessels played a crucial role in this maritime pursuit. During this period, wooden vessels underwent significant improvements, with copper sheathing technology standing out as a key advancement. Initially implemented to protect wooden hulls from damage by marine organisms, copper sheathing notably enhanced both the speed and durability of vessels. However, its introduction presented challenges, particularly the accelerated corrosion of iron fastenings due to galvanic reactions with the copper sheathing. The British Royal Navy addressed this issue by experimenting with copper alloys and eventually adopted "hardened" copper bolts for use below the waterline, a practice later adopted by other European navies.

The transfer of copper sheathing technology from Great Britain to France, Spain, and beyond was a result of both industrial espionage and technological exchange. This technology spread further, extending to merchant vessels, particularly through the British East India Company. By the mid-19th century, advancements in copper alloys, such as Muntz metal, enhanced the efficiency and cost-effectiveness of sheathing and fastenings for vessels (1–8).

**Brief Overview of Selected Archaeological Sites**

*Carron site, Cayo Nuevo*

This wreck site is located northeast of Cayo Nuevo Reef on a limestone bed at a depth ranging from 5 to 7.9 m (Fig. 1). Scattered metallic sheets, concentrated primarily on the southern end, are found alongside other diagnostic remains, including 43 iron guns, 5 anchors, musket balls, lead fragments, and iron rudder hinges. Notably, one gun is inscribed with the foundry name (*CARRON*) and the manufacture date (*1775*) on its trunnion face (9). The use of copper-alloy sheathing, bolts, and sheathing tacks suggest a *terminus post quem* for the wreck events of about the early 19th century (10–13).

Moreover, two 16th-century artifacts—a bronze demi-culverin (dated 1552) and an anchor—were discovered nearby (9,10,12). The broad time range of the identified objects suggests a palimpsest, indicating that the remains of at least two wrecks are likely presented. Analysis of copper-alloy fastenings may provide insights for the contextual assessment of sites.

*Ancla Macuca and RMS* Forth *(1849) sites, National Park Alacranes Reef*

Natural site formation processes have resulted in an overlap of these shipwreck remains, creating a palimpsest (13) (Fig. 1). Materials associated with both vessels, including copper-based sheets and fastenings, present technical similarities, complicating their identification and association with a particular vessel. The Ancla Macuca site, likely a merchant vessel from the late 18th century, yielded a remarkable assemblage of artifacts, including 236 gold jewels (23-carat), emeralds, diamonds, silver macuquina coins (1620–1650), and six iron guns (13–15).

The wreck of RMS *Forth* (1849) revealed structural remains, including the steam propulsion system. Historical records indicate that it belonged to a fleet of 14 steamers from the Royal Mail Steam Packet Company, which was regularly engaged in a transoceanic mail route. Built in 1841, the ship's hull was constructed of oak and teak and equipped with a 450 HP side-lever single steam engine (10,13,16).

*El Pesquero site, Champotón*

This site covers approximately 900 m², with remains embedded in a coral formation measuring about 14 m in length and oriented east-west (Fig. 1). Due to the tropical marine environment, only limited portions of the wooden hull have survived. The assemblage includes an iron stove, bricks (likely from the ship's kitchen), six guns ranging from 3 to 9 pounds, round shot, pig iron, and shingle ballast. Sheathing tacks, a spike, and fragments of lead were also recovered. A highly corroded sheet containing tacks was discovered positioned parallel to the area with the greatest concentration of archaeological remains (Fig. 6).

Eighty meters north of the main assemblage, an anchor was located, though its association with the site remains undetermined. These materials, particularly the copper-alloy fastenings, could offer insights into the ship's construction and potential trade networks (12,17,18).

## Methodology

A historiographic review of the production cycle of copper sheathing and fastenings used in shipbuilding was conducted and compared with the archaeological data gathered from the selected sites. In addition, characterization studies were performed on samples of sheeting, sheathing tacks, nails, and bolts samples from these sites (11)[1]. Photogrammetry and 3D modeling were employed to record the shape and dimensions of the objects. X-ray imaging was employed to analyze metallic remains in severely deteriorated sheathing.

The metallographic examination of copper-based samples to determine microstructural features was conducted using light microscopy (LM) and scanning electron microscopy (SEM).

[1] Samples were labeled with an acronym of the archaeological site and a number (e.g., SASY, AM, PI).

Additionally, semi-quantitative elemental composition analysis was performed through energy dispersive X-ray spectroscopy (EDX) and X-ray fluorescence (XRF). The samples were embedded in thermoplastic resin, then ground and polished to achieve a specular surface. To reveal the microstructure, a hydroalcoholic solution of ferric chloride was applied. For brass samples, the areas unaffected by selective corrosion (dezincification) were selected.

Vickers microhardness testing was conducted on polished sections of the samples to evaluate their mechanical properties (Hardness, 1999). A load of HV 0.2 was applied to each sample for 10 seconds. This measurement was performed using a Duramin-40 microhardness tester from Struers®. These data provided insights into the manufacturing techniques employed, such as cold working and annealing.



**Results and discussion. Metallurgical analysis and findings**

*Carron*

At the Carron wreck site, two types of brass bolts were identified, both shared a similar composition but exhibited differences in shape and microstructure (Fig. 2). Bolt SASY-016 is characterized by a partially recrystallized structure with grains displaying a high level of corrosion (Figure 2a, b, c). Elongated metallic inclusions in the longitudinal direction suggest that the bolt was manufactured through plastic deformation, likely by hot (or possibly cold) forging, followed by annealing. Slip bands near the surface suggest slight cold working. The alloy composition is 65% Cu and 35% Zn, with trace amounts of Pb and Fe. In contrast, bolts SASY-015 feature a wedge-shaped tip and display a Widmanstätten-type grain structure, likely a result of rapid cooling after the hot deformation process (Figure 2d, e, f).

According to the Cu-Zn phase diagram, the α phase precipitates from the single-phase ß during cooling, forming α laminations within a ß matrix (19).[2] The different microstructures of the bolts suggest at least these two possibilities: a) they were manufactured for different purposes, such as securing distinct parts of the hull, and b) they were produced in different workshops using different methods. Similar microstructural variations in brass have also been documented by Bram and colleagues in the Akko Tower wreck (20,21).

Sheathing tack SASY 014 exhibits a dendritic microstructure, with larger grains concentrated at the head where solidification was slower (Figure 2g, h, i, j). These characteristics are typical of casting and solidification without subsequent thermomechanical treatment. The alloy consists primarily of Cu (65.9%) and Zn (33.7%), with minor Pb content (0.2%) precipitating in the interdendritic regions.

The microstructure of sheet SASY 020 displays equiaxed grains of various sizes (20-200 µm) with recrystallization twins, indicating that the sheet was manufactured by rolling, either hot or cold, followed by annealing (Fig. 2k, l, m). The sheet is made of brass and features elongated Pb inclusions in the direction of hammering or rolling. The brass alloys documented at the site resemble the composition of Muntz metal (about 60% Cu - 40% Zn), patented in 1832 (8,22–26).

*Ancla Macuca and RMS* Forth *(1849)*

At Alacranes Reef, the correlation between historical records and archaeological remains enabled the identification of one shipwreck—the RMS *Forth*, a steamship that sank in 1849. In contrast, the archaeological remains of the Ancla Macuca wreck suggest that this second vessel might date to the second half of the eighteenth century. Analysis of copper-base fastenings and

[2] For duplex brasses, the α phase is a solid solution of Zn in Cu, crystallizing in a face-centered cubic (FCC) structure and readily deformable in cold working. The ß phase is an intermetallic compound with an approximate 1:1 composition ratio. The ß phase forms once the α phase reaches saturation and crystallizes in a body-centered cubic (BCC) structure (19).

sheets at this location revealed two distinct compositional groups: one of unalloyed copper (Fig. 3) and the other consisting of brass and bronze alloys (Fig. 4-5).

The use of brass in shipbuilding began in the early nineteenth century, with applications including bolts, nails, and sheathing (1,8,25,26). Consequently, the brass remains were associated with the RMS *Forth* (1849). In contrast, the unalloyed copper elements, introduced into the European shipbuilding practices in the last third of the eighteenth century, may correspond to the Ancla Macuca wreck. However, this does not exclude the possibility that some components of unalloyed copper might also belong to the British steamship, as a single vessel could incorporate materials from different periods and origins (10). Additionally, the prolonged use of unalloyed copper in certain naval contexts must be considered.

From the Ancla Macuca site, bolt AM–063 exhibits a microstructure of equiaxed grains of unalloyed copper of variable grain sizes (10-100 µm) and recrystallization twins (Fig. 3a, b, c). In the longitudinal section, the grains are elongated (Fig. 3a). This bolt was likely produced by plastic deformation, probably through hot forging. The presence of deformation lines and elongated grains at one end of the bolt suggests hammering, possibly occurring during the vessel's construction.

Sheathing sheet PI–07 is also composed of unalloyed copper (Fig. 3d-h). Its microstructure displays equiaxed grains, recrystallization twins, and metallic inclusions (Pb, As, Bi), elongated along the manufacturing direction (Fig. 3f, g). This evidence indicates that the sheet was produced by rolling, potentially either hot or cold, followed by annealing. They, while somewhat aligned, vary in thickness and length. This feature suggests that the sheet may have been further shaped by hammering. If the vessel is of Spanish origin, as suggested by contextual evidence, historical information raises several considerations (14,15). Copper sheathing was first introduced in Spain in 1782, but no rolling mill was established there until 1790 (10,27). Therefore, it is plausible that the vessel was sheathed in the late eighteenth century. However, given the presence of clandestine activities in the Gulf of Mexico, it is also conceivable that the vessel was of English origin, operating in the Campeche Sound. If so, it may date to an earlier period, as the British merchant fleet began adopting copper sheathing for hulls in the last third of the eighteenth century (28,29).

At the RMS *Forth* (1849) site, sheet AM-084 is composed of brass with 62-66% Cu and 38-34% Zn. Its microstructure consists of equiaxed grains of various sizes (40-300 µm) and recrystallization twins (Fig. 4a, b, c). The sheet also contains metallic inclusions of Pb with minor amounts of Bi, As, and Fe and non-metallic of S. These data, along with the alignment of the inclusions, suggest that the sheet was manufactured by rolling—either hot or cold, with annealing in the latter case (Fig. 4a, b, c).



For the bolts, the composition is consistent with Muntz brass. Bolts PI-021 A, B, C, and D show an average composition of Cu 64%, and Zn 35%, with traces of Pb, Mn, and Fe. Brass bolts AM 072 (63-65% Cu - 37-35% Zn), PI-021-C (66% Cu - 34% Zn, with traces of Fe), and PI 020 (67% Cu - 33% Zn) share similar compositions (Fig. 4). In cross-section, bolts PI 021C (Fig. 4d, e) and PI 020 (Fig. 4i, j, k) exhibit a microstructure of equiaxed grains of varying sizes and recrystallization bands, indicative of plastic deformation in the manufacturing process. Slip bands along the surface likely resulted from cold working in the final production stage. In the cross-section of bolt PI-020, a peripheral zone with smaller grains indicates intense deformation and partial recrystallization during the final production stage (Fig. 4j). In the longitudinal section, the grains are elongated, likely due to plastic deformation in the manufacturing process

(Fig. 4l, m). This bolt also displays significant dezincification, resulting from selective Zn dissolution in the marine environment (Fig. 4n).[3]

The square-bodied nails, like the bolts and sheets, can be grouped based on composition. Of the four square-bodied nails (PI 016 A, B, E and PI 022A) (Fig. 5), PI 016A and B exhibit similar dendritic microstructures and ternary bronze compositions (85-89% Cu, 6-7% Zn, and 3-4% Sn, with traces of Fe), and numerous pores in the matrix (Fig. 5a-f). Nail PI 016E shows advanced intergranular corrosion, with marine environment minerals filling its pores (Fig. 5k-m). Its originally dendritic microstructure is partially recrystallized, and its composition (82% Cu, 6% Zn, 6.8% Sn, and 3.3% Pb) differs slightly from the others. The microstructural characteristics suggest potential heat exposure, either during manufacturing (e.g., annealing) or as a result of the vessel's sinking. The fourth square-bodied nail (PI 022A) is in an advanced state of corrosion, yet still retains a visible dendritic with a slightly different composition (62-66% Cu, 30-33% Zn, 1-3% Sn, and traces of Pb) (Fig. 5g-j).

At this site, three sheathing tacks (PI 16C, PI016D and AM 052) were analyzed, displaying a composition consistent with quaternary bronze. The average composition of these tacks is 77-87% Cu, 6-11% Zn, 4-7% Sn, and 3-6% Pb, with traces of Fe (Fig. 5n-w).

The dendrites within the tacks have an approximate composition of 82% Cu, 10% Zn, 5% Sn, and 2% As. In the interdendritic regions, the Sn percentage increases to 23% (Fig. 5m, p). Below 320°C, copper and tin exhibit limited mutual solubility, leading to precipitation in these areas. The elevated Sn concentration is attributed to segregation during solidification (Fig. 5r). Lead inclusions, mostly containing traces of As, Ni, and Fe, are observed; as Pb, is practically insoluble

[3] Zinc dissolution occurred along the grain boundaries of the brass microstructure, in some instances penetrating to the core of the metal (Fig. 4m).

in copper alloys, it segregates and precipitates within shrinkage voids during solidification (19) (Fig. 5s, u, v).

Pb concentration increases from the tip to the head of the nail, correlating with the cooling pattern of the alloy, as the head is oriented upward in the mold. Micro-shrinkage occurs due to the contraction of the metal across the nail head during cooling (Fig. 5t, w). Elemental mapping using EDX confirmed that areas with Pb also contain S and As (Fig. 5m, p). SEM imaging revealed a dark phase in the form of angular particles in the peripheral areas of the Pb inclusions or scattered within the alloy's microstructure (Fig. 5u). These particles primarily consist of Zn (62%), S (23%), Cu (14%), and Sn (1%). The presence of As impurities likely reflects the ore source and limitations in refining technology of the period (30).

*El Pesquero*

At El Pesquero site, a thin and highly deteriorated sheet containing three nails embedded within the corrosion products was recovered (PQ 060) (Fig. 6). X-ray analysis revealed a retained metallic matrix within a concretion, which was carefully removed (PQ 060D) (Fig. 6a, b). SEM-EDS and metallographic studies determined that the sheet's composition is predominantly copper (99-100%), with localized inclusions of Bi and As. Its microstructure displays equiaxed grains with deformation twins (Fig. 6a, b).

Three sheathing tacks, PQ 060 A, B, and C, attached to the corroded sheet PQ 060, were made of a quaternary brass (88-90.5% Cu, 3-4% Zn, Sn 1-4.5% Sn, and 2.5-3.5% Pb, with traces of Fe and As) and exhibit a dendritic and biphasic microstructure, indicative of a casting process (Fig. 6c-n). Micro-shrinkages formed during solidification are evident in the head area, and carbon particles were detected in two of the tacks (Fig. 6e). As expected, Pb precipitated within the interdendritic spaces (Fig. 6f, i, m, r).

An additional sheathing tack, PQ 020, was found isolated approximately five meters apart from the main concentration of archaeological remains. It is composed of a quaternary bronze, similar to the other artifacts (91-92% Cu, 4-5% Sn, 2-5% Zn, and 1% Pb), but lacks traces of Fe or As (Fig. 6o-r). The slight compositional differences are likely attributable to the inherent heterogeneity of such artifacts, exacerbated by alterations induced by corrosion processes. This tack also displayed dendritic microstructure as cast.All sheathing tacks displayed segregation of a Zn-rich phase within the interdendritic spaces,with a compositional gradient correlated to variations in hardness. The PQ 020 tack exhibited slip bands, more pronounced at the tip than in the body and head, likely due to cold working.Whether this feature results from manufacturing or subsequent use is difficult to determine.During the vessel’s sinking, fastenings in the ship's structure might have experienced differential stresses depending on their location and hull integrity.

The square-bodied nail PQ 044 is composed of a quaternary bronze, primarily Cu (89-91%), with smaller percentages of Zn (3-4%), Sn (3-4%), Pb (1-3%), and traces of Fe. It displays a dendritic microstructure indicative of a casting process (Fig. 6s, t, u). The nail’s composition closely aligns with that of the analyzed sheathing tacks. The compositional analysis of the sheets, sheathing tacks, and nails, and their correlation with other site remains, suggest that this vessel dates from the late 18th to early 19th century.

*Influence of metallurgical processes on microhardness*

The microhardness of the studied alloys varies notably based on both metallurgical processing and alloy composition, offering insights into the behavior and durability of the artifacts. In brass bolts, for instance, the differences in microstructure between SASY 015 (Longitudinal hardness

(LH): 110.17 HV – Transverse hardness (TH): 126.58 HV) and SASY-016 (LH: 144.27 HV – TH: 148.4 HV) illustrate the impact of distinct manufacturing processes on hardness. These variations are critical for understanding the functionality of these bolts within shipbuilding, where hardness influences the durability and mechanical strength of fasteners.

Similarly, the dendritic microstructure of sheathing tacks and nails, such as SASY-014 (LH: 132 HV – TH: 172.5 HV) and PQ-060A (LH: 143.5 HV – TH: 118.4 HV), indicates that the solidification without subsequent thermo-mechanical treatments results in heterogeneous microhardness. In particular, the segregation of Pb in interdendritic spaces and the precipitation of Zn-rich phases create localized areas of lower hardness, which could adversely affect the structural strength of these components.

Cold working, as observed in brass sheets and bolts [SASY-020 (LH: 103.5 HV – TH: 123.3 HV), PI-020 (LH: 140 HV – TH: 149 HV)], increases hardness by inducing slip bands, which enhance material strength. Recrystallization, conversely, restores ductility in cold-worked bronze, although it decreases hardness compared to material worked without annealing.

In summary, the microhardness of the studied materials is directly related to the metallurgical techniques employed, such as casting, forging, and rolling. Copper and its alloys show variabilities in hardness due to elemental segregation as well as cold or hot working processes.

**Conclusions**

This research contributes on two levels: first, by providing specific microstructural and compositional data for the sheathing and fastenings used in different vessels, and second, by offering broader insights into the formation processes and identification of the wreck sites.

The archaeometallurgical analysis of copper and copper-alloy sheathing, sheathing tacks, nails, and bolts from shipwrecks located in the Campeche Bank has revealed several key technological features: a) composition, b) manufacture, c) use, and d) deterioration processes. These findings contribute to a more nuanced understanding of the materials used for shipbuilding during the late 18th to mid-19th centuries.

The development and adoption of copper sheathing varied across European nations during the last third of the 18th century. Our findings are significant for maritime archaeology in the Gulf of Mexico, particularly for assessing unidentified wreck sites. However, to address the origin or nationality of the vessels, additional historical research and further analysis of archaeological remains are required.

This research also enabled a detailed examination of the palimpsest formed by the wrecks of the Ancla Macuca (ca. late 18th century) and RMS *Forth* (1849). The metallurgical analyses provided valuable data for correlating the composition of the fastenings and sheathing remains with a specific period, serving as a reference frame for the metals used in shipbuilding. Another example of palimpsest is the Carron site, which contains archaeological evidence ranging from the 16th-century bronze demi-culverin to 18th-century iron guns (one, dated from 1775) and a brass sheathing and fastenings. This suggests that the site may represent at least two different shipwrecks occupying the same area. An alternative interpretation considers that the site could correspond to a 19th-century vessel transporting earlier materials, similar to the Spanish frigate *Nuestra Señora de las Mercedes*, built in 1788 and sunk in 1804, whose cargo included bronze guns from the late 16th and early 17th centuries (31). Both general and specific aspects of the methodology employed in this study could be applied to other shipwrecks from the same period.

In summary, this study underscores the value of integrating metallurgical analysis with historical and archaeological evidence from shipwrecks to study metals used in wooden shipbuilding. This integrated approach not only enhances our understanding of the materials and techniques employed but also highlights the broader historical context in which these innovations were applied.

The tropical conditions and specific contexts of the studied wreck sites have led to significant corrosion of the fastenings and sheathing, in brasses, dezincification in the marine environment was a major factor. In this work, the microstructure and composition of samples were examined in areas unaffected by corrosion to identify the manufacturing processes and material characteristics. Given the advanced state of degradation of the archaeological remains, this research highlights the importance of developing a detailed record and analysis of samples. Such documentation is essential for assessing the wreck sites comprehensively, alongside other findings such as guns, hull elements, cargo, and other material cultural carried on board. This is especially crucial in contexts where wooden hulls have been almost destroyed by the action of wood-boring organisms.

This research demonstrates the value of integrating historical, archaeological, and archaeometric data to reconstruct the technologies used in modern naval shipbuilding. Such an interdisciplinary approach enriches our understanding of both the materials and techniques used for copper-based artifacts applied to wooden shipbuilding. To advance this research, further historical review is needed to identify three of the four wrecks and establish the nationality of the vessels. Moreover, analyzing other types of archaeological remains, such as the wood species used in shipbuilding, could greatly enhance our current understanding of the sites and can also offer a more comprehensive insight into the construction and navigation practices of the period.



**Acknowledgments**

The authors are very grateful for the funding provided by the projects PIPY-SAS-INAH and CONACYT - LANCIC LN315853 and LN314846, and the CICORR research center of the Autonomous University of Campeche, in Mexico. We also extend our gratitude to the Spanish State Research Agency, Ministry of Science, Innovation and Universities (State Plan I+D+i 2017-2020, EQC2018-004947-P). We are grateful to the Historical Metallurgy Society for supporting the presentation of this research. Finally, we thank our collaborators Rodrigo Ortiz for the photogrammetry of the El Pesquero site, and Abiud Piza Chávez and Gabriel Quetz León for their contributions to the historical research and archaeological record.

**References**

1. Ciarlo N. Experimentación, transparencia tecnológica y conservadurismo: notas sobre la introducción del aforro de cobre en los barcos de madera del siglo XVIII. *Revista del Centro de Estudios de Arqueología Histórica*. 2017;6:9–27.

2. McCarthy M. *Ships' Fastenings: From Sewn Boat to Steamship*. Texas A&M University Press; 2005. 229 p.

3. Thompson L. *Copper on the Northwest Coast: A Material Investigation of Cultural Entanglements Experienced During the Fur Trade and Colonial Periods*. [PhD Dissertation]. Sheffield, UK: University of Sheffield; 2019.

4. Knight RJB. The introduction of copper sheathing into the Royal Navy, 1779–1786. *The Mariner's Mirror* [Internet]. 1973 Jan 1 [cited 2020 Jun 20];59(3):299–309. Available from: https://www.tandfonline.com/doi/abs/10.1080/00253359.1973.10657911

5. Solar PM, Rönnbäck K. Copper sheathing and the British slave trade. *Economic History Review*. 2015;68(3):806–29.

6. Harris JR. Copper and Shipping in the Eighteenth Century. *Economic History Review* [Internet]. 1966 Dec [cited 2020 Jun 20];19(3):550–68. Available from: http://doi.wiley.com/10.1111/j.1468-0289.1966.tb00988.x

7. Harris JR. *Industrial Espionage and Technology Transfer: Britain and France in the Eighteenth Century*. New York, NY: Routledge, Taylor & Francis Group; 1998. Available

from: https://www.google.com.mx/books/edition/Industrial_Espionage_and_Technology_Tran/6zorDwAAQBAJ?hl=es&gbpv=0~~https://books.google.com.mx~~

8. Ciarlo N. Industrialization, Warfare, and Science: An archaeological-historical insight into technological changes of mid-18th to early 19th-century European naval ships. *International Journal of Nautical Archaeology*. Forthcoming 2023;

9. Barba-Meinecke H. *Naufragios en el Seno Mexicano: El pecio Ancla Macuca, Yucatán, Golfo de México* [Master's Thesis]. Cádiz, España: Universidad de Cádiz, EIDEMAR, CEIMAR; 2019.

10. Arano Recio DE. *Historia y metalurgia de los revestimientos metálicos en embarcaciones de propulsión a vela de la España peninsular y americana circa 1780-1820* [Internet] [Doctoral Dissertation]. Cádiz, España: Universidad de Cádiz; 2023 [cited 2024 Apr 6]. Available from: https://rodin.uca.es/handle/10498/31641

11. Arano Recio D, González-Sánchez J, Bethencourt M, Ciarlo N. Metalurgia de revestimientos y sistemas de sujeción en embarcaciones de madera y propulsión a vela. El caso de tres naufragios localizados en la Sonda de Campeche, México. *In:* XIII Congreso Ibérico de Arqueometría; 2019.

12. Arano Recio D, Barba-Meinecke H, Bethencourt Núñez M, Ciarlo N, Carrasco González G. The metal sheathing and fastenings of wooden ships. Archaeometallurgical study of Carron, Ancla Macuca, HMS Forth and El Pesquero sites located at the Gulf of Mexico (late 18th to mid-19th Centuries). *In:* 43rd International Symposium on Archaeometry; 2022. Lisboa, Portugal.

13. Arano Recio D, Barba-Meinecke H, Bethencourt Núñez M, Ciarlo N, Carrasco González G. Un acercamiento a la problemática del palimpsesto en naufragios: estudio de dos contextos arqueológicos subacuáticos en el arrecife Alacranes, México. *In:* Cerezo Andreo F, Pérez-Reverte Mañas C, editors. I Congreso Iberoamericano de Arqueología Náutica y Subacuática (CIANYS

2021). Cádiz, España: Universidad de Cádiz, Campus de Excelencia Internacional del Mar; 2022. p. 330–3.

14. Barba-Meinecke H, Junco R, Trujeque JR. El tesoro de Alacranes: estudio multidisciplinario del precio Ancla Macuca, Yucatán. *Arqueología Mexicana*. 2020;28(164):58–63.

15. Barba-Meinecke H, Junco Sánchez R, Reyes Trujeque J, Silva León I, Espinosa Morales Y, Domínguez-Bella S, et al. El tesoro de Alacranes. Estudio multidisciplinario del naufragio Ancla Macuca, Yucatán, Golfo de México. Primeros acercamientos. *In:* Elkin D, Delaere C, editors. Entre a tierra y el agua: El patrimonio subacuático costero en América Latina. Gainesville, FL: University Press of Florida; 2023.

16. Barba-Meinecke H, Chávez AP. Los pecios RMS Tweed y RMS Forth: historia y análisis arqueológico de dos naufragios identificados en el Parque Nacional Arrecife Alacranes, Yucatán. *Glifos*. 2019;(22):12–23.

17. Barba-Meinecke H. Arqueología Subacuática en la costa de Campeche. El caso del pecio "El Pesquero, Champotón" Primeros acercamientos en torno a su investigación. *In:* XVII Encuentro Los Investigadores de la Cultura Maya; 2007. Campeche, México: Universidad Autónoma de Campeche.

18. Barba-Meinecke H. Arqueología subacuática en la costa de Campeche: Pecio El Pesquero. Primeros acercamientos en torno a su investigación. *In:* XVI Simposio Román Piña Chán; 2011, Museo Nacional de Antropología, INAH. CDMX, México.

19. Scott DA. *Metallography and Microstructure in Ancient and Historic Metals.* Los Ángeles, CA: Getty Publications;1992.

20. Bram M, Iddan N, Ashkenazi D, Cvikel D. The Nineteenth-Century Molyneux's Boat: Archaeometallurgical Perspective of its Metal Fastenings. *Metallography, Microstructure, and Analysis.* 2020;9(5):721–43.

21. Cohen M, Ashkenazi D, Kahanov Y, Stern A, Klein S, Cvikel D. The Brass Nails of the Akko Tower Wreck (Israel): Archaeometallurgical Analyses. *Metallography, Microstructure, and Analysis.* 2015 Jun 24;4(3):188–206.

22. Ashkenazi D, Cvikel D, Stern A, Klein S, Kahanov Y. Metallurgical Characterization of Brass Objects from the Akko 1 Shipwreck, Israel. *Materials Characterization* [Internet]. 2014 Jun 1 [cited 2020 Sep 27];92:49–63. Available from: https://www.sciencedirect.com/science/article/abs/pii/S1044580314000667

23. Ashkenazi D, Cvikel D, Iddan N, Mentovich E, Kahanov Y, Levinshtein M. Archaeometallurgical Study of the Brass Cases from the Akko 1 Shipwreck. *Journal of Archaeological Science* [Internet]. 2011 Sep 1 [cited 2020 Sep 27];38(9):2410–9. Available from: https://www.sciencedirect.com/science/article/abs/pii/S0305440311001579

24. Ashkenazi D, Inberg A, Cvikel D. Analysis of Naturally Etched Surface of Brass Sheathing from a Nineteenth-Century Shipwreck. *Journal of Mining and Metallurgy, Section B: Metallurgy.* 2018.

25. Bingeman JM. Copper and Muntz Metal Sheathing: A Global Update. *International Journal of Nautical Archaeology.*2018;47(2):460–71.

26. Zuccolotto Villalobos AR. *Las Láminas de Muntz del Pecio "El Ángel": Un Caso de Navegación Comercial en el Caribe Durante el Siglo XIX*,.- Master's Thesis, ~~Zamora, México~~:Available from El Colegio de Michoacán, Centro de Estudios Arqueológicos, México; Thesis completed December, 2020.

27. Quintero González J. La Introducción de los Forros de Cobre en el Sur. *In:* La Economía Marítima en España y las Indias: 16 Estudios. San Fernando, Cádiz, España; 2015. p. 255–80.

28. Rees G. Copper Sheathing: An Example of Technological Diffusion in the English Merchant Fleet. *The Journal of Transport History* [Internet]. 1971 Sep 25;ss-1(2):85–94. Available from: http://journals.sagepub.com/doi/10.1177/002252667100100202

29. Staniforth M. The Introduction and Use of Copper Sheathing: A History. *Bulletin of the Australian Institute for Maritime Archaeology*. 1985;9(1/2):21.

30. Viduka A, Ness S. Analysis of Some Copper-Alloy Items from HMAV *Bounty* Wrecked at Pitcairn Island in 1790. *In:*Proceedings of Metal 2004, National Museum of Australia Canberra ACT. Canberra, Australia: National Museum of Australia; 2004 [cited 2020 Sep 30]. p. 160–72. Available from: www.nma.gov.au

31. Oliver Laso JJ, Ramírez Pernía A. "Bernardino de Texeda Me Fecit": Artillería Virreinal del Perú a Finales del Siglo XVI. *Gladius.* 2021 Jul 20;41:153–76.


Fig. 1. Map depicting the locations of the Ancla Macuca, RMS Forth (1849), Carron, and El Pesquero shipwrecks. Also shown are the position of Campeche Sound in the southeastern region of Mexico, along with the locations of PNAA, Cayo Nuevo, and the Campeche Coast. ©SAS-YUC Archive, INAH (2023). Credit: Ma. Fernanda Ramírez Islas.

296x209mm (300 x 300 DPI)

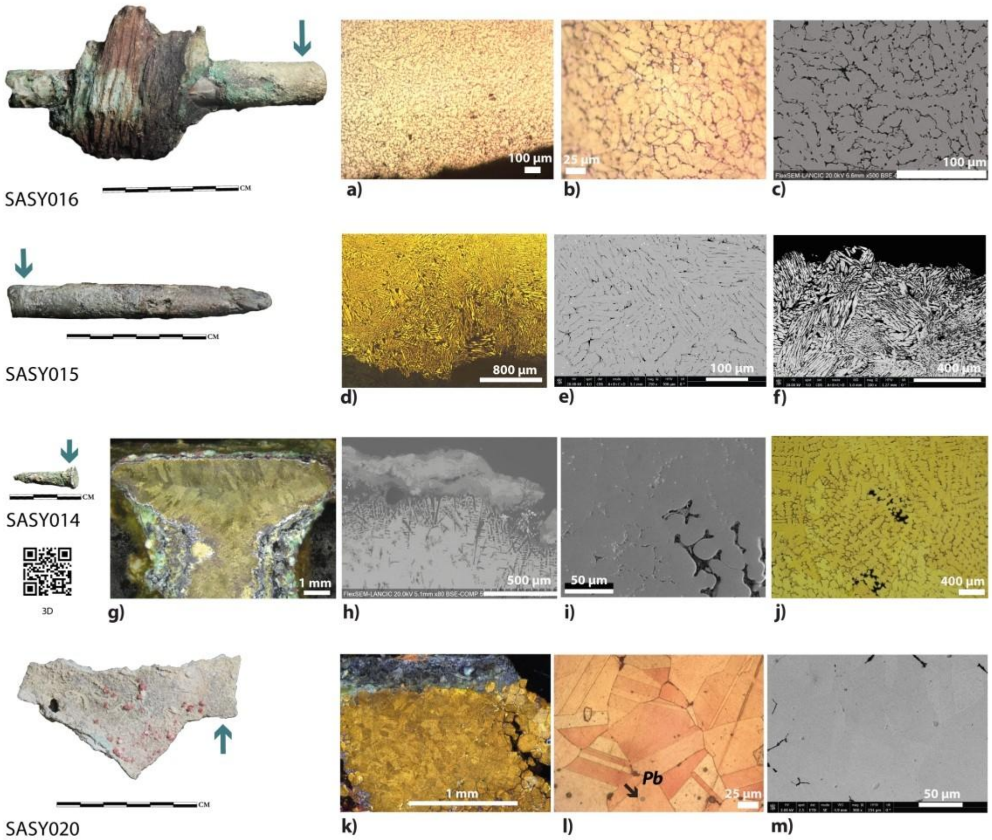


Fig. 2 Carron site. The image shows bolts SASY015 and SASY016, sheathing tack SASY014, and sheet SASY020, along with the photomicrographs displaying their microstructure (LM and SEM). The arrow indicates the sample area. (a–c) Cross-sections: (a) Partially recrystallised structure with a high degree of dezincification, etched; (b, c) Higher magnification views. (d, e, f) Cross-section and edge portion (LM without etching and SEM), showing a Widmanstätten-type grain structure. (g–j) Cross-section of the head: (g, j) LM, showing α and β phases in the dendritic microstructure, etched; (g) arrows indicates the presence of two phases; (h, i) SEM, with (i) showing a higher magnification of the interdendritic space. (k–m) Equiaxed grains with recrystallisation twins: (k, l) LM, Etching: hydroalcoholic ferric chloride; (m) SEM.

534x473mm (118 x 118 DPI)

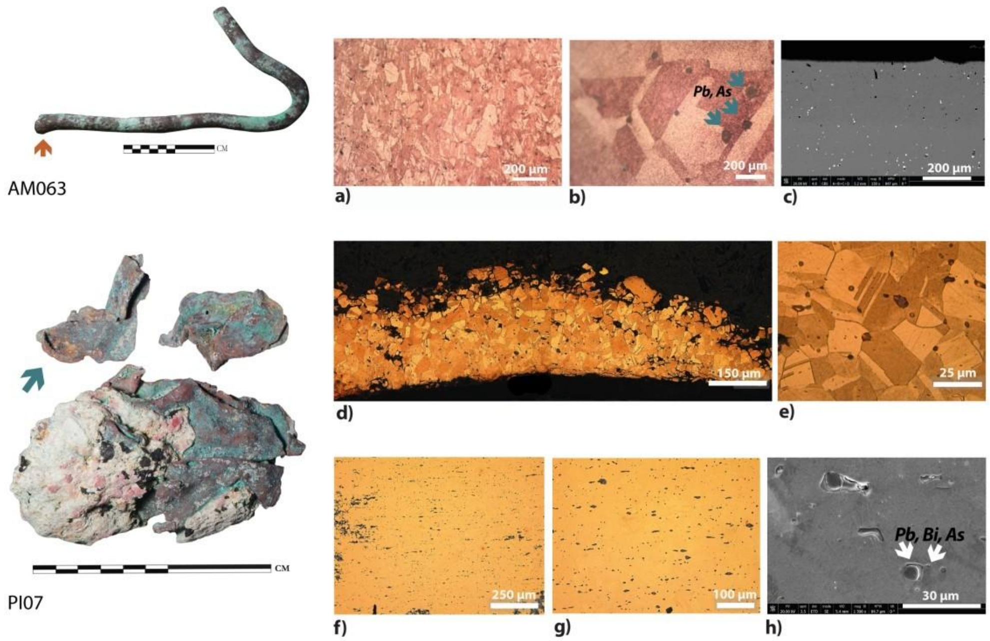


Fig. 3 Ancla Macuca site. Equiaxed grains of unalloyed copper of bolt AM063: (a) Longitudinal section (LS), viewed under LM, etched; (b) Cross-sections (CS), viewed under LM, etched; (c) CS, SEM. Unalloyed sheathing sheet PI07: (d, e) CS under LM, etched. (f, g) Metallic inclusion (Pb, As, Bi) elongated following the manufacturing direction, longitudinal section (LS), non-etched. (h) SEM view. Etching: hydroalcoholic ferric chloride. The arrow indicates the sample area.

534x365mm (118 x 118 DPI)

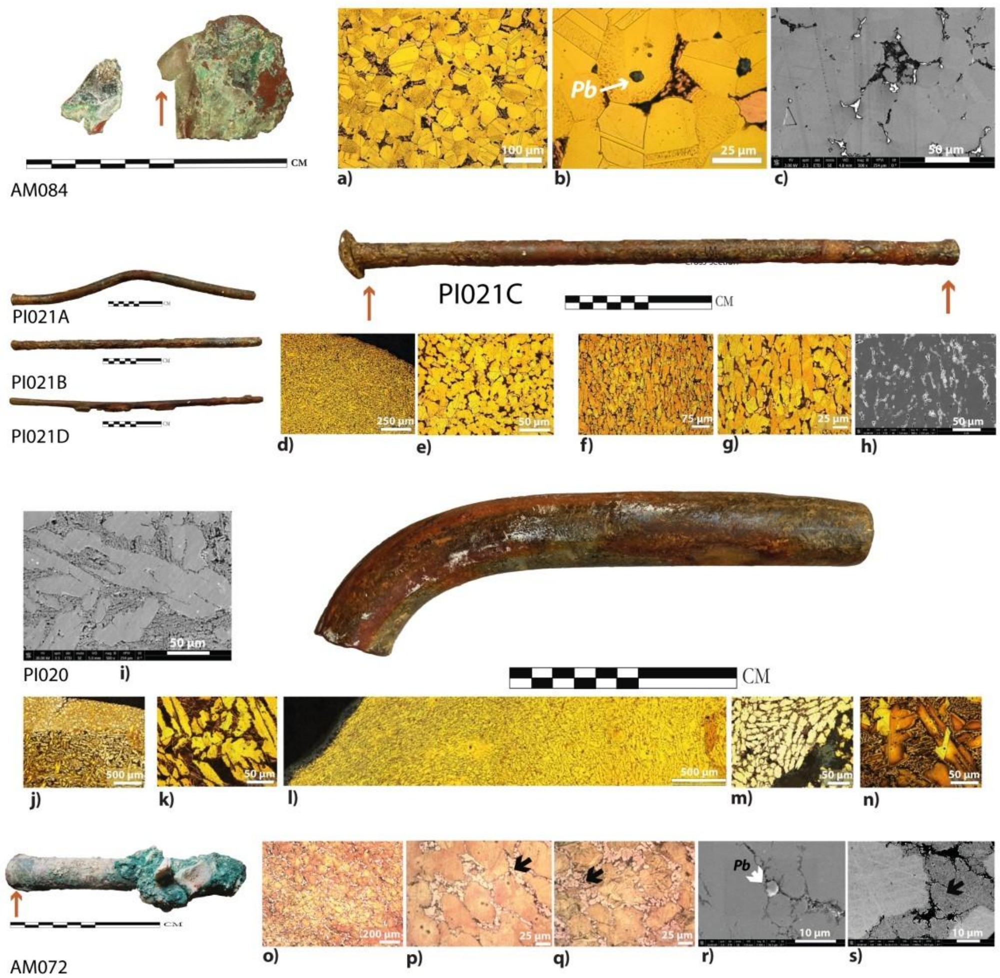


Fig. 4 RMS Forth (1849) site. Equiaxed grains of brass in sheathing sheet AM084: (a, b) Cross-sections (CS) under LM, etched; (c) SEM image. Brass bolt PI021C: (d, e) CS under LM, etched; (f, g, h) Longitudinal section (LS) showing elongated grains; (f, g) LM, etched; (h) SEM, non-etched. Brass bolt PI020: (i) CS, SEM view; (j, k) CS, LM, etched; (l, m, n) LS, LM, etched. Brass bolt AM072 (black arrow indicates dezincification area): (o) LS, LM, etched, showing elongated grains; (p) higher magnification center; (q) same magnification border; (r) SEM showing Pb inclusions at grain boundaries; (s) SEM showing higher magnification of the dezincification process. Etching: hydroalcoholic ferric chloride. The arrow indicates the sample area.

548x581mm (118 x 118 DPI)

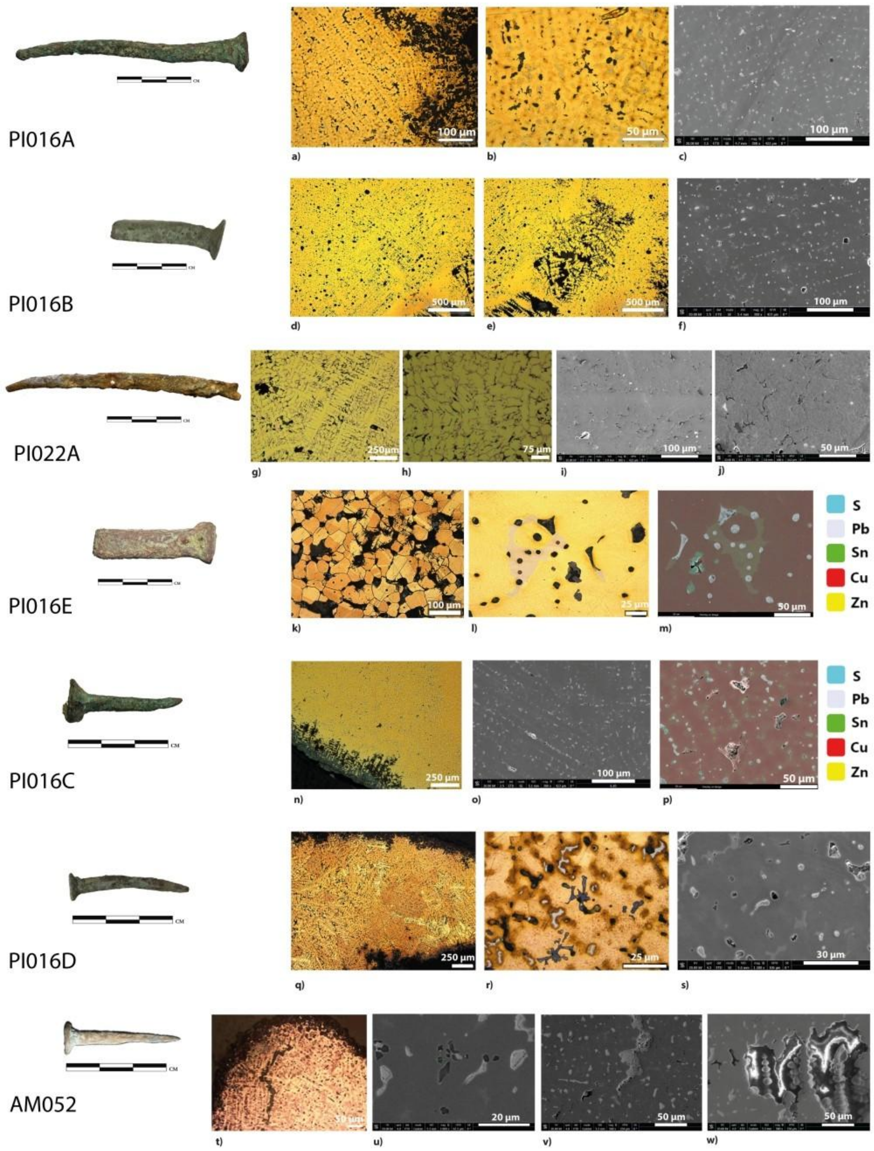


Fig. 5 RMS Forth (1849) site. Nails (PI016 A, B, E, PI022A) and sheathing tack (PI016 C, D, AM052). PI016A: (a, b) Cross-sections (CS) viewed under LM, etched; (c) CS under SEM, non-etched. PI016B: (d, e) CS under LM, etched; (f) CS under SEM, non-etched. PI022A: (g) CS under LM, non-etched; (h) Longitudinal section (LS) under LM, non-etched; (i) LS under SEM, non-etched; (j) CS under SEM, non-etched. Partially recrystallised grains of nail PI016E: (k, l) CS under LM; (k) etched; (l) higher magnification, non-etched; (m) SEM, non-etched, same area as (l), EDS map. PI016C: (n) CS under LM, non-etched; (o) CS under SEM, non-etched; (p) CS, higher magnification under SEM, EDS map. PI016D: (q) CS under LM, etched; (r) CS under LM, etched, higher magnification; (s) CS under SEM, non-etched. AM052: (t) CS under LM, etched; (u) CS under SEM, non-etched; (v) CS under SEM, non-etched, micro-shrinkage filled with Pb; (w) CS under SEM, non-etched, dendrites in micro-shrinkage space. Etching: hydroalcoholic ferric chloride.

534x731mm (118 x 118 DPI)

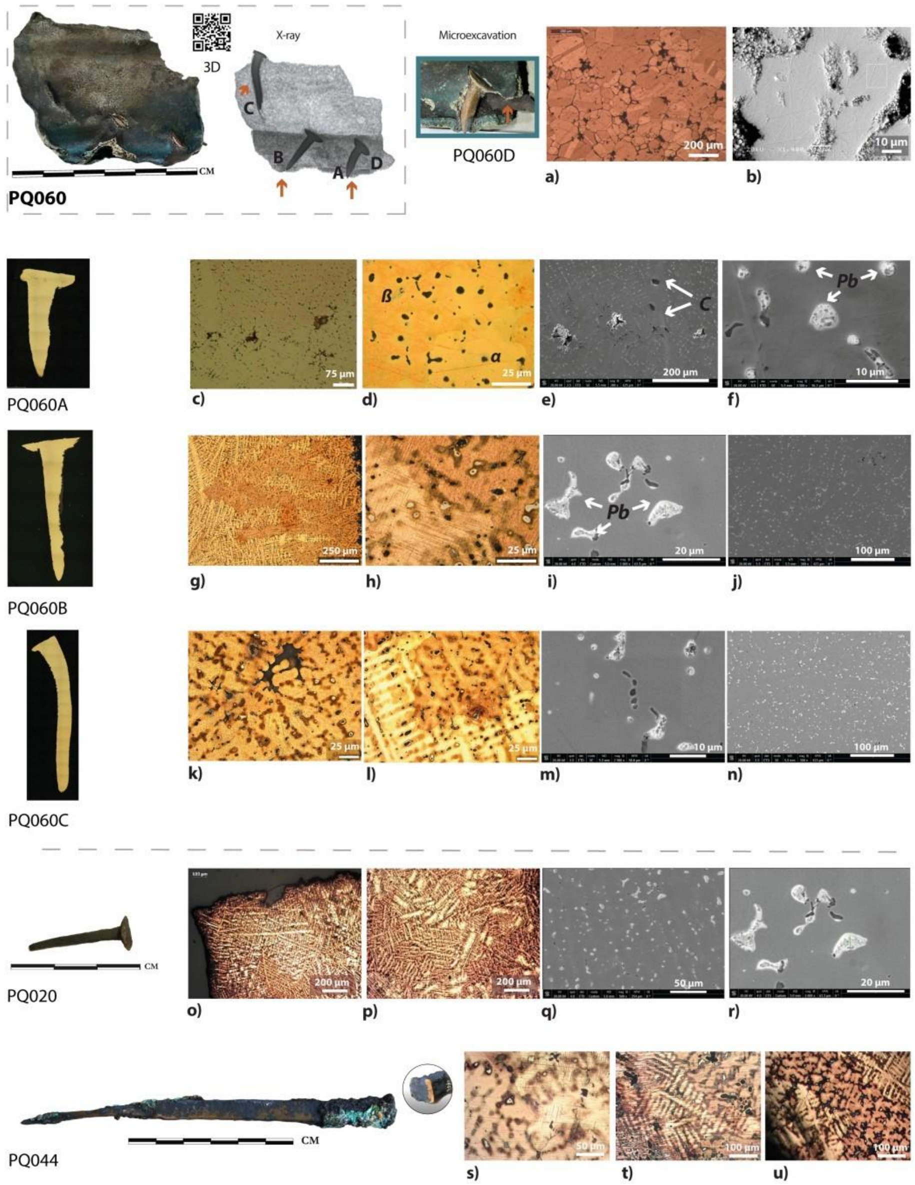


Fig. 6 El Pesquero site. Unalloyed copper sheathing sheet PQ060D: (a) Cross-sections (CS) viewed under LM, etched; (b) CS under SEM, non-etched. Tacks composed of quaternary bronze exhibit a dendritic microstructure: PQ060A, B, C, and PQ020. PQ060A: (c, d) CS under LM, non-etched; (e, f) CS under SEM, non-etched, showing non-metallic and metallic inclusions. PQ060B: (g, h) CS under LM, etched; (i, j) CS under SEM, non-etched, showing Pb segregates. PQ060C: (k, l) CS under LM, etched; (m, n) CS under SEM, non-etched, showing non-metallic and metallic segregates. PQ020: (o, p) CS under LM, etched; (q, r) CS under SEM, non-etched, showing non-metallic and metallic segregates. Square nail of quaternary bronze PQ044: (s, t, u) CS under LM, etched. Etching: hydroalcoholic ferric chloride.

548x710mm (118 x 118 DPI)

Fig. 1. Map depicting the locations of the Ancla Macuca, RMS Forth (1849), Carron, and El Pesquero shipwrecks. Also shown are the position of Campeche Sound in the southeastern region of Mexico, along with the locations of PNAA, Cayo Nuevo, and the Campeche Coast. ©SAS-YUC Archive, INAH (2023). Credit: Ma. Fernanda Ramírez Islas.

Fig. 2 Carron site. The image shows bolts SASY015 and SASY016, sheathing tack SASY014, and sheet SASY020, along with the photomicrographs displaying their microstructure (LM and SEM). The arrow indicates the sample area. (a–c) Cross-sections: (a) Partially recrystallised structure with a high degree of dezincification, etched; (b, c) Higher magnification views. (d, e, f) Cross-section and edge portion (LM without etching and SEM), showing a Widmanstätten-type grain structure. (g–j) Cross-section of the head: (g, j) LM, showing α and β phases in the dendritic microstructure, etched; (g) arrows indicates the presence of two phases; (h, i) SEM, with (i) showing a higher magnification of the interdendritic space. (k–m) Equiaxed grains with recrystallisation twins: (k, l) LM, Etching: hydroalcoholic ferric chloride; (m) SEM.

Fig. 3 Ancla Macuca site. Equiaxed grains of unalloyed copper of bolt AM063: (a) Longitudinal section (LS), viewed under LM, etched ; (b) Cross-sections (CS), viewed under LM, etched; (c) CS, SEM. Unalloyed sheathing sheet PI07: (d, e) CS under LM, etched. (f, g) Metallic inclusion (Pb, As, Bi) elongated following the manufacturing direction, longitudinal section (LS), non-etched. (h) SEM view. Etching: hydroalcoholic ferric chloride. The arrow indicates the sample area.

Fig. 4 RMS *Forth* (1849) site. Equiaxed grains of brass in sheathing sheet AM084: (a, b) Cross-sections (CS) under LM, etched; (c) SEM image. Brass bolt PI021C: (d, e) CS under LM, etched; (f, g, h) Longitudinal section (LS) showing elongated grains; (f, g) LM, etched; (h) SEM, non-etched. Brass bolt PI020: (i) CS, SEM view; (j, k) CS, LM, etched; (l, m, n) LS, LM, etched. Brass bolt AM072 (black arrow indicates dezincification area): (o) LS, LM, etched, showing elongated grains; (p) higher magnification center; (q) same magnification border; (r) SEM showing Pb inclusions at grain boundaries; (s) SEM showing higher magnification of the dezincification process. Etching: hydroalcoholic ferric chloride. The arrow indicates the sample area.

Fig. 5 RMS *Forth* (1849) site. Nails (PI016 A, B, E, PI022A) and sheathing tack (PI016 C, D, AM052). PI016A: (a, b) Cross-sections (CS) viewed under LM, etched; (c) CS under SEM, non-etched. PI016B: (d, e) CS under LM, etched; (f) CS under SEM, non-etched. PI022A: (g) CS under LM, non-etched; (h) Longitudinal section (LS) under LM, non-etched; (i) LS under SEM, non-etched; (j) CS under SEM, non-etched. Partially recrystallised grains of nail PI016E: (k, l) CS under LM; (k) etched; (l) higher magnification, non-etched; (m) SEM, non-etched, same area as (l), EDS map. PI016C: (n) CS under LM, non-etched; (o) CS under SEM, non-etched; (p) CS, higher magnification under SEM, EDS map. PI016D: (q) CS under LM, etched; (r) CS under LM, etched, higher magnification; (s) CS under SEM, non-etched. AM052: (t) CS under LM, etched; (u) CS under SEM, non-etched; (v) CS under SEM, non-etched, micro-shrinkage filled with Pb; (w) CS under SEM, non-etched, dendrites in micro-shrinkage space. Etching: hydroalcoholic ferric chloride.

Fig. 6 El Pesquero site. Unalloyed copper sheathing sheet PQ060D: (a) Cross-sections (CS) viewed under LM, etched; (b) CS under SEM, non-etched. Tacks composed of quaternary bronze exhibit a dendritic microstructure: PQ060A, B, C, and PQ020. PQ060A: (c, d) CS under LM, non-etched; (e, f) CS under SEM, non-etched, showing non-metallic and metallic inclusions. PQ060B: (g, h) CS under LM, etched; (i, j) CS under SEM, non-etched, showing Pb segregates. PQ060C: (k, l) CS under LM, etched; (m, n) CS under SEM, non-etched, showing non-metallic and metallic segregates. PQ020: (o, p) CS under LM, etched; (q, r) CS under SEM, non-etched, showing non-metallic and metallic segregates. Square nail of quaternary bronze PQ044: (s, t, u) CS under LM, etched. Etching: hydroalcoholic ferric chloride.

# Seminarios de la Sociedad Española de Mineralogía

16

## XLI Reunión científica de la Sociedad Española de Mineralogía (SEM) y XXVII Reunión científica de la Sociedad Española de Arcillas (SEA)


Editores: Mª Pilar Ortiz Calderón
Adolfo Miras Ruiz

SEM SEA Sevilla 2025

Seminarios de la Sociedad Española de Mineralogía

Volumen 16

# “Caracterización y Diagnóstico del Patrimonio Cultural”

Seminario celebrado en Sevilla,
15 de enero de 2025

Editores: Mª Pilar Ortiz Calderón y Adolfo Miras Ruiz

## Foto de portada

Paño de representación de Sevilla en la Plaza de España. Se muestra la **Feria de Abril** en la década de los años veinte. Aparece la faceta más ganadera de la celebración, con una serie de personajes vestidos a la manera tradicional, rodeados del ganado y con la catedral y la Giralda de fondo.

Seminarios de la Sociedad Española
de mineralogía


Museo Geominero del Instituto Geológico
y Minero de España
Ríos Rosas, 23
28003 Madrid

Editores
Mª Pilar Ortiz Calderón y Adolfo Miras Ruiz

Diseño y maquetación
Adolfo Miras Ruiz

ISSN
2659-9872

2025

# Foreword / Prólogo

La **Mineralogía Aplicada al estudio del Patrimonio Histórico** se inicia en España con trabajos como los del **Prof. Emilio Galán** en edificios emblemáticos como la Alhambra de Granada, la Catedral de Málaga, el Ayuntamiento y la Torre del Oro de Sevilla, la Catedral de Cádiz, en los que el objetivo era la caracterización de rocas y morteros, el estudio de sus patologías y los agentes de alteración, la evaluación de tratamientos de restauración y su eficacia, o la puesta a punto de técnicas no destructivas como la termografía o la propagación de ultrasonidos. Desde entonces este campo de la mineralogía se ha extendido a muchas otras materialidades propias de las obras de arte, como son los vidrios, metales, pintura mural y de caballete, la policromía sobre madera, la cerámica, los huesos, …, abarcando piezas desde la prehistoria hasta el arte contemporáneo.

El conocimiento exhaustivo de estratos pictóricos, vidrios, metales, cerámicas, … permite conocer la obra del artista y ahondar en la tecnología de la época así como en el estudio de las rutas comerciales o en el desarrollo local de la artesanía, por otra parte, las modificaciones que han sufrido esos materiales en función del ambiente en el que ha discurrido su vida, en grandes ciudades, ambientes costeros, en montaña, enterrados o sumergidos, define las formas de alteración que dependen de su composición química y mineralógica, su textura y estructura, y de las labores de corte, pulido, tallado y finalizado de obra.

Los efectos ambientales como la contaminación atmosférica, la lluvia, la temperatura, el viento, …dañan patrimonio tan diverso, como cuevas y abrigos rupestres, conjuntos arqueológicos, monumentos, museos, jardines históricos, archivos, bibliotecas, templos, …, lo que ha llevado a los expertos de mineralogía aplicada al diagnóstico a investigar la evolución para conservar y salvaguardar el patrimonio cultural material e inmaterial de una forma efectiva.

Por ello, en este curso organizado por la Sociedad Española de Mineralogía y la Sociedad Española de Arcillas, diversos autores reflexionan sobre la caracterización de diversos materiales desde pigmentos, vidrios, aleaciones, rocas o cerámicas, desvelándonos como se han usado a lo largo de la historia, las técnicas que se están empleando para su caracterización con o sin toma de muestra y los procesos de alteración que pueden sufrir.

Desde el Comité Organizador queremos agradecer el esfuerzo y dedicación para difundir el conocimiento en Mineralogía Aplicada al Patrimonio Cultural a los ponentes y autores de este libro, sin olvidarnos de maestros como el Prof. Emilio Galán, pionero en España en esta rama de la Mineralogía.

Pilar Ortiz

Catedrática de Cristalografía y Mineralogía

Universidad Pablo de Olavide de Sevilla

Comité Organizador de la XLI Reunión Científica de la SEM y XXVII Reunión Científica de la SEA

# Index / Índice

# Arqueología subacuática: casos de estudio

**Manuel Bethencourt Núñez (1), Nicolás C. Ciarlo (2)**

(1) Departamento de Ciencia de los Materiales e Ingeniería Metalúrgica y Química Inorgánica. Universidad de Cádiz. Laboratorio de Estudios y Conservación del Patrimonio Histórico. Ed. CASEM, Campus de Puerto Real, 11510, Puerto Real (España)
(2) Consejo Nacional de Investigaciones Científicas y Técnicas (CONICET) – Instituto de Arqueología, Facultad de Filosofía y Letras, Universidad de Buenos Aires. 25 de Mayo 221, 3er piso (C1002ABE), Ciudad Autónoma de Buenos Aires (Argentina)

## *Abstract*

This article summarizes a selection of the works of characterization, diagnosis and safeguarding of underwater cultural heritage (UCH) of metallic nature in which the University of Cadiz, through the Laboratory of Studies and Conservation of Historical Heritage (LEC-PH), has participated. This activity has been divided into three lines of action: the characterization of metallic materials belonging to the UCH, the proposal of stabilization measures against corrosion processes, and the implementation of in situ conservation actions following the UNESCO's guidelines. The cases presented are the result of the collaboration between the University of Cadiz and other research centers and companies, with the university leading the work in some cases and participating in it in others. These cases are among those that will be presented at the seminar on the Characterization and Diagnosis of Cultural Heritage in SEM-SEA 2025.

## *Resumen*

En este artículo se resume una selección de los trabajos de caracterización, diagnóstico y salvaguarda del patrimonio cultural sumergido (PCS) de naturaleza metálica en los que la Universidad de Cádiz, a través de Laboratorio de Estudios y Conservación del Patrimonio Histórico (LEC-PH), ha participado. Esta actividad se ha dividido en tres líneas de actuación: la caracterización de materiales metálicos pertenecientes al PCS, la propuesta de medidas para su estabilización frente a los procesos de corrosión, y la implementación de acciones de conservación *in situ* siguiendo las recomendaciones de la UNESCO. Los casos presentados son el resultado de la colaboración de la Universidad de Cádiz con otros centros de investigación y empresas, en algunos casos liderando el trabajo y en otros participando en los mismos. Estos forman parte de algunos de los ejemplos que se presentarán en el seminario Caracterización y Diagnóstico del Patrimonio Cultural del SEM-SEA 2025.

*Palabras clave:* patrimonio cultural sumergido, caracterización, diagnóstico, salvaguarda, metales.

## 1. Introducción

El litoral de la provincia de Cádiz, con más de 280 km de extensión y bañado por dos mares, cuenta en sus fondos con un patrimonio cultural sumergido (PCS) de excepcional valor. Pecios, puertos, fondeaderos, etc., son testimonios materiales de las relaciones históricas mantenidas con y por el mar por las sociedades establecidas en el entorno del Estrecho de Gibraltar a lo largo de milenios.

La comprensión y conservación de este PCS es crucial, por tratarse de un bien inmaterial que aporta respuestas de nuestro pasado y posee un destacado valor desde el punto de vista histórico, estético y antropológico. Por otra parte, el PCS debe desempeñar un papel clave en el desarrollo sostenible como motor económico, tal y como ha sido reconocido por la Unión Europea (UE), la Organización de las Naciones Unidas para la Educación, la Ciencia y la Cultura (UNESCO) o el Consejo Internacional de Monumentos y Sitios (ICOMOS). En este sentido, entre los objetivos estratégicos de los programas económicos, el turismo, el ocio y otras actividades culturales han sido identificados como una de las grandes prioridades y oportunidades para España y Europa.

En este escenario, el Grupo del Plan Andaluz de I+D+I "Corrosión y Protección- TEP-231" de la Universidad de Cádiz (UCA), inició en el año 2004 una línea de investigación en arqueometalurgia, con el objetivo de estudiar materiales arqueológicos subacuáticos de origen metálico y proponer tratamientos de conservación y análisis de los mismos. Con el transcurso de los años y gracias a la experiencia acumulada, esta línea se transformó en el Laboratorio de Estudios y Conservación del Patrimonio Histórico de la UCA, cuya misión es ofrecer a los investigadores y profesionales pertenecientes a esta universidad y a otras instituciones de investigación y empresas, una serie de servicios que comprenden desde la realización de estudios y análisis del patrimonio hasta la ejecución de proyectos de conservación y restauración del material cultural, histórico y arqueológico. De este modo, ha contribuido a consolidar el área de especialización de "El Valor Cultural del Mar" del Campus de Excelencia Internacional del Mar (CEIMAR).

En este documento se resume una selección de los trabajos realizados y publicados a lo largo de estos años, y, si se dio el caso, relacionarlos con las "Normas relativas a las actividades dirigidas al patrimonio cultural subacuático", recogidas en el Anexo de la Convención sobre la Protección del Patrimonio Cultural Subacuático de la UNESCO, firmado en París el 2 de noviembre de 2001 y ratificado por España en 2005. Estos trabajos se encuentran debidamente citados para su posterior consulta por aquellos lectores que puedan estar interesados.

## 2. La conservación in situ como principio básico

El Anexo de la referida convención de la UNESCO (2001) inicia su andadura en la **Norma 1**, indicando que "La conservación in situ será considerada la opción prioritaria para proteger el patrimonio cultural subacuático". Y en el caso de que sea necesario intervenir, la **Norma 3** expresa que "las actividades dirigidas al patrimonio cultural subacuático no deberán perjudicar más de lo necesario para los objetivos del proyecto". Sobre esta idea se incide en la **Norma 4** que indica que "las actividades dirigidas al patrimonio cultural subacuático deberán servirse de técnicas y métodos de exploración no destructivos, que deberán preferirse a la recuperación de objetos".

Esta nueva estrategia de protección del PCS obliga necesariamente a entender cómo afectan los distintos agentes, físicos, químicos y biológicos, a la preservación de los restos en el medio acuático (sobre todo, marino) y, en su caso, proponer medidas que ralenticen el deterioro de los mismos. En la **Norma 15** de este mismo anexo se indica que la evaluación preliminar de la importancia de un determinado patrimonio cultural subacuático, del entorno que lo rodea y de su vulnerabilidad "incluirá además estudios previos de los datos históricos y arqueológicos disponibles, las características arqueológicas y ambientales del sitio y las consecuencias de cualquier posible intrusión en la estabilidad a largo plazo del patrimonio cultural subacuático objeto de las actividades".

Siguiendo estos preceptos, investigadores de la UCA (Bethencourt et al., 2018) estudiaron la artillería de dos pecios vinculados a la Batalla de Trafalgar (1805), en el marco del proyecto ARQUEOMONITOR (2010) aplicando un enfoque holístico e interdisciplinar basado en el desarrollo de estas cuatro de las treinta y seis normas de la referida Convención. Por un lado, se desarrolló una técnica de prospección no destructiva para obtener información de los cañones y anclas dispersos en el fondo marino sin alterar su estado (**Norma 4**). Se trataba de un sistema combinado de desconcreción, documentación y control de la corrosión como alternativa para una documentación «suficiente» in situ y con una mínima alteración del objeto (**Norma 3**). Este sistema se basa en los trabajos descritos por MacLeod (1995, 2002) y Gregory (1995), y patentado en Bethencourt et al. (2005), tal como se aprecia en la Figura 1.

Tras el acceso a las zonas de interés documental, eliminando de forma selectiva la concreción, se procedía al registro del sector expuestos de la pieza. Para reposicionar el hierro en la zona de pasividad en el diagrama de Pourbaix empleamos un recubrimiento que aísla el metal del medio agresivo. Este mecanismo, denominado efecto barrera, se basa en la protección del objeto mediante el aislamiento eléctrico que se produce al interponer una película sólida y continua entre el metal y el medio corrosivo, en este caso una resina epoxi de dos componentes.

Los trabajos realizados proporcionaron información sobre las marcas de fábrica, que a su vez brindaron indicios sobre ambos pecios, el Fougueux y el Bucentaure, dos navíos de línea de la Marina de Guerra francesa. Asimismo, mediante el procedimiento aplicado fuer posible caracterizar el estado de conservación pieza sin poner en peligro su futura preservación en el medio marino. Además, las mediciones de las principales variables físicas, químicas y biológicas que interaccionan con las piezas permitieron correlacionar el estado de conservación en cada sitio con las condiciones del medio marino (**Norma 15**). Así, mediante la técnica propuesta fue posible obtener información sobre las capas de concreción en cañones de hierro (de las que hablaremos con más detalle en el siguiente apartado) localizados en ambos yacimientos, y relacionar algunas diferencias en su estado de conservación con la situación que ocupaban en el lecho marino (sustrato arenoso-rocoso, grado de enterramiento, etc).

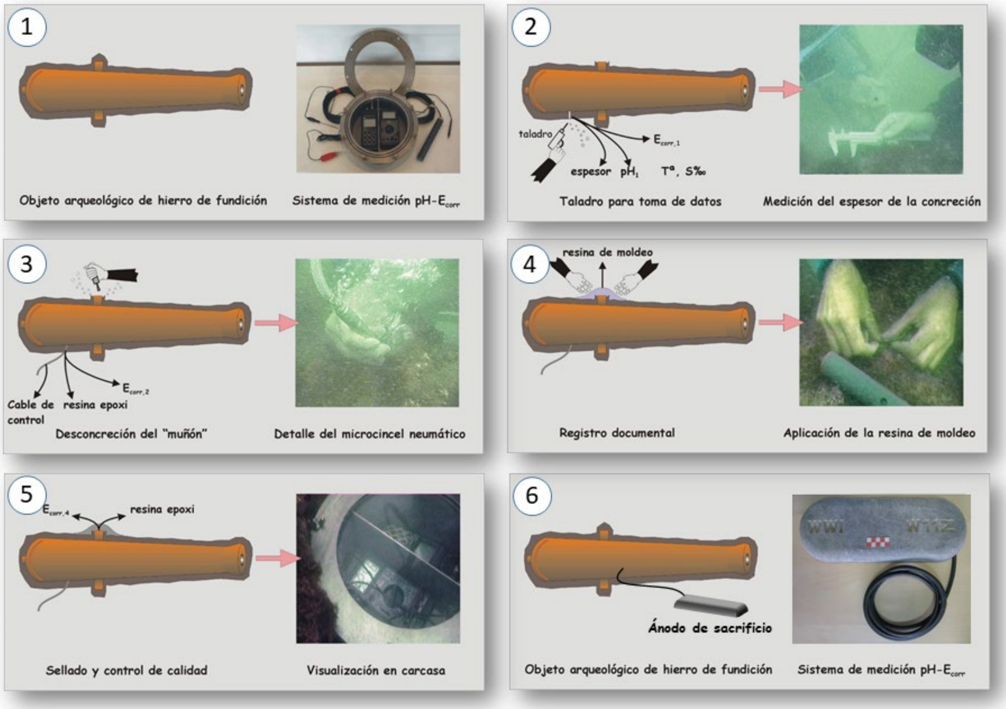


**Fig. 1.** *Etapa 1 a 5: pasos seguidos en la desconcreción parcial controlada y posterior protección de zonas de interés documental en un cañón. Etapa 6: protección mediante ánodo de sacrificio (adaptado de Bethencourt et al., 2005).*

A pesar de la proximidad espacial de los dos yacimientos, que son de la misma época, existen diferencias en el estado de conservación de los restos asociados. Se ha observado que las concreciones biológicas asociadas a los 18 cañones estudiados en el *Fougueux* son diferentes a las de los 16 examinados en el *Bucentaure*. Frente a la capa de concreción calcárea de los cañones de *Fougueux*, uniforme y delgada (de unos 5 mm de espesor medio), los cañones del *Bucentaure* presentan una capa de concreción más gruesa, de hasta 30 mm de espesor. Además, se midió el pH en el interior de las concreciones y el potencial de corrosión ($E_{corr}$) asociado a cada uno de los cañones estudiados. Con estos datos se pudieron establecer las ecuaciones de velocidades de corrosión para cada yacimiento siguiendo la propuesta de MacLeod (1995):

$$\text{Log}\,(V_{corr}) = M \cdot E_{corr} + C \qquad \text{(Ecuación 1)}$$

Así, en el pecio de *Fougueux*, pudo determinarse que los grandes objetos de hierro se están corroyendo a un ritmo más elevado (entre 0,180 y 0,246 mmpy) debido a la elevada removilización y transporte de sedimentos inducidos por el oleaje, causando daños por efecto mecánico directo sobre el material metálico y por la eliminación de la capa de productos de corrosión desarrollada sobre los artefactos. Por otro lado, la artillería del *Bucentaure*, cubierta por gruesas capas de concreción biológica, está bien conservada, con índices de corrosión más bajos (de 0,073 a 0,126 mmpy). Por último, se evaluó la eficacia de la protección catódica como medida temporal de conservación *in situ* (**Norma 1**) en un cañón del *Bucentaure*. Finalmente, el empleo de un ánodo de sacrificio (Figura 1.6) durante 9 meses redujo la velocidad media de corrosión de uno de los cañones de 0,103 a 0,064 mmpy, y el porcentaje de velocidad de corrosión en un 37,9%.

## 3. Cuando hay que extraer

La Convención de la UNESCO reconoce que la opción prioritaria (conservación *in situ*) no es siempre la preferible y, en ciertas circunstancias la propia **Norma 1** indica que la extracción de los objetos "podrá autorizarse cuando constituyan una contribución significativa a la protección, el conocimiento o el realce de este patrimonio". Así, en 2005 la Consejería de Cultura de la Junta de Andalucía autorizó la extracción de dos piezas de artillería del *Bucentaure* para su estudio, conservación y posterior musealización. Para plantear el tratamiento más óptimo se llevó a cabo una experiencia previa con una bala de cañón descontextualizada (Gil et al., 2003).

Estas piezas de fundición, bala y cañones, estaban recubiertas por gruesas concreciones de naturaleza calcárea proveniente de material esquelético de organismos marinos, que interacciona con especies metálicas en difusión $Fe^{2+}$ y $Fe^{3+}$ procedentes del metal subyacente, que producen modificaciones químicas en su composición. El resultado es una envoltura mineral compacta adaptada a la superficie del objeto. En el interior de la concreción, el objeto sufre un proceso de corrosión que transforma el hierro en compuestos químicos distribuidos en fases uniformes desde el núcleo metálico remanente hasta la zona exterior grafitizada, compuesta por $H_2O$, FeO(OH), $SiO_2$, $Fe_3C$, cloruros de hierro y grafito. En función del tiempo de inmersión y de las condiciones físico-químicas del entorno, en el núcleo del metal estarán presentes ferrita y perlita no corroídas o parcialmente corroídas, en secciones contiguas a la zona grafitizada. En ambientes con un exceso de iones cloro libres, estos se incorporan en la primera monocapa de algunos productos de corrosión.

Debido a las condiciones anteriores, si el objeto arqueológico se seca parcialmente al aire, los componentes del cloruro de hierro se descomponen para formar $Fe_2O_3$, $FeCl_3$, HCl y FeO(OH), que proporcionan unas condiciones ideales para la corrosión. El proceso de degradación total está determinado en gran medida por dichos iones $Cl^-$ que están presentes en la zona grafitizada en concentraciones de entre el 6-12 % en peso. La alta concentración de $Cl^-$ presente en estos objetos procedentes del medio marino, es directamente responsable de su deterioro mediante un proceso local de acidificación conocido como corrosión activa, y el fin de todo tratamiento de conservación de hierro arqueológico debe ser su eliminación. En este trabajo se eligió la electrólisis, aplicando intensidades bajas de corriente que minimizasen la evolución de hidrógeno en el cátodo y aumentasen la velocidad de extracción de los $Cl^-$, al incrementar el área disponible para su difusión.

Un examen de diferentes técnicas de limpieza de cloruros, ha mostrado que el paso limitante en la liberación de los mismos, es su difusión desde los productos de corrosión. El aumento de la velocidad de difusión de los $Cl^-$ en los productos de corrosión se consigue transformando los compuestos de hierro en otros más densos mediante su reducción. Dicha reducción se puede llevar a cabo por varios medios, siendo la electrólisis uno de los más eficaces. Adicionalmente, el empleo de intensidades de corriente bajas permite conseguir la consolidación de la zona grafitizada debido a la reducción de los oxihidróxidos de hierro que la componen, principalmente akaganeita $Fe^{3+}O(OH)(Cl_x)$, que se transforma inicialmente en goethita a FeO(OH) y posteriormente en magnetita $Fe_3O$ o $FeO{\cdot}Fe_2O_3$. Este compuesto, más denso, favorece la difusión de los iones cloruros desde el interior de la pieza y consolida la parte metálica externa evitando posteriores oxidaciones.

A diferencia de otros estudios, los productos de corrosión del hierro fueron analizados desde un punto de vista estructural y mineralógico, lo que permitió utilizar el análisis de los patrones de difracción de rayos X para comprobar la eficacia del tratamiento electrolítico en la extracción de cloruros. El análisis de estos patrones se llevó a cabo mediante el método Rietveld, superando el inconveniente que tiene el uso de tales perfiles en el análisis primario de los productos de corrosión de hierro, debido al solapamiento de picos de difracción que presentan los diferentes óxidos y oxihidróxidos. La composición interna del objeto correspondía a $\alpha$-Fe, cementita y cuarzo, compuestos minerales de los principales elementos presentes (Fe, Si, C) que tienen su origen en el proceso de fundición. Esta composición permaneció inalterada tras el tratamiento. El análisis de Rietveld de los patrones XRD de la superficie corroída antes del tratamiento, permitió la identificación de akaganeita, por deconvolución del pico de mayor intensidad, con una estequiometría $Fe^{3+}O(OH)(Cl_{0,19})$. La presencia de este compuesto se confirmó mediante SEM y análisis elemental del espectro EDX correspondiente. Tras el tratamiento de electrólisis, las fases minerales presentes en la superficie que contenían hierro fueron goethita a FeO(OH) y magnetita $Fe_3O$ o $FeO{\cdot}Fe_2O_3$, que no presentan $Cl^-$ (Figura 2).

De este hecho, se dedujo que la electrólisis produjo la extracción de los cloruros de la pieza, dato que confirmó el espectro EDX, induciendo la inestabilidad estructural de akaganeita y su desaparición. Por tanto, el análisis de Rietveld de los espectros XRD, se muestra como una herramienta muy útil que permite monitorizar el tratamiento electrolítico, controlando la presencia de akaganeita en la muestra. Una vez comprobada la eficiencia del tratamiento en la bala, se procedió al tratamiento de los dos cañones extraídos del *Bucentaure*. Este mismo método fue empleado para la estabilización a mayor escala de 17 cañones en 2009, procedentes de la Batería del Caballero Zuazo, San Fernando (Cádiz) (Sánchez Pedreño et al., 2022).

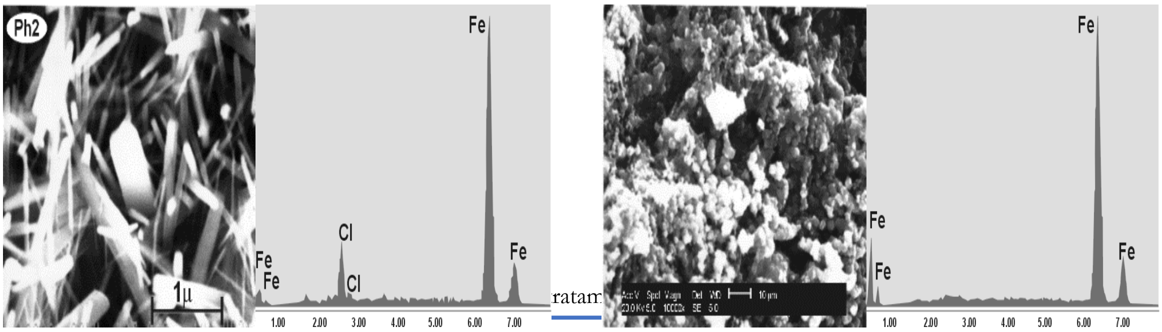


**Fig. 2.** *Imágenes SEM y espectros EDX de: Izquierda: la muestra sin tratar, mostrando estructuras de akaganeita y presencia de $Cl^-$. Derecha: la muestra tratada, mostrando estructuras de goethita y ausencia de $Cl^-$ (adaptado de Gil et al., 2003).*

## 4. La información contenida

Una de las líneas de trabajo del LEC-PH es el análisis de los restos de procedencia subacuática, principalmente de pecios, con el objetivo de profundizar el conocimiento sobre la tecnología náutica y metalúrgica. Desde una perspectiva integral, documental, arqueológica y arqueométrica, se han estudiado evidencias arqueológicas de numerosos sitios de época antigua y moderna. En particular, destacan los trabajos realizados sobre elementos vinculados al casco, equipamiento, artillería y cargamentos de diferentes embarcaciones de madera. En su mayoría, los estudios han sido realizados sobre restos de naturaleza metálica: materiales ferrosos y no ferrosos, y entre estos últimos, principalmente de cobre y sus aleaciones (bronces y latones).

Dentro de este contexto, la aplicación de técnicas instrumentales analíticas para la caracterización físico-química de objetos metálicos de procedencia arqueológica permite obtener nuevos datos para discutir aspectos vinculados a los materiales y procesos utilizados para su fabricación. La selección de los medios empleados se realiza en función de los interrogantes de investigación, siendo habitual la combinación de más de una técnica. La interpretación de los datos obtenidos, según el caso, se lleva a cabo utilizando bases de datos de referencia, herramientas estadísticas, información histórica y paralelos arqueológicos. En este sentido, estudios a nivel comparado (al interior de cada sitio y entre diferentes pecios) permiten superar los límites propios del objeto y discutir aspectos más generales acerca de los conocimientos y prácticas de la época, e incluso procesos a mayor escala, como el cambio tecnológico.

Entre los casos de estudio, mencionamos como ejemplo la caracterización de un conjunto de cañones de bronce y subproductos de fundición transportados como chatarra a bordo de un barco mercante neerlandés que se hundió en el puerto de Cádiz hacia el tercer cuatro del siglo XVII (Ciarlo et al., 2023). Los cañones fueron identificados a través de su diseño, decoración y marcas, rasgos que se asocian a un renombrado taller de fundidores de campanas y cañones que estableció Matthias Benningk en Lübeck, norte de Alemania, que tuvo una importante trayectoria a lo largo del siglo XVII (Figura 3). Por comparación con piezas de museos asociadas a esta familia, es probable que los cañones estudiados hayan sido fundidos hacia el segundo o tercer cuarto de aquella centuria. Entre los restos recuperados, uno exhibe una variante del escudo de armas de Hamburgo, lo que sugiere que la pieza fue hecha por encargo para esta ciudad. Cabe destacar que los productos defectuosos y subproductos de fundición solían reciclarse (refundirse), al igual que sucedía con los cañones deteriorados por el uso, de allí que semejantes materiales no suelen preservarse en contextos arqueológicos. El caso bajo estudio, por ende, constituye una fuente de singular interés para conocer los pormenores del proceso de fundición de cañones.

El análisis de las piezas fue realizado a nivel macroscópico, microestructural y de composición química. Una inspección visual permitió, en el caso de los fragmentos de cañones, reconocer el diseño, decoración y marcas de fábrica de las piezas, así como diferentes evidencias vinculadas a la fallida producción. Esta última se analizó de forma más exhaustiva por medio de metalografía, utilizando microscopía óptica y microscopía electrónica de barrido. En relación con lo anterior, los elementos mayoritarios y minoritarios de la aleación se determinaron por medio de EDX. Los datos recabados, evaluados a la luz de tratados de metalurgia y fundición de la época, permitieron discutir aspectos sobre la calidad y manufactura de los cañones y las dificultades técnicas asociadas a este laborioso y costoso arte. En particular, se analizaron los defectos asociados a errores cometidos en las diferentes etapas de la producción: preparación del patrón y molde del cañón; encendido del horno y fundición de la materia prima; y proceso de colada y enfriamiento. Así, con base en una aproximación interdisciplinaria, se aportó nueva evidencia sobre los conocimientos y práctica cotidiana de una familia de fundidores renacentistas del norte de Europa.

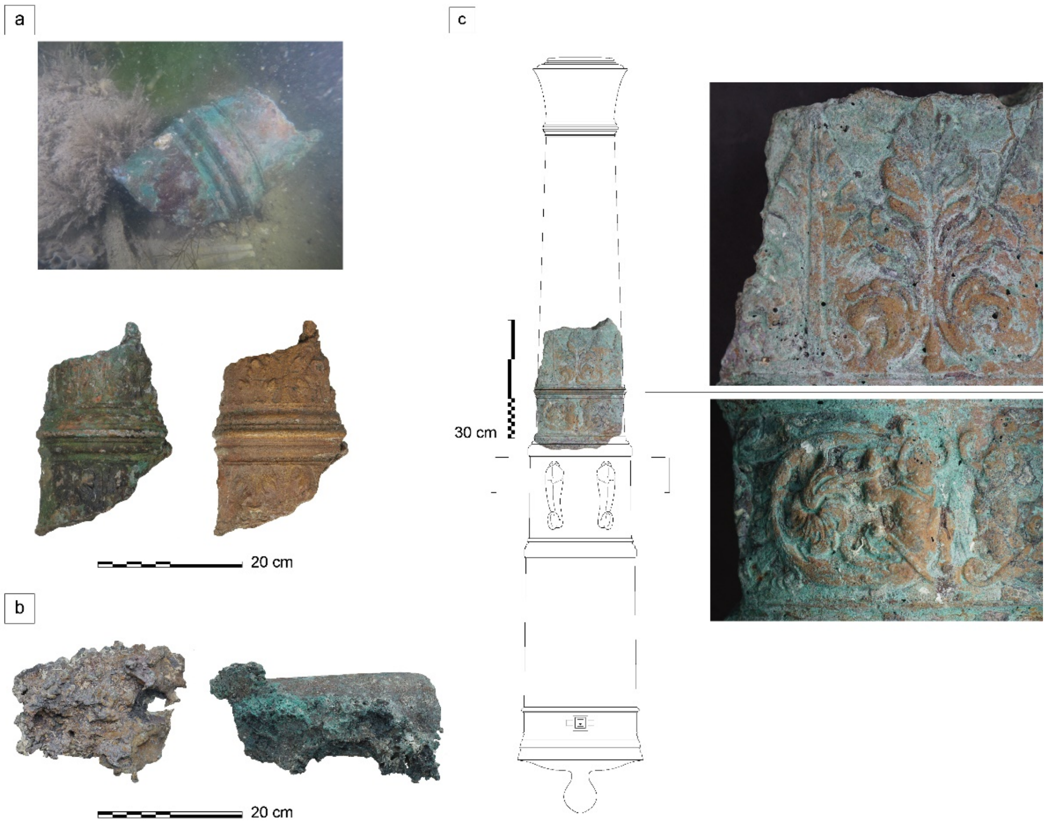


**Fig. 3.** *Restos de cañones de bronce recuperados del pecio Delta I: a) imágenes de un fragmento* in situ *y una vez extraído, previo y posterior a su conservación; b. subproductos de fundición, amorfos y adheridos a partes del cuerpo de las piezas; y c) trozo de cañón, decorado con hojas de acanto y motivos figurativos (extraído de Ciarlo et al., 2023: fig. 1).*

## 5. Palabras de cierre

El patrimonio cultural sumergido debe ser protegido y estudiado, a través de estrategias y acciones en línea con los principios de la Convención de la UNESCO (2001) y dando preferencia a la preservación *in situ*. Una forma de contribuir con lo anterior, además de las medidas de salvaguarda necesarias, es a través de su diagnóstico y caracterización. La información derivada de la investigación de los restos de pecios y otros sitios arqueológicos que se encuentran en contextos sumergidos ha contribuido no solamente a comprender nuestro pasado y arrojar luz sobre aspectos poco conocidos, además, resulta fundamental para definir y aplicar mecanismos adecuados de puesta en valor dentro de las comunidades. En la actualidad, existen numerosos recursos que permiten potenciar esta línea de trabajo. Dentro del LEC-PH de la UCA, se ha promovido un espacio que nuclea a especialistas de la arqueología y otros campos del conocimiento, en colaboración con centros de gestión e investigación del patrimonio. Allí, con base en una perspectiva interdisciplinar e intersectorial, desde su creación se han desarrollado y aplicado diferentes herramientas para el estudio y protección de diferentes sitios, con énfasis en los metales asociados a restos de naufragios.

## Referencias

ARQUEOMONITOR (2010): Estudio de las condiciones físicas, químicas y biológicas en el deterioro y salvaguarda del patrimonio cultural subacuático, Ministerio de Economía y Competitividad, Proyecto CTM2010-16363.

Bethencourt, M., Fernández-Montblanc, T., Izquierdo, A., González-Duarte, M.M., Muñoz-Mas, C. (2018): Study of the influence of physical, chemical and biological conditions that influence the deterioration and protection of Underwater Cultural Heritage. Science of the Total Environment, 613–614, 98–114. https://doi.org/10.1016/j.scitotenv.2017.09.007

Bethencourt, M., Botana, F.J., Marcos, M. (2005): Sistema combinado para el registro y la conservación arqueológica subacuática in situ. Patente: 2-221-525, España. Registro: 24/05/2002. Publicada: 08/09/2005.

Ciarlo, N.C., Martí Solano, J., Bethencourt, M., Fernández Tudela, E., Toboso Suárez, E.J., González Gallero, R. y Zuccolotto Villalobos, A. (2023): New remarks on the mid-17th-century gun founding in Northern Europe: archaeometric analysis of scrap bronze ordnance recovered from a Dutch merchant vessel lost off Cadiz, Spain. Archaeological and Anthropological Sciences, 15, 136. https://doi.org/10.1007/s12520-023-01835-z

Gil, M.L.A., Santos, A., Bethencourt, M., García, T., Fernández-Bastero, S., Velo, A., Gago-Dupor, L. (2003): Use of X-ray and other techniques to analyse the phase transformation induced in archaeological cast iron after its stabilisation by the electrolytic method. Analytica Chimica Acta, 494, 245–254. https://doi.org/10.1016/j.aca.2003.08.012

Gregory, D. (1995): Experiments into the deterioration characteristics of materials on the Duart Point wreck site: an interim report. Int. J. Naut. Archaeol. 24 (1), 61–65. https://doi.org/10.1111/j.1095-9270.1995.tb00712.x

United Nations Educational, Scientific and Cultural Organization – UNESCO (2001): Convención sobre la Protección del Patrimonio Cultural Subacuático. París. http://unesdoc.unesco.org/images/0012/001246/124687s.pdf#page=59,acceso 20 de septiembre de 2024.

MacLeod, I.D. (1995): In situ corrosion studies on the Duart Point wreck. Int. J. Naut. Archaeol. 24, 53–59. https://doi./10.1111/j.1095-9270.1995.tb00711.x

MacLeod, I.D. (2002): In situ corrosion measurements and management of shipwreck sites. In: Ruppé, C.V., Barstad, J.F. (Eds.), International Handbook of Underwater Archaeology. Kluwer Academic/Plenum, New York, pp. 697–714. https://doi-org/10.1007/978-1-4615-0535-8_41

Sánchez Pedreño, I., Salas I., García Amado, J.F., García Trigo, S., Bethencourt, M. (2022): Tratamiento de conservación a gran escala de piezas de artillería pesada de hierro fundido y procedencia subacuática. Procedimientos metodológicos. Ge-conservación, 21, 16–28. https://doi.org/10.37558/gec.v21i1.970

Journal of Cultural Heritage xxx (xxxx) 1–10

Contents lists available at ScienceDirect

Journal of Cultural Heritage

journal homepage: www.elsevier.com

Original article

# Assessment of consolidants for the preservation of *Tituli Picti* on amphorae from the *Ses Fontanelles* late Roman shipwreck (Mallorca, Spain): An analytical approach

Elisa Fernández-Tudela [a, *], Rafael Zarzuela Sánchez [b, 1], Marina Goñalons Lapiedra [b, 2], Almoraima Gil [b, 3], Darío Bernal Casasola [b, 4], Miguel Ángel Cau-Ontiveros [c, 5], Enrique García Riaza [d, 6], Jaume Cardell Perelló [e, 7], Manuel Bethencourt Núñez [b, 8]

[a] *Andalusian Institute of Historical Heritage (IAPH), Center of Underwater Archaeology (CAS), Spain*
[b] *University of Cadiz, Spain*
[c] *ICREA and ERAAUB-IAUB of the University of Barcelona (UB), Spain*
[d] *University of Balearic Islands, Spain*
[e] *Council of Mallorca, Spain*



ARTICLE INFO

*Article history:*
Received 24 November 2024
Accepted 2 April 2025

*Keywords:*
Roman pottery
*Tituli Picti*
Consolidant
Acrylic resin
Nano silica
Underwater archaeology

ABSTRACT

The ceramic materials from the Ses Fontanelles wreck are an exceptional find due to the large number of amphorae with preserved inscriptions and their state of preservation. The presence of *Tituli Picti* is uncommon, and even less so in ceramics altered in an underwater environment. The bibliography on the conservation of these elements is scarce. This manuscript presents the results of a comparative study of two consolidation products: one based on nanoparticles (Nano Estel 1:1) and the other on an acrylic resin based on organic solvents (Paraloid B72 3 % in acetone).This preliminary study aims to establish a methodology for the treatment of the inscriptions painted on Roman amphorae from the Ses Fontanelles wreck (Mallorca), 4th century AD. A suite of analytical techniques was employed, encompassing surface analysis via Scanning Electron Microscopy - Energy Dispersive X-Ray Spectroscopy (SEM-EDX), X-Ray Diffraction (XRD) for the identification of crystalline phases, hardness and micro-indentation testing, peeling test, and measurements of aesthetic alterations using a spectrophotometer and glossmeter. The results obtained from these analyses were found to be highly congruent, underscoring the effectiveness of a long-standing acrylic resin and the potential of the silica nanoparticle-based product, which has seen a surge in utilization. This study also paves the way for further research in this area, as it opens up new avenues for exploration and the potential discovery of additional findings.



## Introduction

The preservation of painted inscription or *Tituli Picti* on amphorae is exceptionally rare, even though this type of marking, made with atramentum (black ink) and calamus or paintbrush type tools, was commonly applied to such recipients in antiquity. It believed that in antiquity most —if not all— amphorae were marked, with at least the majority within each shipment bearing some form of identification [1]. This scarcity poses a significant challenge when attempting to implement established conservation methodologies, particularly for a unique assemblage such as that from Ses Fontanelles shipwreck, where 82 amphorae bearing *Tituli Picti* of different characteristics have been identified.

This paucity poses a significant challenge when attempting to implement established conservation methodologies, particularly for a unique assemblage such as that from the Ses Fontanelles shipwreck, where 82 amphorae bearing *Tituli Picti* of different characteristics have been identified. The search for established methods for the consolidation and preservation of *Tituli Picti* has yielded limited results, with only a few documented cases existing in which *Tituli Picti* have been identified on ceramics recovered from underwater contexts or other terrestrial environments. The Ses Fontanelles wreck is the third such wreck in the Iberian Peninsula, following the Gandolfo wreck (Almería) [2–3] and the Albufereta (Alicante) [4].In the majority of these cases, the conservation processes remain unmentioned. These studies include archaeometry analyses of inks [5,6]. With the exception of the study of the *Tituli Picti* from the Gandolfo shipwreck (Almería, Spain), which addresses both the conservation and the archaeometry analysis of the *Tituli* recovered during the excavation, the extant literature focuses primarily on the conservation of materials such as stones and mortars, all of which are from terrestrial environments [7–8].

Ceramics that have been exposed to an underwater environment for an extended period are susceptible to alterations and contaminations

* Corresponding autor at: Center of Underwater Archaeology (CAS), Andalusian Institute of Historical Heritage (IAPH), Duque de Najera, 3, 11002, Cadiz, Spain.
*E-mail addresses:* Elisa.fernandez.tudela@juntadeandalucia.es (E. Fernández-Tudela), rafael.zarzuela@uca.es (R.Z. Sánchez), marina.gonalons@uca.es (M.G. Lapiedra), almoraima.gil@uca.es (A. Gil), dario.bernal@uca.es (D.B. Casasola), macau@ub.edu (M.Á. Cau-Ontiveros), manuel.bethencourt@uca.es (M.B. Núñez).

[1] Rafael Zarzuela, TEP-243 Nanomaterials Group, Department of Physical-Chemistry, Faculty of Sciences, University of Cadiz (UCA), Campus Universitario Puerto Real s/n, 11510, Puerto Real, Spain.

[2] Marina Goñalons Lapiedra, Marine Research Institute (INMAR) of the University of Cadiz (UCA), Campus Universitario Puerto Real s/n, 11510, Puerto Real, Spain.

[3] Almoraima M.L Gil Montero, TEP-243 Nanomaterials Group, Department of Physical-Chemistry, Faculty of Sciences, University of Cadiz (UCA), Campus

Universitario Puerto Real s/n, 11510, Puerto Real, Spain.

[4] Darío Bernal-Casasola, HUM-440 Research Group, Archaeology Area of the Department of History, Geography and Philosophy, University of Cadiz (UCA), Dr. Gomez Ulla, 1, 11003, Cadiz, Spain.

[5] Miguel Ángel Cau-Ontiveros, Archaeological and Archaeometric Research Team of the University of Barcelona (ERAAUB), Institute of Archaeology of the University of Barcelona (IAUB), University of Barcelona (UB), Montalegre, 6–8, Barcelona, Spain.

[6] Enrique García Riaza, «Civitas (Balius)» Research Group, University of the Balearic Islands (UIB), Valldemossa Km. 7.5, Palma, Spain

[7] Jaume Cardell Perelló, Consell de Mallorca, Palma, Plaça Hospital 4, 07012, Spain; «Civitas (Balius)» Research Group, University of the Balearic Islands (UIB), Valldemossa Km. 7.5, Palma, Spain

[8] Manuel Bethencourt Núñez, Department of Materials Science, Metallurgical Engineering and Inorganic Chemistry, Institute of Marine Science (INMAR), University of Cadiz (UCA), Campus Universitario Puerto Real s/n, 11510, Puerto Real, Spain.

https://doi.org/10.1016/j.culher.2025.04.002
1296-2074/

Note: Low-resolution images were used to create this PDF. The original images will be used in the final composition.

that can impact their chemical and mineralogical composition. Research studies have identified the formation of non-original minerals and the presence of elements such as Ca, F, and S, which are associated with contamination caused by colonizing marine organisms. The occurrence of these post-depositional alterations can be attributed to a combination of intrinsic agents associated with the materials and extrinsic agents influenced by the marine environment [9–11].

Notwithstanding the mechanisms of alteration to which underwater archaeological heritage is exposed, the case of the Ses Fontanelles wreck is exceptional due to the extraordinary state of preservation of its materials. The site has remained virtually intact for centuries, buried in fine sands composed primarily of bioclastic sediments and carbonate lithoclasts [12].

A substantial number of fragments and complete amphorae of at least four types have been recovered, including the Almagro 51c type, the Ses Fontanelles I type, and the flat-bottomed amphorae, as well as the Keay XIX type. The Almagro 51c type is the most abundant, followed by the Ses Fontanelles I type. The classification of these typologies has been previously determined through studies that utilized petrographic analysis, categorizing them as Group 1. These studies have revealed a ceramic assemblage exhibiting similarities in content, with a range of primary inclusions, particularly micas (mostly muscovite), monocrystalline and polycrystalline quartz/quartzite, and fragments of metamorphic rocks likely derived from mica schist, along with other components in smaller quantities [13–15].

The bibliographic search for possible consolidants was initially driven by the need for a product that could be applied from the earliest stages of object treatment (i.e., desalination through progressive baths from saltwater to demineralized water). This requirement arose from observations made during the 2019 excavation campaign, where it was observed that the intensity of the *Tituli Picti* diminished during the post-extraction conservation treatments.

The primary objective of the study was to identify a water-based consolidant that could be introduced during the early stages of treatment, while salts were still being extracted from within the ceramic. The selected product was required to achieve both the consolidation of the ceramic and the stabilization of the *Tituli* without hindering the migration of chlorides to the surface. These stringent requirements substantially narrowed the range of viable options. The existing literature on the subject relied on examples of ceramics that had already undergone prior treatments, such as demineralization, making it challenging to evaluate the potential incompatibilities of these salts with the treatment process. This could lead to undesirable outcomes, such as efflorescence, color changes, or the loss of effectiveness. The utilization of barrier products to safeguard the *Tituli* during desalination was considered but ultimately dismissed due to the contribution of residual substances resulting from post-treatment processes [16].

However, at the outset of the desalination treatment of the materials recovered during the second excavation phase (2021–2022), it was observed that the *Tituli Picti* responded well in static water baths. Nevertheless, after a prolonged exposure and as the baths changed from tap water to deionized water, a gradual loss of intensity in the *Tituli* was noted. Consequently, the ceramics were extracted from the baths following an initial air-drying evaluation, and a resolution was reached to undertake a dry consolidation and fixation process employing either water-based or organic solvent-based consolidants.

This study explores two selected consolidation products, each with a documented history of extensive use on pottery and similar materials [17–24] and compares the results through various analytical techniques. The objective of this research is to evaluate the effectiveness of these treatments in comparable contexts. In summary, the study seeks to explore a methodological framework for assessing conservation approaches for underwater archaeological pottery, particularly those with preserved *Tituli Picti*.

Following the conclusion of the archaeological excavation of the Ses Fontanelles shipwreck's cargo (2021–2022) [13], the amphorae assemblage —both with and without *Tituli Picti*— was divided into two groups. The first group consisted of complete amphorae, some still sealed and containing remnants of their original contents, while the second group comprised small to medium-sized fragments with preserved *Tituli Picti*. The latter group was transferred to the laboratories of the University of Cádiz for further study and conservation.

The present research focuses on the development of an initial methodology applied to these fragments, which can later be extrapolated to the complete amphorae currently undergoing preventive conservation at the Council of Mallorca's facilities.

## Research aims

This study addresses the rare preservation of painted inscriptions, or tituli picti, on amphorae, which were commonly marked in antiquity but are seldom found intact today. This paper aims to investigate two consolidation products for the conservation of archaeological pottery and tituli picti, focusing on their effectiveness in comparable contexts, particularly from the Ses Fontanelles wreck. The main objective is to establish a methodological framework for assessing conservation approaches for underwater archaeological pottery, especially those with preserved tituli picti. This study aims to advance the application of consolidation products for underwater materials, recognizing that their conservation challenges differ from those of terrestrial finds.

## Material and methods

### *Preparation of pottery samples*

A total of 24 samples were extracted from three fragments that were recovered during excavation in areas close to the site. According to the typological classification carried out by the archaeologists, the samples correspond to the two typologies that retain *Tituli*: Almagro 51c (samples A and C) and Ses Fontanelles 1 (sample B).Both feature *Tituli Picti* and exhibit similar petrographic characteristics (classified within petrographic group 1). Their macroscopic features demonstrate a degree of homogeneity, exhibiting relatively fine matrices. Variations in color and texture across some ceramics, even within different areas of the same specimen, suggest potential depositional processes associated with subaqueous environments [13]. However, none of the three fragments used preserved *Tituli*, nor do they coincide with the original fragments treated in the laboratory with *Tituli*. In this study, only one fragment with visible *Tituli* (DSF-469) was utilized for the examination of its microscopic surface characteristics. The fragments were designated as A, B, and C, and the samples were numbered in consecutive order while maintaining the initial letter of the fragment from which they were extracted (Fig. 1). Fourteen samples were utilized in the present study, while the remaining ten were reserved for future investigations.

The extraction process involved the use of a Bosch grinder and a Dremel cutter, both equipped with diamond discs. The dimensions of the samples were adjusted according to the specific requirements of each test (Table 1).

### *Consolidate products and application method*

A comprehensive review of the extant literature was conducted to identify two products that are frequently utilized in the conservation of archaeological materials. Paraloid B-72, a copolymer of ethyl methacrylate and methyl acrylate soluble in organic solvents, which remains the most widely used consolidant for various types of archaeological materials. Resins, however, are not without their drawbacks. These include sensitivity to ultraviolet radiation, which can lead to discoloration and cracking. Resins also exhibit low permeability and lim-

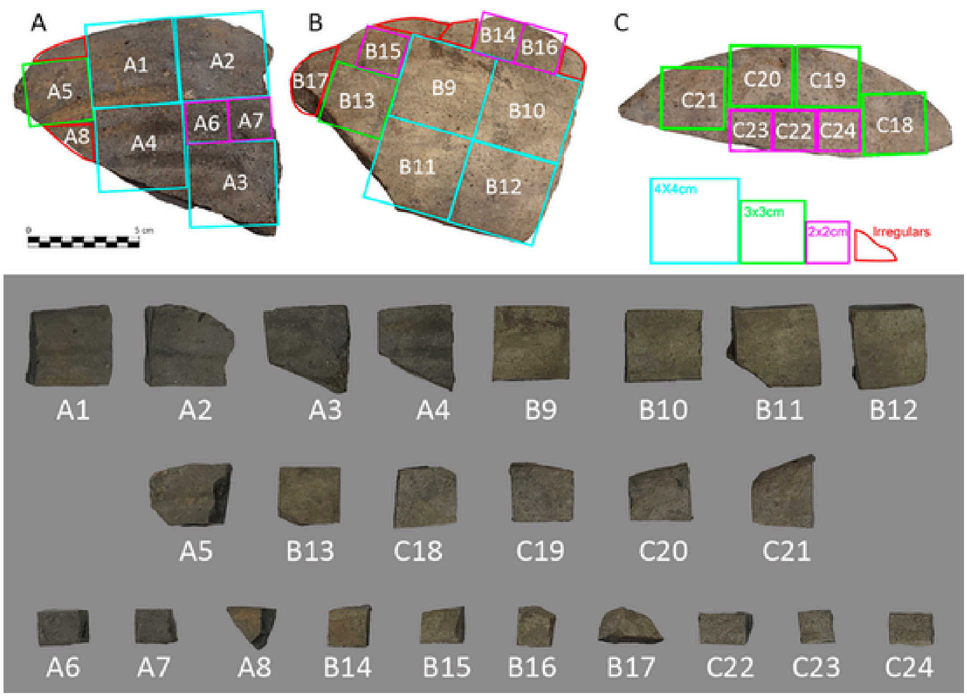


**Fig. 1.** Image of the samples.

**Table 1**
Summary of sample size and tests performed.

| *Treatment Applied* | Paraloid B-72 | Nano Estel | Untreated | Sample dimensions (cm) |
|---|---|---|---|---|
| *Control Samples* | A1 | B9 | – | 4 × 4 |
| *Mineralogical and Petrological characterization* | | | | |
| (XRD) | A2, B11 | A3, B12 | A4, B10 | Powder |
| *Chemical Analysis* | | | | |
| (SEM-EDX) | A2, B11 | A3, B12 | A4, B10, DSF-469* | Fragment |
| *Physical and Mechanical Analysis* | | | | |
| Colorimetry | A2, B11 | A3, B12 | A1, B9 | 4 × 4 |
| Brightness | A2, B11 | A3, B12 | A1, B9 | 4 × 4 |
| Water behavior | A2, B11 | A3, B12 | A1, B9 | 4 × 4 |
| Drilling resistance (DRMS) | B11 | B12 | A4, B10 | 4 × 4 |
| Indentation Microhardness | A2, B11 | A3, B12 | A4, B10 | 4 × 4 |
| Peeling Test | B15, C23 | B16, C24 | B13, C18 | 3 × 3 |

* Untreated sample with *Tituli Picti*.

ited chemical interaction with mineral substrates [25–26]. However, these limitations are particularly pronounced when materials are exposed to outdoor conditions or in aggressive environments. Paraloid B-72 remains a prominent consolidant, underscoring the necessity for a comprehensive evaluation of its effectiveness and compatibility with archaeological materials.

The second product is Nano Estel, a newer consolidant based on aqueous colloidal silica dispersion of 10–20 nm nanoparticles, with 30 % solid content and stabilized with NaOH at pH 9.8–10.4. Despite certain drawbacks, the selection of a water-based consolidant is predicated on the material's inherent characteristics (i.e., its submerged origin) and the prospective feasibility of treating fragments in a moist state without the necessity of a prior dehydration process, a prerequisite for solvent-based consolidants. This product has shown promising results in the treatment of ceramics and other archaeological materials [7].

The selected application method was a drip technique, which minimizes surface disruption by avoiding the application of pressure or friction. Paraloid B-72 was applied at a rate of 3 % in acetone and Nano Estel in a 1:1 ratio of deionized water. Each sample was subjected to two surface applications of consolidant, allowing 72 h of drying time between each application at room temperature. All samples were left to dry for one month at controlled room temperature before testing.

*Methodology for the evaluation of pottery samples*

A digital microscope Leica DV6, with a magnification range of 46x to 675x, was utilized to examine and evaluate the pottery samples prior to treatment. This microscope was equipped with Leica Application Suite X (LAS X) software, which facilitated the analysis.

The mineralogical composition was determined semi-quantitatively using randomly oriented powder samples from treated and untreated fragments. The analysis was performed using a Bruker D8 Advance Diffractometer, equipped with a secondary monochromator and Cu Kα radiation. The instrument scanned a range of 10° to 75° 2θ at a rate of 0.020° 2θ every 0.19 s. Two specimens from each sample were prepared, and the resulting XRD patterns were compared using EVA software.

Morphological surface analysis was conducted using a Nova NanoSEM 450 Scanning Electron Microscope (FEI) and a Dual Beam Scios2 (Thermo Fisher Scientific), operating at an acceleration voltage of 20 kV and coupled with Energy-Dispersive X-ray spectroscopy (EDX). The Scios2 system was also equipped with a focused ion beam (FIB) using a gallium ion source. Prior to observation, the samples were sputtered with thin layers of platinum and graphite, and a thin platinum coating was deposited around the area of interest for a smooth cross-section via FIB. Seven samples were examined for each group: untreated (A4, B10), treated with B72 (A2, B11), treated with Nano Estel (A3, B12), and DSF-469 (untreated with *Tituli Picti*). Images were observed at magnifications of 65x, 250x, 500x, 1200x, 2000x, 4000x, and 6000x in secondary electron (SE) and backscattered electrons (BSE) modes.

The determination of the physical and mechanical properties was conducted using a variety of instruments. The mechanical resistance of the untreated and treated samples was evaluated through the implementation of the Drilling Resistance Measurement System (DRMS) from SINT Technology [27,28]. The experimental setup incorporated a rotation speed of 600 rpm, drill bits with a diameter of 4.8 mm, and a penetration depth rate of 10 mm/min.

The mechanical response of the samples was examined through a series of tests using a Struers Duramin-40 A1 nanoindenter. The Vickers (HV) method was employed, with a force range of 10 kg (kgf) being applied. To ensure accuracy in measurement, DuraminTM software and a Leica Digital microscope DV6 were utilized to analyze the indentation shape.

The cohesion of the material on the surface was evaluated using the non-destructive Scotch Type test, with five repetitions following the procedure described in Drdácký et al. (2015) [29]. The samples were untreated (C18 and B13), treated with B72 (C23 and B15), and treated with Nano Estel (C24 and B16). The double-sided 3 M Scotch tape, measuring 40 mm in width, was employed as the adhesive agent. Following a 90-second application period, the tape was removed at a 90° angle.

A ColorFlex solid reflection spectrophotometer (HunterLab) was utilized to evaluate the potential color alterations induced by the treatments. The total color difference (ΔE*ab) was determined in the CIE L*a*b* color space, adhering to the UNE-EN 15,886:2011 protocol [30], under the stipulated conditions: illuminant D65, CIE 10° observer (CIE 1964 standard).

$$\Delta E * ab = [\Delta L * 2 + \Delta a * 2 + \Delta b * 2]\, 1/2$$

Gloss measurements were performed in duplicate on the same samples using a PCE-GM 60 Plus glossmeter, an instrument that determines the specular reflection of light from the surface at a specific angle, following the ISO 2813:2014 procedure [31].

For the water absorption test, the samples were weighed before and after being immersed in ultrapure water for 24 h. A balance with an accuracy of 0.00010 g was used to ensure precise measurement of the samples' weight before and after the immersion process.

The water absorption coefficient was then calculated using the following equation:

$$water\ absorption\ ratio = \frac{W_t - W_0}{W_0}\ x\ 100\%$$

$W_t$ is the weight of the sample after 24 h of immersion and $W_0$ is the original weight of the sample.

The contact angle test was also performed to provide complementary insights into the hydrophilicity of the surface. Other analyses, such as accelerated aging analysis or water contact angle measurements, have not been deemed necessary, given that these objects are intended to be exposed and conserved in controlled museum environments with stable conditions.

## Results and discussion

### *Mineralogical composition: XDR*

The X-ray diffraction results indicate that the six samples evaluated (A2–4 and B10–12) are predominantly composed of muscovite ($KAl2(AlSi3O10)(OH)2$), quartz ($SiO2$), gypsum ($CaSO4·2H2O$), and pyrite ($FeS2$) (Fig. 2). These findings are consistent with the conclusions of previous petrographic analyses, which identified two petrographic groups with highly homogeneous clay compositions. The samples utilized in this study are classified as Petrographic Group 1, which is distinguished by muscovite-rich fabrics, containing metamorphic rock fragments such as quartzite, phyllites, and schists [13].

The presence of gypsum and pyrite is typically indicative of alterations in the raw material and environmental burial conditions. In marine environments, gypsum has been associated with pyrite formation or calcite dissolution and reaction with sulfates in acidic conditions. Both of these phenomena can occur in a buried deposit with a low oxygen environment and abundant decomposing organic matter, along with other elements that acidify the environment, such as iron objects.

In a similar vein, the presence of gypsum has been linked to sulfate precipitation from seawater [10]. The presence of pyrite indicates the decomposition of iron oxides, which are reduced and subsequently dissolved through two primary mechanisms: hematite hydroxylation to goethite and the subsequent dissolution of goethite by bacterial reduction or reaction with hydrogen sulfide in water solution [11].

### *Superficial characterization and elemental analyses: digital microscope and SEM-EDX*

The initial macroscopic documentation of the pottery surface was provided by the digital microscope. Two ceramic types depicted in Fig. 3 (A-B) exhibited substantial deterioration in their untreated states, with the use of *Tituli Picti* (DSF-469) serving solely as a means to assess the state of conservation. The samples displayed areas where ink preservation was minimal. At higher magnifications, it becomes evident that in specific regions, the material forming the lines is barely visible, penetrating surface imperfections (Fig. 3-C).

SEM micrographs of secondary electrons (Fig. 4) reveal the surface morphology of untreated (A4 and B10) and treated samples with B72 (A2 and B11) and Nano Estel (A3 and B12) at magnifications of 500x and 2000x. Previous studies have demonstrated that B72 forms a uniform and dense film on pottery surfaces, reducing porosity. This effect is barely visible in Fig. 4 (C, D), likely due to the low percentage of B72.No clear film details were observed in the micro cross-section analysis FIB (Fig. 5).

The samples treated with Nano Estel exhibited two different states, as illustrated in Figs. 4 (E and F). The product formed a homogeneous surface coating in some areas while concentrating in specific spots in others, resulting in an incomplete coverage of the entire surface. This phenomenon of microcracking has been documented in the literature as a consequence of the capillary pressure generated during the solvent drying process [32]. It is noteworthy that, despite the $SiO2$ nanoparticles being smaller than the typical pore size in pottery, the formation of larger aggregates and solvent evaporation impede their penetration into the material. The cross-section of the sample treated with Nano Estel reveals an irregular product layer, measuring 1–2 μm in thickness, exhibiting apparent cohesion deficiency in specific areas (Fig. 5).

The EDX analysis indicates an elemental distribution consistent with the clays and mineral phases identified in the XDR analysis, including Si, Al, K, Ca, S, and Fe. Furthermore, trace elements such as Mg, Mn, Na, and Ti were detected, likely originating from clay impurities or depositional alteration and/or contamination.

EDX analysis of both the surface and cross-section was conducted. No detectable elements associated with the ink were found, likely due to the organic nature of the pigment. It is possible that the ink originated from combustion products such as plant matter or bones, rather than from iron-based ink [5,6,33].

### *Colour alteration measurement and gloss variation*

The visual alterations induced by the treatments are imperative for the assessment of their compatibility with archaeological objects. The total color difference values (ΔE*ab) documented prior to and following treatment (Table 2) are consistent with the acceptable range for conservation treatments in cultural heritage (ΔE*ab < 5). According to the criteria established by Delgado Rodríguez and Grossi [34], the measured ΔE*ab values indicate changes that are either imperceptible or minor, with the exception of sample B11 (treated with B72), which exhibited a significant color shift (ΔE*ab = 7.14).

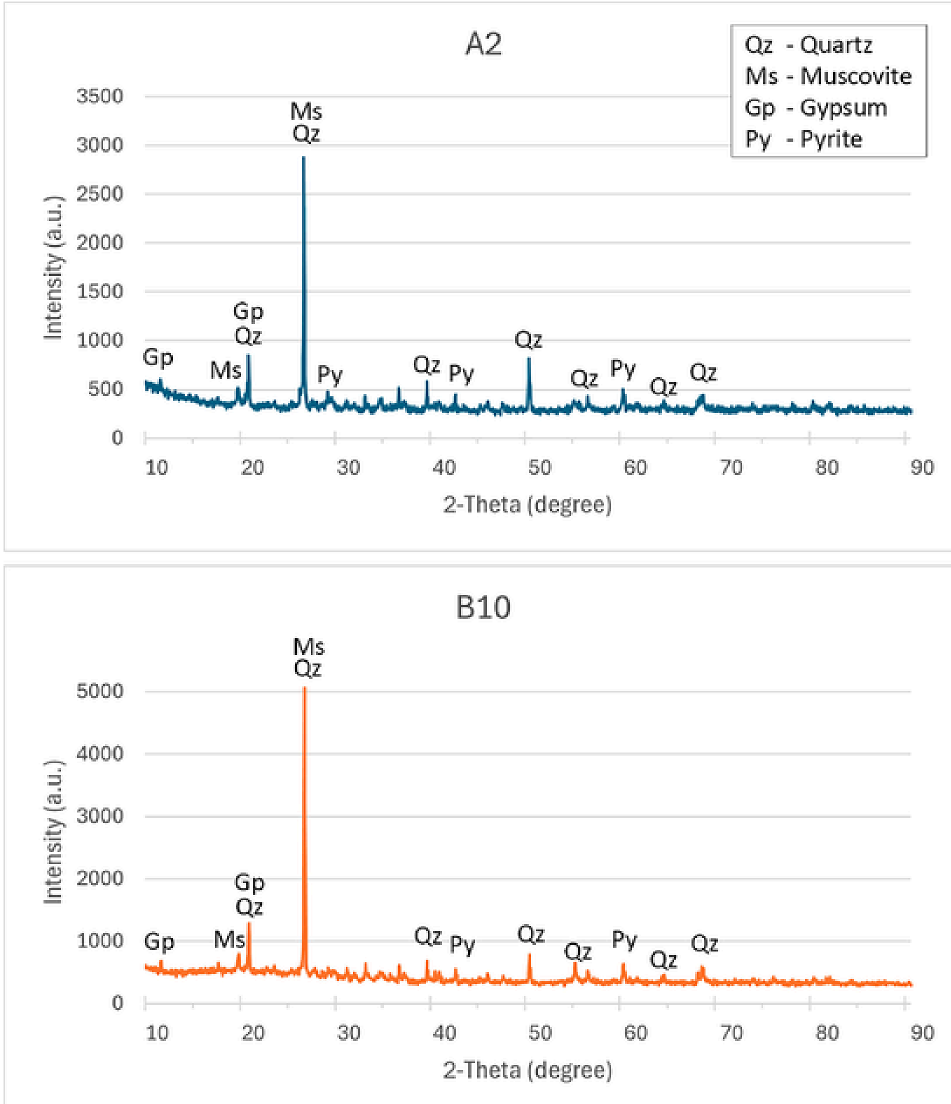


**Fig. 2.** Example of similar XRD analysis results of two of the samples (A2 and B10).

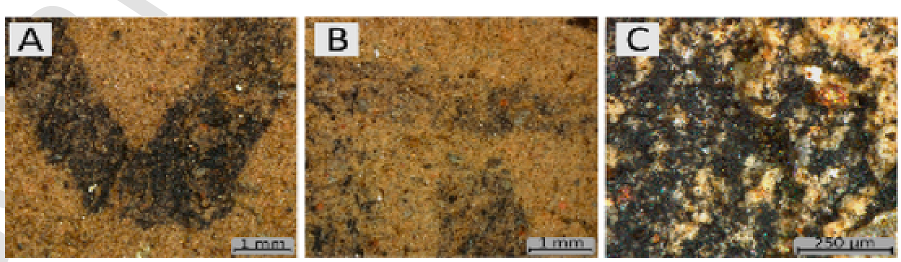


**Fig. 3.** Different preservation states of the markings on the ceramic surface of untreated sample (DSF-469).

As illustrated in Fig. 1, sample B11 exhibits a lighter coloration compared to A2. The predominant factor contributing to this variation is a reduction in the L* coordinate. A prevalent phenomenon associated with resin treatments is that the surface of the material tends to resemble the appearance of the underlying material (which is darker in hue). This effect is more pronounced in light-colored samples, as evidenced by the L* coordinates of both samples prior to treatment, which indicate this tendency. However, it is imperative to exercise caution when interpreting these results, as another B72-treated sample (A2) exhibited an acceptable value ($\Delta E^*ab = 2.45$).

The results of the study demonstrate that the treatments resulted in slight but acceptable color alterations. It is imperative to consider these changes in conjunction with gloss variations.

Gloss measurements, obtained from two angles to account for the low sheen of the pottery, demonstrate minor increases in gloss for both treatments (Table 3). However, sample B11 (treated with B72) exhib-

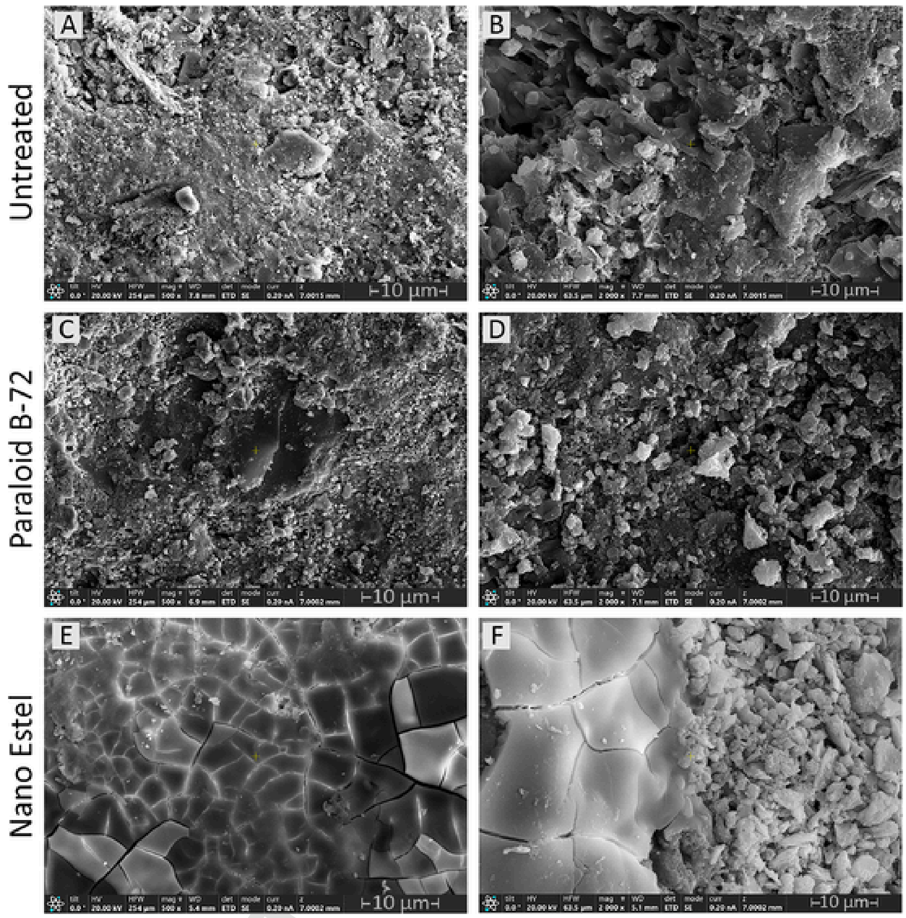


**Fig. 4.** Untreated sample A4 (A) and B10 (B) at different magnifications; treated with Paraloid B72 sample A2 (C) and B11 (D) and treated sample with Nano Estel A3 (E) and B12 (F).

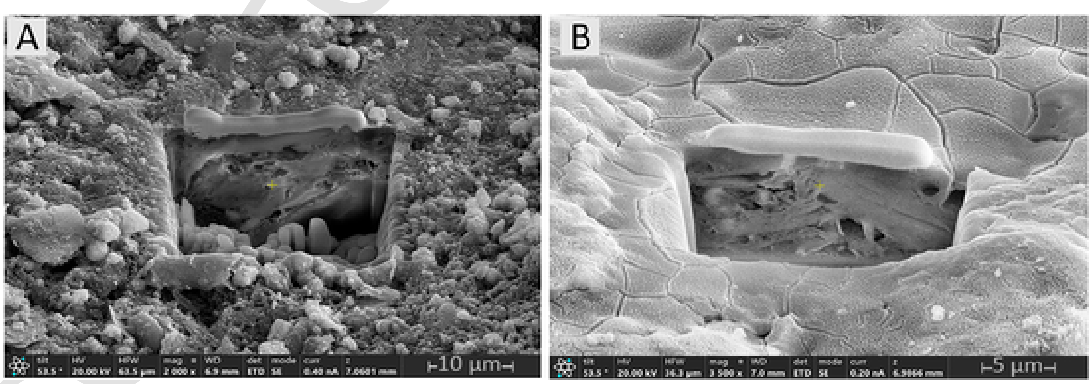


**Fig. 5.** Cross-section details of A2 treated with Paraloid B72 (A) and A3 treated with Nano Estel (B).

ited an unexpected gloss reduction, which is consistent with its substantial color change. Samples treated with Nano Estel (A3 and B12) exhibited a slight increase in gloss at 60° compared to those treated with B72 (A2).

In the context of color alteration, the a* and b* coordinates exhibited minimal contribution to the observed changes, with the L* coordinate demonstrating greater relevance. This suggests that the alterations are not indicative of hue, such as the yellowing of resin, but rather of lightness, resulting in a darker coloration. In the case of Paraloid, this change can be attributed to the resin making the material more similar in color to wet material (this occurs because the refractive index of resins is different from that of air). However, this effect was only noticeable in the lighter colored sample [35].

With regard to gloss, the untreated material itself exhibits low gloss values initially. As such, it is designated a matte surface, and the measurement to be utilized according to the standard (ISO 2813) is 85° Subsequent to the application of the treatment, there is negligible change in the values, thereby confirming that the gloss does not increase significantly. Consequently, a surface is designated as "semi-glossy" when the gloss index at 60° falls between 10 and 70 [36].

**Table 2**
Total Colour Difference (*ΔE*ab*) values.

| Sample | Before treatment | | | After treatment | | | ΔE*ab |
|---|---|---|---|---|---|---|---|
| | L | a | b | L | a | b | |
| **A1 (Un)** | 50.97 | 1.81 | 10.32 | – | – | – | – |
| **B9 (Un)** | 58.98 | 2.39 | 15.72 | – | – | – | – |
| **A2 (B72)** | 52.19 | 0.99 | 7.58 | 50.13 | 1.79 | 8.43 | 2.45 |
| **B11 (B72)** | 60.82 | 1.82 | 15.27 | 53.96 | 2.92 | 16.9 | 7.14 |
| **A3 (NE)** | 49.81 | 1.22 | 8.08 | 47.15 | 2.11 | 9.99 | 2.45 |
| **B12 (NE)** | 59.84 | 2.21 | 14.18 | 57.9 | 2.54 | 15.02 | 2.24 |

**Table 3**
Gloss measurement results.

| *Sample* | Before treatment | | After treatment | | Increase | |
|---|---|---|---|---|---|---|
| | 60° | 85° | 60° | 85° | 60° | 85° |
| ***A1 (Un)*** | 0.9 | 0.1 | – | – | – | – |
| ***B9 (Un)*** | 0.9 | 0.1 | – | – | – | – |
| ***A2 (B72)*** | 0.8 | 0.1 | 1 | 0.5 | 0.2 | 0.4 |
| ***B11 (B72)*** | 1.1 | 0.2 | 0.9 | 0.4 | −0.2 | 0.2 |
| ***A3 (NE)*** | 0.9 | 0.2 | 1.6 | 0.6 | 0.7 | 0.4 |
| ***B12 (NE)*** | 0.9 | 0.2 | 1 | 0.3 | 0.1 | 0.1 |

While there are no discernible disparities in brightness, it is imperative to deliberate on the factors that influence the brightness of treatments such as those utilized in this study. A higher refractive index has been shown to be associated with an enhancement in brightness. This phenomenon underlies the common occurrence of glossy appearances in resin treatments, as they result in the formation of a transparent film with a refractive index (typical values of ~1.5) that exceeds that of air (1.0003). However, the SEM images do not provide evidence of the formation of such a film by the Paraloid, as it has been appropriately diluted. In the case of the Nano Estel, while the silica has a similar refractive index (~1.4, as confirmed through research) and the SEM images do show the formation of a 1–2 µm film, the brightness does not increase noticeably either. It is crucial to acknowledge that the film's relative thinness and irregularity, coupled with the roughness of the surface evident at the micron scale (as observed in the SEM), contributes to the observed nano-roughness. This, in turn, is known to be associated with a decrease in brightness, which likely compensates for the potential effect of the refractory index.

*Water behavior of samples*

The findings of the study demonstrated that there was no decline in absorption observed in the treated samples in comparison to the untreated samples (Fig. 6). The objective of this evaluation was to ascertain whether alterations in water absorption would emerge as a compatibility criterion [17].

A comparative analysis of static contact angle measurements revealed only moderate differences between untreated and treated samples. Furthermore, the study found that none of the treatments rendered the surface hydrophobic. However, it was observed that both consolidants increased the hydrophobic grade (Fig. 6).

It has been demonstrated that certain consolidants possess the capacity to render the material hydrophobic, a consequence of their chemical composition or incomplete reaction. In certain applications, this phenomenon can give rise to complications, manifesting as disparate water absorption properties between the treated and untreated zones. Illustrative scenarios include materials exposed to soluble salts or volume differences arising from water absorption, which can lead to distinct zones with varied properties. In certain applications where protection from water is imperative, the exposure of ceramic pieces to the elements is to be avoided.

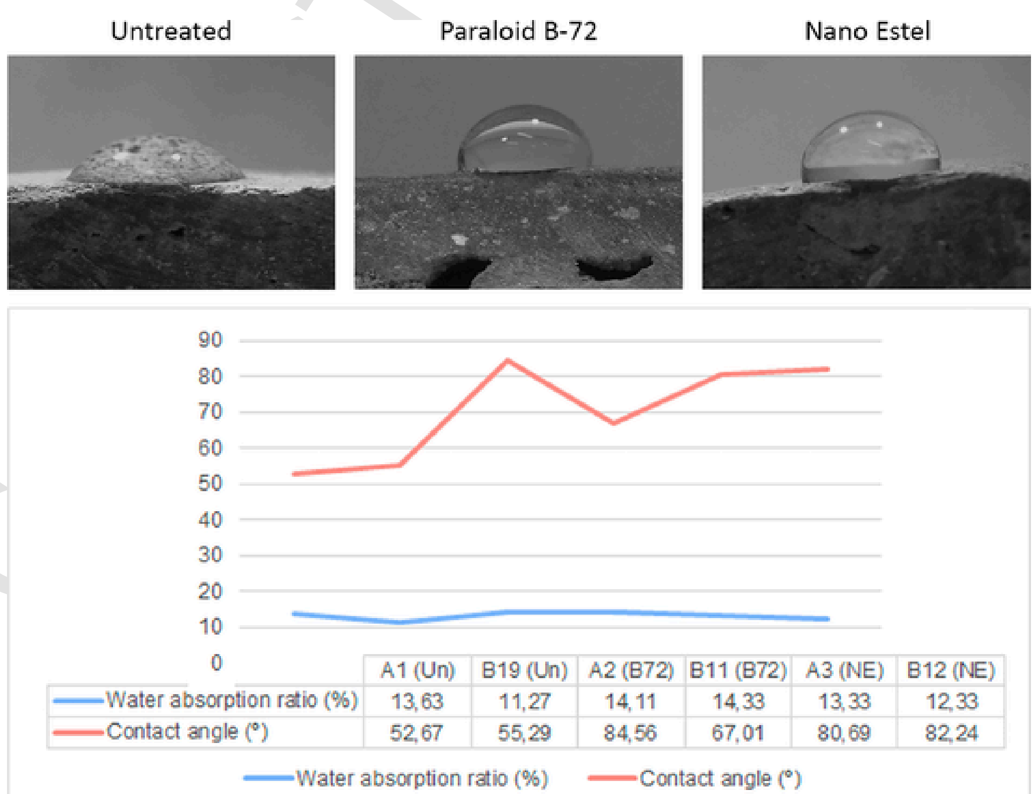


**Fig. 6.** Water absorption and contact angle results.

In the case of the consolidants utilized, both exhibit hydrophilic properties due to their chemical composition. Specifically, Nano Estel is amorphous SiO2, and Paraloid B-72 is an acrylic resin, both of which possess hydrophilic characteristics. Despite the observed discrepancies between the untreated samples, these samples do not undergo a transition to a hydrophobic state, provided that the contact angle is greater than 90° [34].

*Evaluation of strength and surface hardness*

In order to assess the enhancement of cohesion, a total of four drilling resistance measurements were obtained for each specimen. Owing to the inherent heterogeneity in the material's strength, samples of the same ceramic fragment were utilized. The treated samples exhibited augmented resistance to the surface (0–1 mm), which persisted until approximately 4 mm, at which point the resistance commenced a decline (Fig. 7). In contrast, the untreated samples demonstrated more uniform drilling resistance across their entire depth.

The results of the study indicate that the treated samples appear to increase at the surface, presumably due to the penetration of the consolidants. At greater depth, certain areas exhibited higher resistance; however, the differences were subtle, likely attributable to material inconsistencies.

The micro-indentation test revealed higher surface hardness in samples treated with Nano Estel, whereas the samples treated with B72 tended to lose surface hardness (Fig. 7). This phenomenon can be attributed to the unique surface layers formed by each consolidant. B72 forms a relatively soft acrylic resin layer, while Nano Estel creates a harder layer composed of silica nanoparticles. Notably, B72-treated samples exhibited more uniform hardness across the entire surface, suggesting a potential advantage in terms of consistency and predictability in hardness distribution.

The findings of the peeling test demonstrate that the Paraloid B72-treated samples exhibited enhanced surface cohesion in comparison to the untreated samples. Conversely, the Nano Estel-treated samples exhibited reduced peeling resistance compared to the B72-treated samples. This phenomenon may be attributed to the increased cohesion of the surface layers induced by each of the consolidants. Notably, despite demonstrating superior surface resistance in the indentation test, the Nano Estel-treated samples exhibited a higher degree of mass loss following peeling. This phenomenon may be attributed to several factors. Firstly, the samples exhibited an increased propensity for detachment when subjected to the peeling test. Secondly, the presence of microfractures within the coating could have exacerbated the detachment process. This hypothesis is further substantiated by the SEM images (Figs. 4–5). Additionally, the heterogeneity of the coating, character-

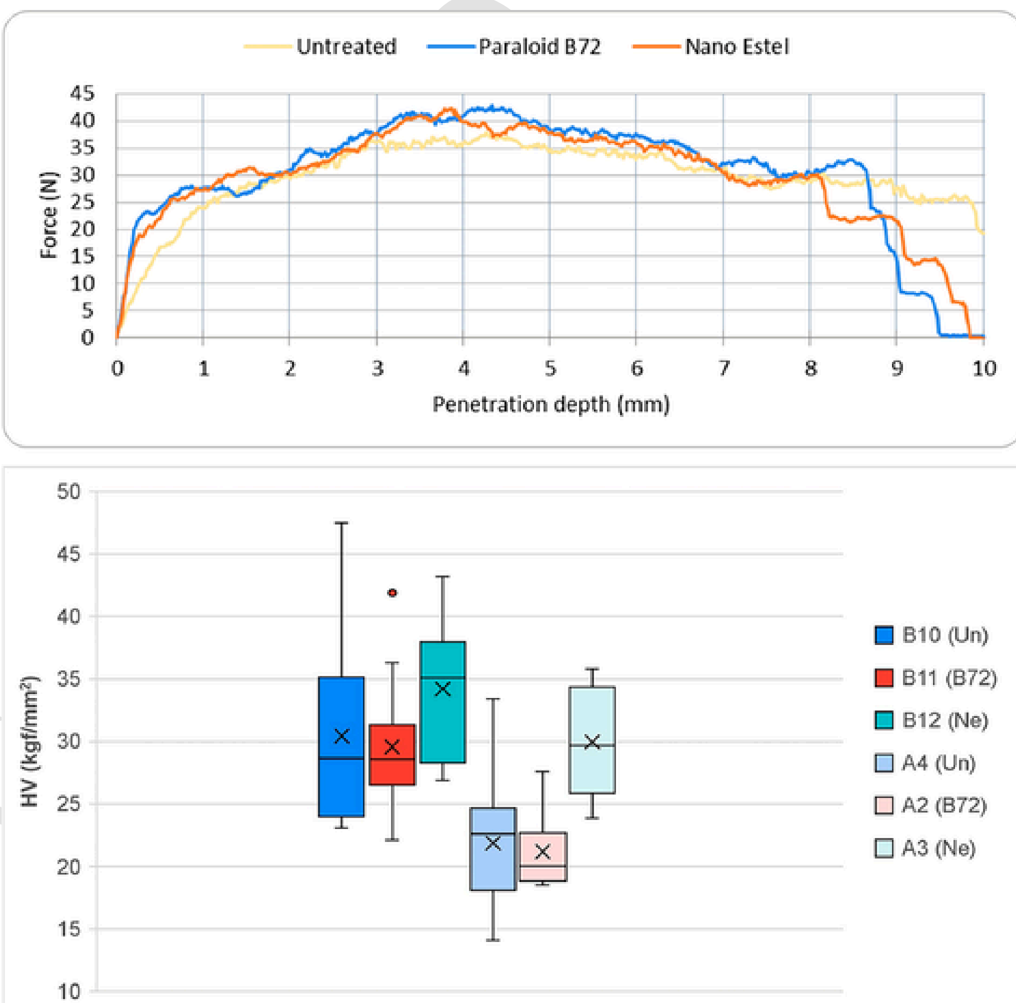


**Fig. 7.** Strength and surface hardness results. Top, drilling resistance profiles for untreated and treated samples; bottom, box plots of microhardness results from ten tests per sample.

ized by the presence of uncoated areas, may contribute to a reduction in peeling resistance.

## Conclusions

The result of this comparative study between two widely used consolidants for archaeological ceramics — Paraloid B72 and Nano Estel — demonstrates that both products have good consolidating and protective properties for the ceramic surfaces. SEM-EDX analysis reveals that Paraloid B72 forms a thin, uniform, and compact layer, while Nano Estel creates a homogeneous layer with microfractures in some areas, though it does not consistently cover the entire surface.

The observed variations in color and gloss are negligible and comparable for both products. While there is a slight color change and an increase in gloss, the changes fall within the acceptable range for conservation treatments of cultural heritage. Notably, the gloss on surfaces treated with Nano Estel is marginally higher than that of surfaces treated with Paraloid B-72. Nonetheless, these changes are not visually disruptive and remain within limits that are considered compatible with conservation standards.

The drilling resistance results indicate that both consolidants enhance surface resistance and penetrate sufficiently into the ceramic structure to provide internal reinforcement. However, Paraloid B72 demonstrates slightly better performance. This phenomenon can be attributed to Paraloid B72′s organic solvent-based composition, which facilitates deeper penetration compared to Nano Estel's water-based formulation. A notable distinction between the two consolidants was observed in the microhardness tests. Treatment with Paraloid B72 resulted in a decline in surface hardness, likely attributable to the formation of a softer acrylic resin layer on the surface. Conversely, the samples treated with Nano Estel exhibited a slight increase in surface hardness compared to untreated samples, which may be attributed to the silica nanoparticle composition of the consolidant. In the peeling test, Paraloid B72-treated samples exhibited superior cohesion and significantly reduced surface drag compared to those treated with Nano Estel. This disparity may be attributed to the enhanced surface adhesion of Nano Estel, which, despite its superior hardness, exhibits a higher propensity for detachment under mechanical stress.

A comparison of the two products reveals that they exhibit similar consolidating characteristics, rendering them suitable candidates for the conservation of ceramics from the Ses Fontanelles shipwreck, including the protection of its *Tituli Picti*. However, the decision regarding the utilization of either product should take into account several factors: Paraloid B72 has a well-documented history of long-term behavior, whereas Nano Estel is a more recent formulation and requires further long-term evaluation; Nano Estel may offer better compatibility with ceramic substrates, especially given its inorganic nature; Paraloid B7 Furthermore, at a 3 % concentration, Paraloid B72 has been observed to penetrate deeper than Nano Estel at a 1:1 ratio, potentially offering enhanced structural reinforcement. In addition, Paraloid B72 has been associated with higher toxicity risks and the presence of surface residues, while Nano Estel has been deemed less toxic and has been shown to leave minimal residues.

Treatments based on nanoparticles have potential disadvantages, as indicated in the discussion, but there is also evidence indicating their effectiveness. The other type of treatments that are more common are alkoxysilanes (e.g., ESTEL1000, Wacker OH100), which were indeed raised as an option. However, the number of samples was limited, and a selection of two types of consolidant was made. Alkoxysilanes have demonstrated superior penetration and chemical interaction with the substrate; however, they are also associated with potential issues such as slow reaction times (resulting in hydrophobic behavior or color changes), cracking during drying, and their effectiveness being contingent on the humidity conditions during the curing process.

These considerations underscore the intricacy inherent in the selection of a consolidant for conservation purposes, wherein the particularities of each case must serve as the guiding principle in the decision-making process. This study offers invaluable data that can serve as a valuable foundation for future research and contribute to the ongoing refinement of conservation practices for archaeological ceramics.

There is a paucity of research on the protection of inscriptions on ceramic material of underwater origin. Although the two products studied yield optimal results, both present disadvantages. This study represents a significant step forward in the application of consolidating products to materials of underwater provenance, pottery with inscriptions, as the alteration mechanisms and the resulting state of conservation of these materials differ considerably from those of terrestrial deposits.

In the subsequent research, two lines of investigation are proposed. First, the effectiveness of other formulas will be studied. This will be achieved by either varying the characteristics of the tests or by trying new consolidating products. Conversely, there is a need to prioritize the investigation of products with an aqueous base that can consolidate and protect both inscriptions and ceramics during the initial phase of desalination treatment. This is crucial to prevent the loss of inscriptions caused by prolonged exposure to aqueous baths. In this regard, the products utilized must be compatible with chlorides, or alternatively, facilitate the migration of salts to the exterior of the material without compromising its conservation.

## Acknowledgments

This work has been supported by the ARQUEOMALLORNAUTA project, together with the Universitat de Barcelona, Universidad de Cadiz & Universitat de les Illes Balears. This study was undertaken within the framework of the Laboratory of Historical Heritage Studies and Conservation (LEC-PH, INMAR) and the Nanomaterials Group (TEP-243) of the University of Cadiz. Projects GARVM IV (PID2022–138814OB-I00/MCIN/AEI) and MEDUSA (PCM_00031) have also been involved.

## References


[1] A.Font Jaume Soler, P. Berni, E. García Riaza, D. Bernal-Casasola, M.Á.Cau Ontiveros, J. Cardell, S. Munar Llabrés, El singular conjunto de *Tituli Picti* del pecio de Ses Fontanelles (Mallorca, islas Baleares) y su contribución a la epigrafía anfórica tardorromana hispánica, CuPAUAM 47 (2021) 287–317, https://doi.org/10.15366/cupauam2021.47.1.010.

[2] B. Liou, E.Rodríguez Almeida, Les Inscriptions Peintes Des Amphores Du Pecio Gandolfo (Almería), Mélanges de l'école Française de Rome, 2000, pp. 7–25.

[3] R. Pascual i Guasch, El Pecio Gandolfo (Almería), Pyrenae, 1968, pp. 141–155.

[4] A. Fernández Izquierdo, P. Berni Millet, A. Aguilera Martín, El pecio romano Albufereta I (siglo I d.C.): el cargamento, in: R. Azuar, O. Inglese (Eds.), El pecio romano Albufereta I (siglo I d.C.): el cargamento, Carta Arqueológica Subacuática De Alicante I (2017) 99–114.

[5] J. Martínez, Una inscripción inédita de Pecio Gandolfo. El complejo análisis delos *Tituli Picti* en ánforas salarias y el comercio de salsamenta. Cetariae 2005: Salsas y Salazones De Pescado En Occidente Durante La Antigüedad ; Actas Del Congreso Internacional (Cádiz, 7 - 9 Noviembre De 2005), Universidad de Cádiz, Cádiz, 2007, pp. 391–400.

[6] J. Martínez, J.L. Ferrero, C. Roldán, J. Álamo, Los *Tituli Picti*, estudio sobre el atramentum y su composición, Conservas, Aceite y No De La Bética En El Imperio Romano (1998) 1221–1229.

[7] S.A. Ruffolo, N. Rovella, A. Arcudi, V. Crupi, D. Majolino, M. Osanna, R. Pace, A. Pantuso, L. Randazzo, M. Ricca, N. Ruggieri, V. Venuti, M.F. La Russa, New insights to assess the consolidation of stone materials used in built heritage: the case study of ancient graffiti (*Tituli Picti*) in the archaeological site of Pompeii, Herit. Sci. 8 (2020) 49, https://doi.org/10.1186/s40494-020-00393-0.

[8] M.C. Galvín, A. Quevedo, Protocolo de conservación-restauración en un ánfora africana tardía con dipinti (isla del Fraile, Águilas). Actas Del VI Congreso Internacional de La SECAH (Zaragoza, 2022), Monografías EX OFFICINA HISPANA, Zaragoza, 2024, pp. 593–601.

[9] C.M. Belfiore, M.F. Russa, L. Randazzo, G. Montana, A. Pezzino, S.A. Ruffolo, P. Aloise, Laboratory tests addressed to realize customized restoration procedures of underwater archaeological ceramic finds, Appl. Phys. A 114 (2014) 741–752, https://doi.org/10.1007/s00339-013-7878-x.

[10] U. Sanchez-Garmendia, J.G. Iñañez, G. Arana, Alterations and contaminations in ceramics deposited in underwater environments: an experimental approach, Minerals 11 (2021) 766, https://doi.org/10.3390/min11070766.

[11] M. Secco, L. Maritan, C. Mazzoli, G.I. Lampronti, F. Zorzi, L. Nodari, U. Russo, S.P. Mattioli, Alteration processes of pottery in lagoon-like environments,

Archaeometry. 53 (2011) 809–829, https://doi.org/10.1111/j.1475-4754.2010.00571.x.

[12] C. Jaume, J.J. Fornós, Composició i textura dels sediments de platja del litoral mallorquí, Boll. Soc. Hist. Nat. Balears (1992) 93–110.

[13] D. Bernal-Casasola, M.Á. Cau Ontiveros, Estudio preliminar del cargamento del pecio tardorromano de Ses Fontanelles (Palma de Mallorca): inventario, catalogación y primeras analíticas, 2020.

[14] D. Bernal-Casasola, M.Á. Cau-Ontivero, C.D. Juan Fuertes, S. Munar Llabres, J. Cardell Perelló, E. García Riaza, J.A. Moya Montoya, J. Oviedo Callealta, J.L. Portillo-Sotelo, J.A. Retamosa Gámez, L. Fantuzzi, Repensando el comercio maritimo de Carthago Spartaria: acerca del pecio tardorromano de Ses Fontanelles (Mallorca): acerca del pecio tardorromano de Ses Fontanelles (Mallorca), Drassana 31 (2024) 156–185, https://doi.org/10.51829/Drassana.31.713.

[15] M.A. Cau-Ontiveros, D. Bernal-Casasola, A. Pecci, L. Fantuzzi, L. Picornell Gelabert, A. Valenzuela, J. Retamosa, J. Portillo-Sotelo, J. Perelló, S. Llabrés, C. De Juan, E. Riaza, Multianalytical approach to the exceptional late Roman shipwreck of Ses Fontanelles (Mallorca, Balearic Islands, Spain), Archaeol. Anthropol. Sci. 16 (2024), https://doi.org/10.1007/s12520-024-01952-3.

[16] A. Dittus, R.E. Bisbing, R. Norton, Residues from cyclododecane consolidation following desalination. Subliming Surfaces: Volatile Binding Media in Heritage Conservation, University of Cambridge Museums, 2019, pp. 101–108, https://doi.org/10.17863/cam.49280.Barberio.

[17] M. Barberio, S. Veltri, A. Imbrogno, F. Stranges, A. Bonanno, P. Antici, TiO2 and SiO2 nanoparticles film for cultural heritage: conservation and consolidation of ceramic artifacts, Coat. Technol. (2015).

[18] G. Cultrone, F. Madkour, Evaluation of the effectiveness of treatment products in improving the quality of ceramics used in new and historical buildings, J. Cult. Herit. 14 (2013) 304–310, https://doi.org/10.1016/j.culher.2012.08.001.

[19] M.M. Ibrahim, W.S. Mohamed, H.M. Mohamed, Evaluation of the efficacy of traditional and nano paraloid B72 for pottery consolidation, Int. J. Conserv. Sci. 13 (2022) 15–30.

[20] P. Manoudis, S. Papadopoulou, I. Karapanagiotis, A. Tsakalof, I. Zuburtikudis, C. Panayiotou, Polymer-silica nanoparticles composite films as protective coatings for stone-based monuments, J. Phys.: Conf. Series 61 (2007) 1361, https://doi.org/10.1088/1742-6596/61/1/269.

[21] H.M. Mohamed, N.M. Ahmed, W.S. Mohamed, M.G. Mohamed, Advanced coatings for consolidation of pottery artifacts against deterioration, J. Cult. Herit. 64 (2023) 63–72, https://doi.org/10.1016/j.culher.2023.08.014.

[22] K. Elert, F. Jroundi, C. Benavides-Reyes, E. Correa Gómez, D. Gulotta, C. Rodriguez-Navarro, Consolidation of clay-rich earthen building materials: a comparative study at the Alhambra fortress (Spain), J. Build. Eng. 50 (2022) 104081, https://doi.org/10.1016/j.jobe.2022.104081.

[23] E.H. Mohamed, Z.M. Ahmed, M.L.A. El-Latif, Evaluation of the effectiveness of traditional and nano materials used in consolidation of sandstone used in Ramesses III Temple, Karnak, Egypt, JMMCE 13 (2025) 18–30, https://doi.org/10.4236/jmmce.2025.131002.

[24] Y. Zhang, X. Li, J. Zhu, S. Wang, B. Wei, Hybrids of CNTs and acrylic emulsion for the consolidation of wall paintings, Prog. Org. Coat. 124 (2018) 185–192, https://doi.org/10.1016/j.porgcoat.2018.08.016.

[25] J.A. Poulis, Y. Mosleh, E. Cansell, D. Cimino, R. Ploeger, E.René De La Rie, C.W. McGlinchey, K. Seymour, Mechanical and physical characterization of natural and synthetic consolidants, Int. J. Adhesion Adhesives 117 (2022) 103015, https://doi.org/10.1016/j.ijadhadh.2021.103015.

[26] P. Kotlík, K. Doubravová, J. Horálek, L. Kubáč, J. Akrman, Acrylic copolymer coatings for protection against UV rays, J. Cult. Herit. 15 (2014) 44–48, https://doi.org/10.1016/j.culher.2013.01.002.

[27] P. Tiano, C. Filareto, S. Ponticelli, M. Ferrari, E. Valentini, Drilling force measurement system, a new standardisable methodology to determine the “superficial hardness” of monument stones: prototype design and validation, Int. J. Restorat. Build. Monuments 6 (2000) 115–132.

[28] E. Vasanelli, A. Calia, M. Masieri, G. Quarta, New insights into the use of drilling test for the characterization of soft lime mortars, Constr. Build. Mater. 316 (2022) 125894, https://doi.org/10.1016/j.conbuildmat.2021.125894.

[29] M. Drdácký, J. Lesák, K. Niedoba, J. Valach, Peeling tests for assessing the cohesion and consolidation characteristics of mortar and render surfaces, Mater. Struct. 48 (2015) 1947–1963, https://doi.org/10.1617/s11527-014-0285-8.

[30] UNE-EN 15886. Conservation of cultural property—test methods—colour measurement of surfaces. (2011).

[31] ISO 2813:2014. Paints and varnishes—determination of gloss value at 20 degrees, 60 degrees and 85 degrees. (2014).

[32] J.S. Pozo-Antonio, D. Noya, C. Montojo, Aesthetic effects on granite of adding nanoparticle TiO2 to Si-based consolidants (Ethyl Silicate or Nano-Sized Silica), Coatings 10 (2020), https://doi.org/10.3390/coatings10030215.

[33] E. Vassiou, D. Lazidou, E. Kampasakali, E. Pavlidou, J. Stratis, Iron gall ink from historical recipes on organic substrates and their study before and after accelerated ageing with μ-RAMAN spectroscopy and SEM-EDS, J. Cult. Herit. 66 (2024) 584–592, https://doi.org/10.1016/j.culher.2024.01.006.

[34] J.D. Rodrigues, A. Grossi, Indicators and ratings for the compatibility assessment of conservation actions, J. Cult. Herit. 8 (2007) 32–43, https://doi.org/10.1016/j.culher.2006.04.007.

[35] W.S. Mokrzycki, M. Tatol, Color difference ΔE : a survey, Mach. Graph.Vision 20 (2011) 383–411.

[36] P.M. Carmona-Quiroga, S. Martínez-Ramírez, M.I.S.D. Rojas, M.T. Blanco-Varela, Surface water repellent-mediated change in lime mortar colour and gloss, Constr. Build. Mater. 24 (2010) 2188–2193, https://doi.org/10.1016/j.conbuildmat.2010.04.039.

Journal of *Marine Science and Engineering*

MDPI

*Article*

# A Risk Assessment of Underwater Cultural Heritage for Wave-Induced Hazards: The Impact of Climate Change on Cadiz Bay

**C. Ferrero-Martín [1,*], A. Izquierdo [1], M. Bethencourt [2] and T. Fernández-Montblanc [3,*]**

[1] Department of Applied Physics, University of Cadiz, INMAR, 11510 Cadiz, Spain; alfredo.izquierdo@uca.es
[2] Department of Materials Science, Metallurgical Engineering and Inorganic Chemistry, University of Cadiz, INMAR, 11510 Cadiz, Spain; manuel.bethencourt@uca.es
[3] Earth Sciences Department, University of Cadiz, INMAR, 11510 Cadiz, Spain
* Correspondence: carmen.ferrero@uca.es (C.F.-M.); tomas.fernandez@uca.es (T.F.-M.)

**Abstract:** The combination of future changes in sea levels and wave climate in coastal areas represents one of the greatest threats to the preservation of underwater cultural heritage (UCH). This study presents a new methodology to assess climate change's impacts on UCH preservation in shallow waters, focusing on wave-induced hazards like decontextualization, scouring, and wear erosion. The approach uses hybrid downscaling of bias-corrected wave fields from the RCP4.5 and RCP8.5 CMIP5 scenarios. The methodology was applied in the Bay of Cadiz, where an overall reduction in wave energy flux was observed. However, local increases were detected in rocky outcrops and coastal areas with high UCH density. As a result, the shallow zones exhibited significant changes in decontextualization and scouring hazards. However, the most relevant risk changes were linked to wear erosion, particularly at sites on rocky outcrops near Cadiz. The methodology proposed in this study is essential for identifying areas with higher risk and for evaluating UCH preservation under future climate conditions. It offers an effective tool for discriminating sites at risk and for conducting a long-term assessment of these risks in coastal environments affected by climate change.

**Keywords:** underwater cultural heritage; climate change; hybrid downscaling; decontextualization risk; scouring risk; wear erosion risk, numerical modelling, ocean waves



Academic Editor: Eugen Rusu

Received: 29 November 2024
Revised: 29 December 2024
Accepted: 30 December 2024
Published: 14 January 2025

**Citation:** Ferrero-Martín, C.; Izquierdo, A.; Bethencourt, M.; Fernández-Montblanc, T. A Risk Assessment of Underwater Cultural Heritage for Wave-Induced Hazards: The Impact of Climate Change on Cadiz Bay. *J. Mar. Sci. Eng.* **2025**, *13*, 136. https://doi.org/10.3390/jmse13010136



## 1. Introduction

The alterations in wave climate attributable to global warming are of vital importance in coastal areas given the fundamental role of waves in shaping coastal dynamics and coastal hazards. These modifications have the potential to change coastal morphology [1] and significantly impact human activities. Assessing the impacts resulting from climate change (CC) in littoral areas is of great interest as these regions not only represent the most densely populated areas but also holds high value in terms of underwater cultural heritage (UCH).

The preservation of UCH is crucial for local communities, and it is necessary to recognize and properly appreciate its value [2] as its degradation not only implies a loss of cultural capital but also reductions in tourism and recreational, educational, and scientific activities, as well as a decline in local ecological knowledge [3]. In this regard, within the framework of the European Green Deal, it is anticipated that the preservation of cultural heritage will serve as a powerful driver of economic recovery [4]. Littoral UCH is continuously subjected to the impact of marine agents that accelerate its degradation. Among these, waves stand out as one of the main factors affecting the preservation and evolution of UCH in shallow water areas exposed to wave action [5,6]. Wave energy is released on the coast, generating three fundamental hazards for submerged cultural heritage: decontextualization, scouring, and wear erosion [7].

The complex interaction among archeological sites, suspended sediment transport, and hydrodynamic processes has been recognized and extensively investigated in the context of the in situ preservation of underwater archeological sites [5,6,8–13]. Changes in sediment budgets can compromise the stability of shipwrecks, leading to the exposure and/or burial of valuable artifacts. Additionally, scouring influences chemical and biological processes affecting the composition of the benthic community. This has effects on metallic materials [14], the corrosion rates of metal [15], and the degradation of stone materials [16] and wood [17].

CC will affect atmospheric and marine conditions, thereby impacting the conservation of coastal and underwater archeological sites. However, despite the relevance and high density of UCH in coastal areas, studies analyzing wave-induced hazards [7,18] have not considered long-term changes in environmental conditions.

Long-term changes in large-scale atmospheric circulation and in local wind patterns, coupled with changes in the occurrence and characteristics of tropical and extra-tropical cyclones, indicate long-term changes in wind wave statistics [19]. Reguero et al. [20] indicated that upper-ocean warming is altering the global wave climate, suggesting that global wave energy has increased by 0.4% per year since 1948. Global-scale studies have assessed projected changes in wave climate under different CC scenarios [21–23], finding a robust increase in the annual mean significant wave height in the Southern Hemisphere, while a reduction has been observed in the Northern Hemisphere. In the case of the North Atlantic, a reduction in significant wave height is expected by the end of the century, with greater decreases under the RCP8.5 scenario (~10%) compared to RCP4.5 (~5%) [24]. Furthermore, the extreme wave height is also projected to decrease in the northeast Atlantic [25–27], with the largest decrease being more than 1 m (12%) occurring south of 45° N [28].

These potential changes in global wave climate, along with sea level rise, underscore the need for further studies to downscale global trends regionally, analyze changes in wave climate in coastal shallow waters, and to evaluate how these changes will affect UCH preservation. Therefore, this study aims to develop a methodology to assess UCH-related risk associated with wave-induced hazards in current and future climates under climate change conditions. This methodology is tested in the Bay of Cadiz, a region characterized by a large number of UCH sites with great diversity. To achieve this, an assessment of wave climate and changes in the main hazards affecting UCH is carried out for the RCP 4.5 and RCP 8.5 scenarios. To attain the spatial resolution demanded by coastal applications and to reduce the uncertainties inherent in using global models for local-scale studies, a hybrid downscaling approach is employed to propagate waves from deep to shallow waters.

The remainder of this paper is structured as follows: The next section introduces the study area; the Methods Section describes the methodology developed and the datasets used for validation; the Results Section presents the downscaled wave climate and the assessment of CC's impact on UCH risks and hazards; the Discussion Section analyzes the applicability, limitations, and potential of the methodology based on the results; and, finally, the main findings of this study are summarized.

*Study Area*

The Bay of Cadiz is located in the southwest of Spain, extending from Punta Candor to the Sancti Petri estuary (Figure 1A). The seabed mainly consists of unconsolidated sediments, with a mean grain size ranging from very fine quartz sand to very fine gravel. Exceptions to this general pattern are localized rocky outcrops in the study area. The bay is a mesotidal shallow estuary with a maximum depth of 20 m at its seaward edge, and it is characterized by dominantly semidiurnal co-oscillating tides with amplitudes of ~1 m for the M2 component and ~0.4 m for the S2 component [29]. The typical waves in the Bay of Cadiz are wind waves with periods below 7 s and significant heights around 0.5 m in summer and 1.0 m in winter, increasing during storm events. The longer swell components of the wave spectrum have periods of 12–15 s and a height of about 1.5 m [30]. The predominant wave direction is from the west, while the most energetic waves (wave heights exceeding the 95th percentile) originate from the west-southwest (Figure 1B). Winds in the Bay of Cadiz show significant seasonality with dominant Atlantic winds from the W and WNW, and less frequent but more intense Mediterranean winds from the ESE. S-SSW winds reaching speeds of 10–20 m·s$^{-1}$ are associated with typical storm event conditions, occurring when low-pressure systems move along a SW-NE trajectory [6].

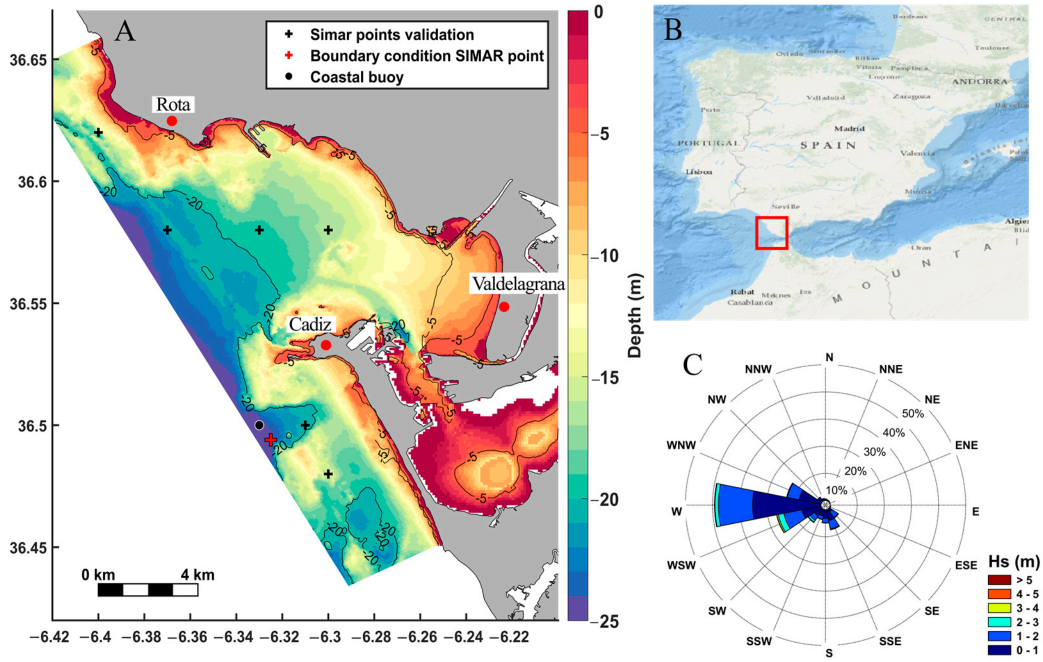


**Figure 1.** (**A**) Study area with overlaid bathymetry. (**B**) Location of the study area, Bay of Cadiz, Andalusia, Spain (**C**) A wave rose diagram of the significant wave height for a directional wave buoy.

The coastline stretching from the mouth of the Guadalquivir River to the Bay of Cadiz is one of the areas with the highest density of shipwrecks in the world owing to the presence of maritime trade routes since ancient times and the navigational hazards characteristic of this zone. The great archeological significance of Cadiz Bay drove their inclusion under the figure of maximum archeological protection of Andalusia in 2008 (BOJA nº48 of 03/10/2008, Resolution of 17 January 2008).

## 2. Methods

The proposed methodology for assessing the impact of climate change on the risk of UCH due to wave-induced hazards is structured into four phases (Figure 2). To better assess the temporal evolution of the risk, three time slices are considered: the baseline (1981–2005), the mid-century period (2036–2060), and the end-of-century (2075–2099) period. For each of these time slices, we create two climate change scenarios corresponding to the Representative Concentration Pathways (RCPs) defined in the Fifth Assessment Report (AR5) of the Intergovernmental Panel on Climate Change (IPCC): RCP4.5 and RCP8.5. RCP4.5 represents a moderate emission mitigation scenario, while RCP8.5 reflects a high-end, business-as-usual scenario.

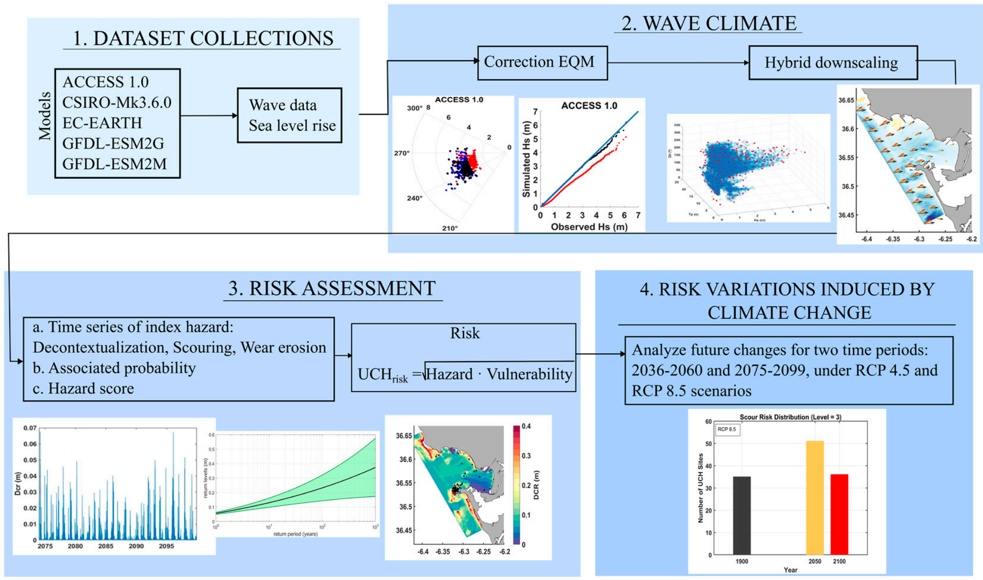


**Figure 2.** The workflow of the methodology developed to assess the impact of climate change on UCH risk due to wave-induced hazards.

In the first phase, time series of wave parameters and mean global sea level rise are extracted from the output of different global climate models corresponding to the historical runs and RCP4.5 and RCP8.5 climate change scenarios [31]. The second phase involves the treatment of RCP4.5 and RCP8.5 wave projections. This includes applying bias correction procedure, followed by propagating the bias-corrected wave field into shallow coastal waters using the hybrid downscaling method while considering sea level perturbation (tide + SLR). In the third phase, a risk assessment is performed for each of the considered hazards: decontextualization, scouring, and wear erosion. Finally, an ensemble mean is calculated using the variables and indices obtained for each of the global climate models, and the impacts of climate change on the risk are analyzed.

### *2.1. Datasets Collection*

#### Wave Data and Sea Level Rise Projections

The historical wave data used in this study are detailed in Table 1. Given the temporal limitation of available data at the coastal buoy of Cadiz (6.33° W, 36.50° N, 21 m water depth), the buoy data are used to correct the longer timeseries from Med-Wav reanalysis [32] (maintained and distributed by the Copernicus Marine Service). The corrected Med-Wav reanalysis is then utilized for bias adjustment of the global climate model wave projection data (Table 2).

**Table 1.** Summary of wave data.

| Name of Product | Spatial Resolution | Temporal Resolution | Available Period | Obser-Model | Bias Adjust | Institution |
|---|---|---|---|---|---|---|
| **Coastal buoy of Cadiz** | - | 3 h (1996–1997)/ 1 h (1998–2014) | Scalar data: 1996–2019; directional data: 2001–2014 | Obser. | none | Puertos del Estado |
| **SIMAR** | 2.8 km | 1 h | From 13-12-2005 to the present | Model | none | Puertos del Estado |
| **MEDSEA-Wav** | ~4.6 km (1/24°) | 1 h | 1993–2016 | Model | EQM by buoy | Copernicus Marine |

**Table 2.** Wave and sea level rise projections. The table includes spatial and temporal atmospheric resolution, bias adjust applied, and affiliated institution.

| Model | Atm. Spatial Resolution | Atm. Temporal Resolution | Bias Adjust | Institution |
|---|---|---|---|---|
| **ACCESS 1.0** | 1.25° × 1.9°, L38 | 3 h | EQM by MEDSEA-WAVE | CSIRO and Bureau of Meteorology |
| **CSIRO-Mk3.6.0** | 1.9° × 1.9°, L18 | 6 h | EQM by MEDSEA-WAVE | CSIRO, Industrial Research Organization & QCCCE |
| **EC-EARTH** | 1.1° × 1.1°, L62 | 3 h | EQM by MEDSEA-WAVE | EC-EARTH consortium |
| **GFDL-ESM2G** | 2° × 2.5°, L48 | 3 h | EQM by MEDSEA-WAVE | NOAA Geophysical Fluid Dynamics Laboratory |
| **GFDL-ESM2M** | 2° × 2.5°, L48 | 3 h | EQM by MEDSEA-WAVE | NOAA Geophysical Fluid Dynamics Laboratory |

The SIMAR reanalysis dataset (provided by Puertos del Estado) is used to validate the wave propagation methodology to shallow waters (downscaling) in the study area. The SIMAR dataset was generated by concatenating two simulated datasets, SIMAR-44 and WANA. To model wave fields over time, two third-generation models, WAM and WaveWatch III, are used with a nested grid scheme. These models are fed with wind data obtained from the HARMONIE-AROME mesoscale model provided by the State Meteorological Agency (AEMET, Spain). First, SIMAR point data (315047108) are used to propagate the wave time series into the Bay of Cadiz. The propagated wave field is then validated using data from SIMAR points located in intermediate waters at eight different locations within the study area (see Figure 1A). The validation period from 13 December 2005 to 1 May 2003 was selected based on the availability of SIMAR data.

The global wave projection data used in this study (Table 2) were generated using the spectral wave model WaveWatch III (version 4.18, [33]) forced by 10 m wind extracted from the Coupled Model Intercomparison Project Phase 5 (CMIP5) models ACCESS 1.0 (CSIRO-BOM, Australia), CSIRO-Mk3.6.0 (CSIRO-QCCCE, Australia), EC-EARTH (EC-EARTH consortium), GFDL-ESM2G, and GFDL-ESM2M (NOAA Geophysical Fluid Dynamics Laboratory USA). These models attain a horizontal resolution of 0.5° and a temporal resolution of 6 h [23]. The selection of these models is based on their high performance in reproducing synoptic situations and inter-annual variability across Europe [34]. CMIP5 models have a typical resolution of around 1°, which means they do not resolve tropical cyclones and poorly represent midlatitude storms [35].

In our analysis, sea level perturbation considers both tides and mean sea level. In CMIP models, ocean dynamic sea level (DSL) is diagnosed as ZOS [36]. However, DSL simulations from global climate models (GCMs) do not include the effect of sea level pressure on sea level (inverted barometer effect). ZOS varies locally due to ocean circulation and horizontal gradients, with its global mean being zero at every time step. As a result, ZOS excludes global mean sea level rise (GMSLR). The mean sea level, due to thermal expansion, changes in salinity affecting density, and water flows from the atmosphere, land, and glaciers, while always maintaining a constant total volume, is represented by ZOSGA. For this reason, as an approximation to sea level, we use the "adjusted ZOS," which is the sum of ZOS and ZOSGA. These variables were retrieved from the Earth System Grid (ESG) for the five global models previously mentioned. For the CSIRO-Mk360 model, ZOSTOGA (global mean thermosteric sea level rise; GMTSLR) is used instead of ZOSGA. Meanwhile, for the EC-EARTH model, only ZOS data are available. These are monthly data, so we interpolate them every 6 h and incorporate the tidal effect in order to later integrate them into the reconstruction of wave patterns within the bay. Furthermore, by using 3 h and 6 h wind fields to force wave models, much of the high-frequency nature of the wind climate is not captured, which could lead to substantial errors when estimating the wave energy resource in a region [37].

### 2.2. Wave Climate Reconstruction

Global wave models are the most comprehensive tools available for simulating past and future wave climate on a global scale. However, they are unable to accurately simulate wave transformation processes in intermediate and shallow waters due to their limited spatial resolution. This limitation prevents the proper representation of bathymetric and coastal features, leading to systematic biases in the coastal zone.

#### 2.2.1. Bias Adjustment of Global Wave Model

To mitigate these uncertainties, outputs from global wave models are corrected in two stages using wave buoy measurement and high-resolution wave reanalysis data (Med-WAV), involving both scalar and directional corrections. Since directional data from the buoy are limited and only available from 2001 onwards, we are unable to use directly observational data to correct the data from the global wave model, so the correction process is performed in two phases. First, the observational data (1983–2014) are used for the correction of the Med-WAV reanalysis at the location closest to the coastal buoy of Cadiz. Subsequently, in a second phase, the corrected Med-WAV model output (1993–2005) is used to adjust the bias in the global wave projections. The correction in both phases involves a scalar correction using the Empirical Quantile Mapping (EQM) method to address biases across different quantiles [38]. Subsequently, directional adjustment is carried out by dividing wave directions into 22.5° sectors. Within each sector, the difference between the mean directions of Med-WAV and global wave projections is calculated and applied as a correction [39]. The bias adjustment process is applied to the entire analysis period (baseline: 1981–2005; projections: 2006–2099), assuming that model biases and correction functions remain stationary over time.

#### 2.2.2. Hybrid Downscaling

The adjusted global wave model time series are downscaled from deep water to shallow water using the hybrid downscaling methodology proposed by Camus et al. [40]. This approach combines a numerical wave model with statistical techniques and involves selecting a limited number of cases, within the range of 189 to 254 cases, based on the slide period and model. These cases ensure a proper representation of the possible sea states through bulk wave parameters (Hs, Tp, and Dir) and sea level (SL) in deep waters using a maximum dissimilarity selection algorithm. SL accounts for the tide and sea level rise associated with each period and model.

The selected sea states are propagated in the Bay of Cadiz using the third-generation wave model SWAN ("Simulating Waves Nearshore"; [41]). The spatial domain is discretized in a regular mesh with 37.5 m resolution. The mesh resolution is selected to balance the computational cost and the accurate representation of the bathymetric features (i.e., rocky outcrops, rocky shoals, and navigation channels) in the study area. We employ 36 directional bins ($\Delta\theta = 10°$) and 24 frequencies, with logarithmic spacing from 0.05 to 1.00 Hz. The range of the frequency is representative of the wave condition measured in the study area provided by the wave buoy used for the correction of MEDSEA-WAV reanalysis (2001–2014), where most of the data exhibit peak periods shorter than 20 s (see Figure 1 and [7]). The Battjes and Janssen [42] formula represents the depth-limited wave breaking. Then, the time series of the parameters of the propagated sea states are reconstructed at each node of the grid using an interpolation technique based on radial basis functions [40].

The effectiveness and accuracy of the EQM correction procedure and the wave propagation method are evaluated according to the following statistical indicators for scalar quantities:

- The correlation coefficient ro $= \sum_{i=1}^{N} \left(S_i - \overline{S}\right)\left(R_i - \overline{R}\right)/\sigma_S\sigma_R$, where N denotes the number of data, $S_i$ and $R_i$ are simulations and reference data, $\sigma_S$ and $\sigma_R$ are their corresponding standard deviations, and the over bar denotes time averaging.
- The symmetrically normalized root mean square error, HH, introduced by Hanna and Heinold [43], $HH = \sqrt{\sum_{i=1}^{N} (S_i - R_i)^2/\sum(S_iR_i)}$. This indicator combines information on the components of average error and dispersion and is characterized by not being biased towards simulations that underestimate the average [44].
- The root mean square error (RMSE), $RMSE = \sqrt{\frac{1}{N}\left[\sum_{i=1}^{N}(S_i - R_i\right))]^2}$.
- The normalized root mean square error (NRMSE):

$$NRMSE = \sqrt{\frac{\sum_{i=1}^{N} (S_i - R_i)^2}{\sum_{i=1}^{N}(R_i)^2}}$$

- The bias (BIAS), $BIAS = \overline{S} - \overline{R}$.
- The normalized bias (NBI), $NBI = \sum_{i=1}^{N} (S_i - R_i)/\sum_{i=1}^{N} (R_i)$.
- The scatter index (SI), $SI = \sqrt{\frac{1}{N}\left[\sum_{i=1}^{N} (S_i - \overline{S}\right)(R_i - \overline{R})]^2}/\overline{R_i^2}$.

For the circular direction (θ), the normalized bias ($NBI_\theta$) and the normalized root mean square error ($NRMSE_\theta$) are normalized by employing a 2π radians angle [45]:

- $NRMSE_\theta = \sqrt{\frac{\sum_{i=1}^{N} mod_{-\pi,\pi}\left(\theta_{Si} - \theta_{Ri})\right]^2/N}{2\pi}}$
- $NBIAS_\theta = \sum_{i=1}^{N} mod_{-\pi,\pi}(\theta_{Si} - \theta_{Ri}\big)/2\pi N$ where the modulo operator $mod_{-\pi,\pi}$ indicates that if $(\theta_{Si} - \theta_{Oi}) > \pi$, a 2π angle is subtracted from the difference, and if $(\theta_{Si} - \theta_{Oi}) < -\pi$, a 2 π angle is added to the difference.

The skill scores are computed for the whole time series but also for the upper tail (>99th) in order to specifically evaluate the capability of the global wave model and downscaling methods to reproduce extreme wave conditions because of their large potential to damage UCH.

### 2.2.3. Bathymetry and Sediment Characterization

The bathymetry and seabed slope required for wave modeling were derived from multibeam echosounder data obtained during a comprehensive eco-cartographic study conducted in 2011 [46]. Additionally, seafloor mapping using multibeam backscatter data allowed for the classification of seafloor types, distinguishing between rocky and unconsolidated sediments. Sediment grain size was determined using 460 samples collected using a Van Veen grab.

### 2.2.4. Archeological Datasets

The archeological database, compiled by Fernández-Montblanc et al. [7], provides information about the main characteristics of UCH sites. This dataset includes attributes such as provenance and chronology; material composition (organized into five categories: metallic, stone, glass, ceramic, and wood/organic materials) and dominant material; metadata, including data source; and basic environmental characteristics of the sites, such depth and seabed type (when available). The archeological database comprises 56 sites of different chronologies spanning from 500 BC to AD 1820.

### 2.3. Risk Assessment

The risk assessment methodology evaluates UCH vulnerability to wave-induced hazards by calculating a risk index specific to each archeological site [7]. Each UCH site is treated as an asset susceptible to wave-induced damage.

The risk index is calculated as a function of vulnerability (determined by archeological materials, seabed slope, and type) and hazard. The analysis focuses on three primary wave-induced hazards that influence the long-term preservation of UCH: archeological decontextualization (DCR), scouring (SC), and erosive wear (EW). Each of these hazards is assessed independently without considering interactions between them. A response-based approach [47] is used, where hazard probability is directly calculated without presupposing underlying drivers or governing variables.

An indicator is defined for each hazard, and its assessment follows three sequential steps [48,49]. First, the time series of the hazard indicator are calculated based on the depth, seabed, grain size, wave characteristics, and sea level perturbation (tide + sea level rise). Second, extreme hazard probabilities are modeled using a transformed-stationary methodology. In this case, storm events are decluttered using a 72 h time window, and a constant threshold (97th percentile) is applied to select extreme events. The selected extreme events are fitted to a generalized Pareto distribution (see [50] for further details). For the case of archeological decontextualization and scour hazard, values corresponding to a 10-year return period are used as intermediate values in the extreme distribution. However, for the case of erosive wear hazard, a 1-year return period is selected to account for the continuous impact of wear on UCH materials. This reflects the high-frequency, cumulative damage of wear rather than isolated extreme events. Hazard indicators for each return period are ranked, and hazard scores (0 to 5) are assigned (see Table 3).

**Table 3.** Hazard indicator scores for decontextualization, scouring, and wear erosion.

| Critical Size of Decontextualized Object, DCR (m) RT10 | Scouring Volume, SV ($m^3$) RT10 | Erosive Wear Potential, EWP ($J/m^3$) RT1 | Scores | Level of Hazard |
|---|---|---|---|---|
| Dcr < 0.02 | SV < 0.05 | $-20 \geq$ EWP $< -18$ | 0 | None |
| $0.02 \geq$ Dcr < 0.04 | $0.05 \geq$ SV < 0.1 | $-18 \geq$ EWP $<-16$ | 1 | Low |
| $0.04 \geq$ Dcr < 0.08 | $0.1 \geq$ SV < 0.15 | $-16 \geq$ EWP $< -13.5$ | 2 | Low/medium |
| $0.08 \geq$ Dcr < 0.12 | $0.15 \geq$ SV <0.3 | $-13.5 \geq$ EWP $< -12.5$ | 3 | High/medium |
| $0.12 \geq$ Dcr < 0.16 | $0.3 \geq$ SV < 0.4 | $-12.5 \geq$ EWP $< -11.5$ | 4 | High |
| Dcr $\geq$ 0.16 | SV $\geq$ 0.4 | EWP $\geq -11.5$ | 5 | Very high |

RT10 corresponds to the value of a 10-year return period and RT1 to a 1-year return period.

Given the limited amount of information about UCH sites, we assume that all of them have the same exposure value. The risk index is calculated as the geometric square root of the product of the hazard and the vulnerability scores [48,51]. The vulnerability index ranges from 1 to 5 and is determined by the material composition of the UCH site and the specific hazard considered (refer to Table 4).

$$\text{UCHrisk} = \sqrt{\text{Hazard} \cdot \text{Vulnerability}} \quad (1)$$

**Table 4.** Vulnerability scores in common material in underwater cultural heritage sites for decontextualization, scouring, and wear erosion hazard.

| | Material Category | Material Type | Vulnerability Score |
|---|---|---|---|
| | Metallic | Gray iron | 1 |
| | Stone | Marble | 2 |
| Decontextualization | Glass | Glass | 3 |

**Table 4.** *Cont.*

| | Material Category | Material Type | Vulnerability Score |
|---|---|---|---|
| Scouring | Ceramics | Coarse ware | 4 |
| | Wood/organic material | Oak | 5 |
| | Glass | Glass | 1 |
| | Metallic | Gray iron | 2 |
| | Ceramics | Coarse ware | 3 |
| | Stone | Marble | 4 |
| | Wood/organic material | Oak | 5 |
| Wear erosion | Stone | Marble | 1 |
| | Metallic | Gray iron | 2 |
| | Ceramics | Coarse ware | 3 |
| | Glass | Glass | 4 |
| | Wood/organic material | Oak | 5 |

Sites are classified as "at risk" when $UCH_{Risk} > 3.2$, a threshold derived as the rounded geometric mean of "low" (2) and "very high" (5) classes. Higher $UCH_{Risk}$ values indicate a combination of medium to very high vulnerability and hazard classes.

### 2.4. Wave Energy Flux

Wave energy flux (WEF) serves as comprehensive indicator of wave climate within the study area.

To account for water depth effects, the WEF calculation follows the methodology outlined by Liang et al. [52]:

$$\mathrm{WEF} = \frac{\pi \rho g h H_s^2}{16 T_e}\left[1 + \frac{2kh}{\sinh(2kh)}\right] \tag{2}$$

where ρ is the water density, g is the gravitational acceleration, h is the water depth taking into account the sea level perturbation (tide and sea level rise), and $H_s$ and $T_e$ are the significant wave height and energy period, respectively, where $T_e$ can be approximated as $T_e = T_p$. $T_p$ denotes the peak period, while $k = 2\pi/L$ represents the wave number, and L is the wavelength. An extreme value analysis of the WEF time series is conducted for each grid node using the methodology in Section 2.3, focusing on a 10-year return period.

### 2.5. Variations in WEF and UCH Risk Induced by Climate Change

From the 5-member model ensemble, and for each considered period and scenario, we calculate the ensemble mean and standard deviation of WEF, hazard indices, and risk.

Model agreement is evaluated based on the coefficient of variation (CV) [53–55]. The CV is defined as the ratio of the standard deviation of the model ensemble, σ, to the ensemble mean value:

$$CV = \frac{\sigma_\alpha}{\overline{\alpha}} \tag{3}$$

where $\sigma_\alpha$ is the standard deviation of the model ensemble and $\overline{\alpha}$ is the ensemble mean. CV decreases as intra-model variability becomes a smaller fraction of the ensemble mean value, implying greater agreement among models and statistical significance of the ensemble mean value. To reduce uncertainty, values with $|CV| > 0.8$ are not considered, corresponding approximately to an average agreement of four out of five models (i.e., 80% probability).

Finally, WEF or UCHrisk variation induced by climate change is assessed by means of absolute changes ($\Delta\alpha$) for each period (mid-century and end-of-century periods) corresponding to the RCP 4.5 and RCP 8.5 scenarios ($\alpha_{RCP}$) with respect to baseline values ($\alpha_{baseline}$):

$$\Delta\alpha = \alpha_{RCP} - \alpha_{baseline} \quad (4)$$

## 3. Results

### *3.1. Wave Climate*

#### 3.1.1. EQM Correction

Global wave model outputs, with and without correction, were compared with corrected Med-WAV (Figure 3). The uncorrected global models underestimate significant wave height (Hs) values and extreme Hs values. This is particularly noticeable for ACCESS 1.0, GFDL-ESM2G, and GFDL-ESM2M (Figure 3A,D,E; also, see Table S1 in SM) where the EQM largely improves the Hs NBI index. CSIRO-Mk3.6.0 and EC-EARTH show better performance (HH ~0.8; Table S1 in SM) with an EQM improvement of ~5% in HH.

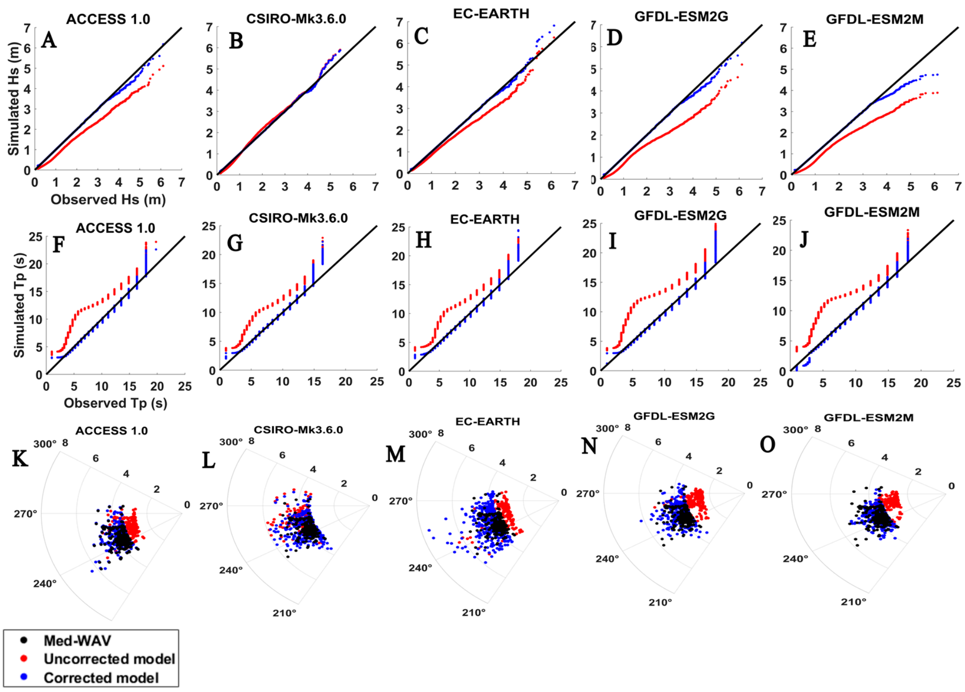


**Figure 3.** Q-Q plot of significant wave height (Hs) (**A**–**E**) peak period (Tp) (**F**–**J**). Polar plot for wave heights exceeding 99th percentile (**K**–**O**). Uncorrected global wave model (red), corrected global wave model (blue), and Med-WAV reanalysis (black) are represented.

The uncorrected global wave model outputs overestimate, in general, the peak period (Tp) (NRMSE ~0.6), with EQM correction improving ~10% for CSIRO-Mk3.6.0 and EC-EARTH models (Figure 3G,H) and ~18% for the rest of the models (Figure 3F,I,J).

For the case of wave directions with an Hs greater than or equal to the 99th percentile (P99), the uncorrected models show a deviation of approximately 25° ($NRMSE_\theta$ ~39°; Figure 3K,L,N,O). After applying the EQM correction, this improves by 63% ($NRMSE_\theta$ ~ 20°), except for the case of EC-EARTH, where the bias increases by 66% (Figure 3M). Overall, in the study area, EC-EARTH and CSIRO-Mk3.6.0 show the best agreement with the Med-WAV reanalysis, both with and without correction. Specifically, CSIRO shows better alignment for Hs, especially for extreme values. On the other hand, EC-EARTH performs better in capturing extreme Tp values compared to the other models. Regarding wave direction, EC-EARTH shows the best agreement among the uncorrected models. However, after applying the EQM correction, CSIRO achieves the most accurate alignment with the observed data.

#### 3.1.2. The Validation of the Wave Propagation Method

This section summarizes the performance of the wave propagation method to reproduce average and extreme wave conditions (>99th). This step is crucial for reducing the uncertainties associated with global models, which do not accurately represent wave transformation processes in intermediate and shallow waters due to their limited spatial resolution. Due to the lack of observational data within the bay, SIMAR points were selected to assess the model's performance within the bay. SIMAR reanalysis was selected as the best alternative due to its wide spatial distribution in the region, good temporal coverage, and frequent use in wave studies conducted across the Iberian Peninsula (e.g., [56,57]). Table 5 shows the average values of skill scores for Hs, Tp, and Dir calculated in the eight SIMAR locations in the Bay of Cadiz. The validation indicates a good performance, especially for extreme wave conditions, for Hs (ro = 0.95; HH = 0.07) and Tp (ro = 0.82; HH = 0.18). The biases related to Hs are practically zero, while Tp is generally affected by a negative bias. However, the results are quite adequate. The wave direction shows also good agreement, although performance worsens in extreme events.

**Table 5.** Statistical scores for mean and extreme significant wave height, peak period, and mean direction between propagated series and SIMAR points.

| | **ro** | **HH** | **NRMSE** | **NBI** |
|---|---|---|---|---|
| Hs (m) | 0.96 | 0.18 | 0.18 | 0.05 |
| P99 Hs | 0.95 | 0.07 | 0.07 | −0.02 |
| Tp (s) | 0.82 | 0.28 | 0.26 | −0.14 |
| P99 Tp (s) | 0.83 | 0.18 | 0.17 | −0.11 |
| Dir (°) | - | - | 2.60 | −1.72 |
| P99 Dir (°) | - | - | 13.42 | 38.39 |

### *3.2. Changes in WEF*

#### Scalar and Direction Climate

The WEF associated with a 10-year return period (RT10) shows maxima (around $15 \times 10^4$ $Wm^{-1}$) in the outer domain and by the rocky outcrops outside the bay. Minima appear by the coast, where shallow depths and the wave breaking limit reduce the WEF, and inside the bay due to the protective effect of the Cadiz tombolo against wave front propagation (Figure 4A). Under RCP4.5, the WEF associated with RT10 shows a general decrease, slightly increasing only by some coastal stretches, over rocky outcrops and inside the bay (Figure 4B,C). The general WEF decrease is weaker in the end-of-century period than in the mid-century period as a result of the larger SLR. The mid-century RCP8.5 WEF change pattern replicates that of the RCP4.5 WEF, but with a weaker general decrease and slightly larger increments located in the shallower areas (Figure 4E). By the end-of-century period in RCP8.5, there is a general WEF increase, with maxima located at shallow waters and rocky outcrops (Figure 4F). Additionally, a southward shift in the WEF direction is evident in all cases except for RCP4.5 in the mid-future period.

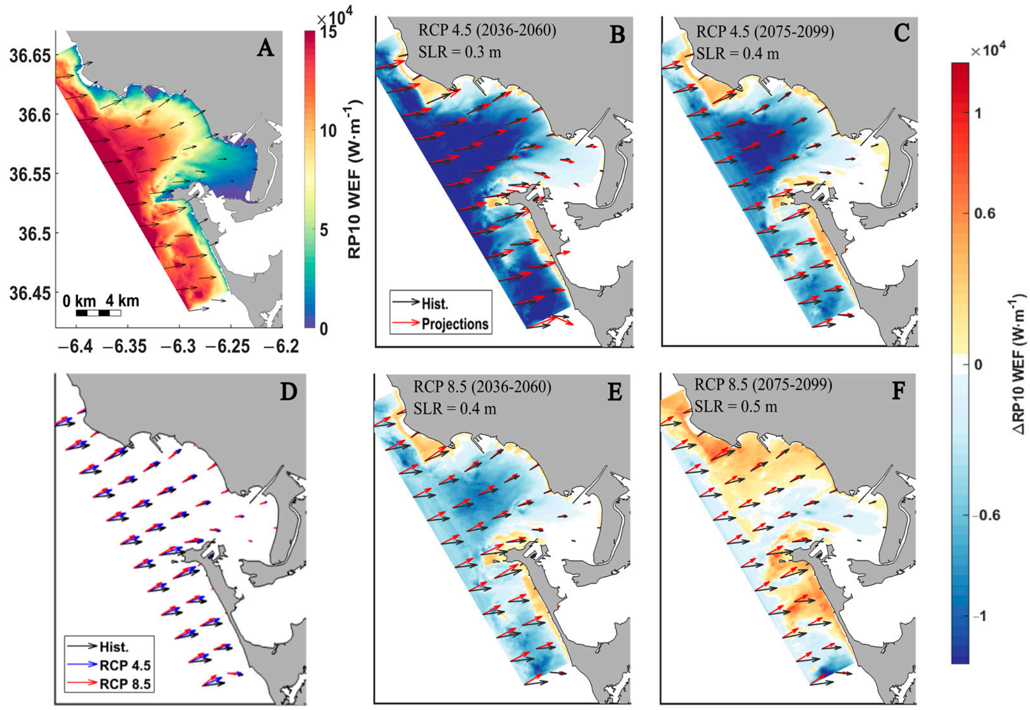


**Figure 4.** (**A**) The wave energy flux corresponding to the 10-year return period and the mean direction associated with the 99th percentile or greater of the WEF (black arrow). The absolute change and mean direction associated with the 99th percentile of the WEF for each simulation (red arrow): (**B**) the 2036–2060 period of the RCP 4.5 scenario, (**C**) the 2075–2099 period of the RCP 4.5 scenario, (**E**) the 2036–2060 period of the RCP 8.5 scenario, and (**F**) the 2075–2099 period of the RCP 8.5 scenario. The sea level rise (SLR) for each period is shown in the bottom left corner and represents the average increase calculated from the five global models used. (**D**) The mean direction associated with the 99th percentile or greater of the WEF for the historical period (black arrow), the end-of-century period of the RCP 4.5 scenario (blue arrow), and the end-of-century period of the RCP 8.5 scenario (red arrow).

Such a direction shift also takes place for the most energetic waves. Figure 4D shows the average of the directions of the extreme waves (>99th) for the historical period and for the end-of-century period in the RCP 4.5 and RCP 8.5 scenarios. While the most energetic waves impact the bay from the west (ca. 263°) during the historical period, they come from 250° in the RCP 4.5 scenario and from 240° in RCP 8.5. This change in the direction of incident waves in the bay leads to an alteration in their propagation within the Bay of Cadiz, resulting in a greater impact on the areas of Rota, Cadiz, and the surrounding areas.

To determine how the increase in sea level affects wave propagation, the methodology is repeated without considering the SLR (Figure 5). These results show a larger WEF decrease than when considering SLR, which is particularly notable over the shallow coastal areas and rocky outcrops, where the depth increase due to SLR makes a substantial contribution to the WEF.

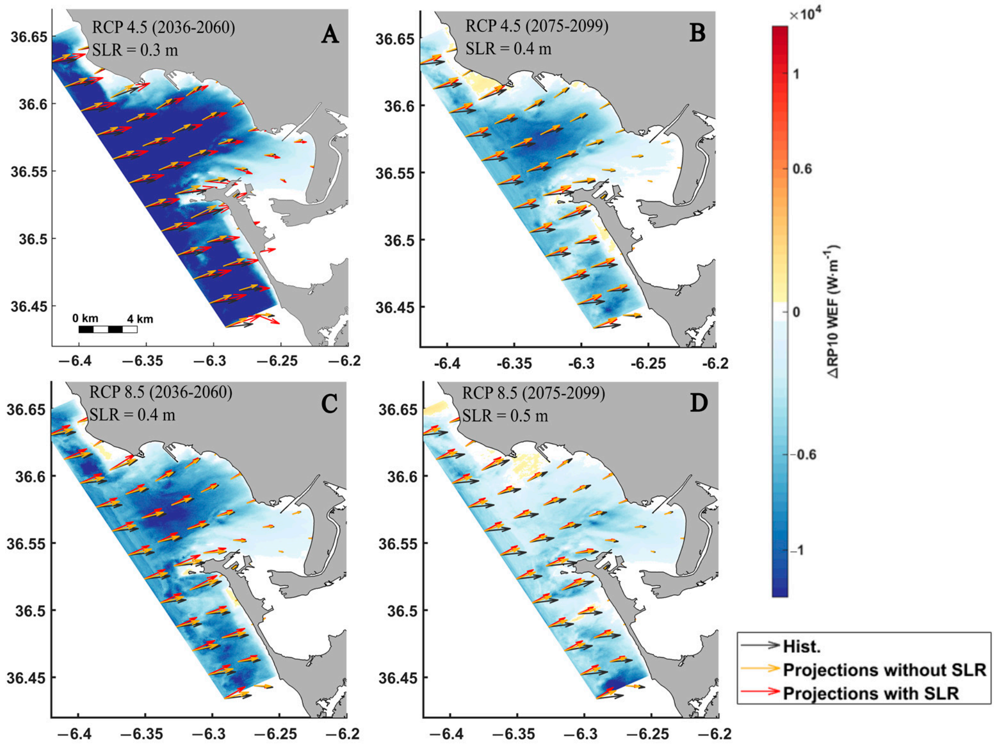


**Figure 5.** The absolute changes in wave energy flux (WEF) with and without sea level rise are shown for the following: (**A**) the 2036–2060 period of the RCP 4.5 scenario, (**B**) the 2075–2099 period of the RCP 4.5 scenario, (**C**) the 2036–2060 period of the RCP8.5 scenario, and (**D**) the 2075–2099 period of the RCP 8.5 scenario. The mean direction associated with the 99th percentile or greater of the WEF for the historical period (black arrow) is shown with sea level rise (red arrow) and without SLR (orange arrow) projections.

### *3.3. Hazard Assessment*

#### 3.3.1. Decontextualization Hazard

We relate decontextualization hazard (DCR) to the maximum critical diameter of an object (we assume sphericity) susceptible to be displaced due to wave action over a 10-year return period (Figure 6). All projections present a slight general reduction in the value of DCR, except for the bay's interior and shallower areas, where local significant increases (up to 25%) are observed compared to the historical period. This result aligns with the projected general reduction in the WEF and its local increase in shallower areas. In shallow areas, the wave-induced bottom stress is larger, but as wave orbital velocity strongly attenuates with an increasing depth (Figure S1), DCR is reduced throughout the rest of the bay. The mid-century RCP4.5 and the end-of-century RCP8.5 scenarios exhibit the most substantial hazard changes. However, the result of these changes reflects only as a decrease in the bay area under a hazard score of 3 and an increase in the bay area as a hazard score of 2. The percentages of the bay area classified as high and very high hazards (scores of 4 and 5; Figure 6D) remain nearly unchanged.

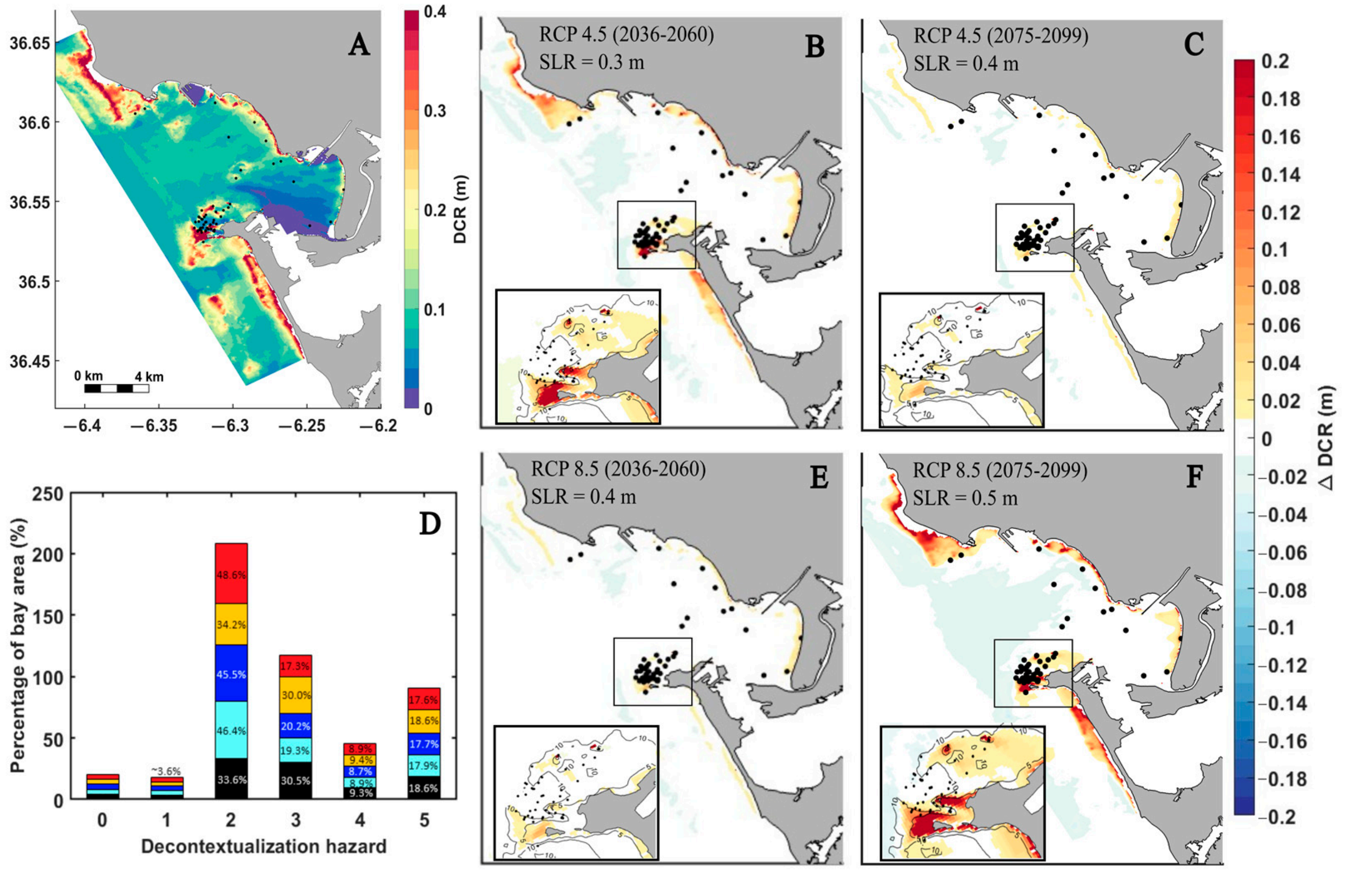


**Figure 6.** (**A**) A map of decontextualization hazard (the critical diameter of an object moved under wave action) for the historical period. The absolute change in this hazard for (**B**) the 2036–2060 period of the RCP 4.5 scenario, (**C**) the 2075–2099 period of the RCP 4.5 scenario, (**E**) the 2036–2060 period of the RCP 8.5 scenario, and (**F**) the 2075–2099 period of the RCP 8.5 scenario compared with the historical period. The black points indicate the locations of UCH sites. (**D**) A histogram of the hazard at UCH sites and hazard classes. The sea level rise (SLR) for each period is shown in the bottom left corner and represents the average increase calculated from the five global models used.

### 3.3.2. Scour Hazard

The scour hazard indicator is represented by the potential volume of scouring corresponding to a 10-year return period (Figure 7). In general, no significant changes in the scouring hazard are observed in the Bay of Cadiz for all the scenarios and periods considered. However, locally significant variations are identified in the shallower areas of the bay (less than 5 m) and in some rocky outcrops, such as those located off Rota and Cadiz. In these areas, the RCP 4.5 scenario for the mid-century period and the RCP 8.5 scenario for the end-of-century period show mostly positive anomalies, while the RCP 4.5 scenario for the end-of-century period and the RCP 8.5 scenario for the mid-century period exhibit mostly negative anomalies. These changes result in an increase in the percentage of the bay area classified as a high hazard level (4), accompanied by a decrease in the very high hazard level (5; Figure 7D). The percentage change is very similar across all periods; however, it is at the end of the century for the RCP 4.5 scenario where the greatest reduction in the percentage of the bay area classified as having a very high hazard level is observed.

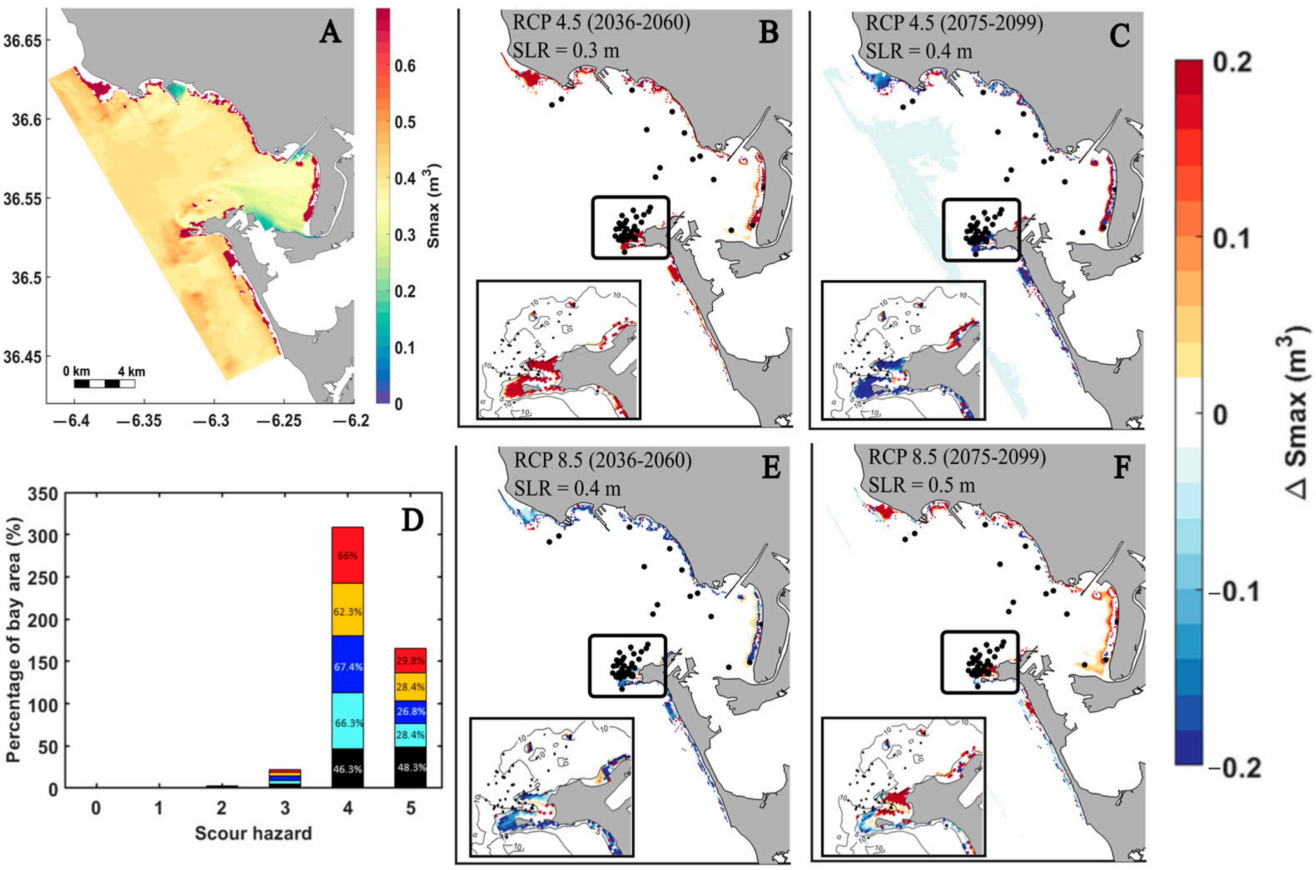


**Figure 7.** (**A**) A map of the scour hazard (scour volume) for the historical period. The absolute change in this hazard for (**B**) the 2036–2060 period of the RCP 4.5 scenario, (**C**) the 2075–2099 period of the RCP 4.5 scenario, (**E**) the 2036–2060 period of the RCP 8.5 scenario, and (**F**) the 2075–2099 period of the RCP 8.5 scenario compared with the historical period. The black points indicate the locations of UCH sites. (**D**) A histogram of the hazard at UCH sites and hazard classes. The sea level rise (SLR) for each period is shown in the bottom left corner and represents the average increase calculated from the five global models used.

### 3.3.3. Wear Erosion Hazard

The indicator erosive wear hazard is analyzed by means of the erosion potential (Figure 8). This hazard exhibits the most significant future changes compared to the historical period. The changes for both scenarios are predominantly positive, indicating an increase in the magnitude of the hazard. These changes are more intense near the southern entrance of the bay, where most UCH sites are located. However, significant negative anomalies are also recorded at the rocky outcrops off the city of Cadiz, being more pronounced in the RCP 8.5 scenario, particularly towards the end of the century. As a result, there is an increase in the percentage of the bay area that will be affected by a very high hazard level (5) for erosive wear hazard (Figure 8D).

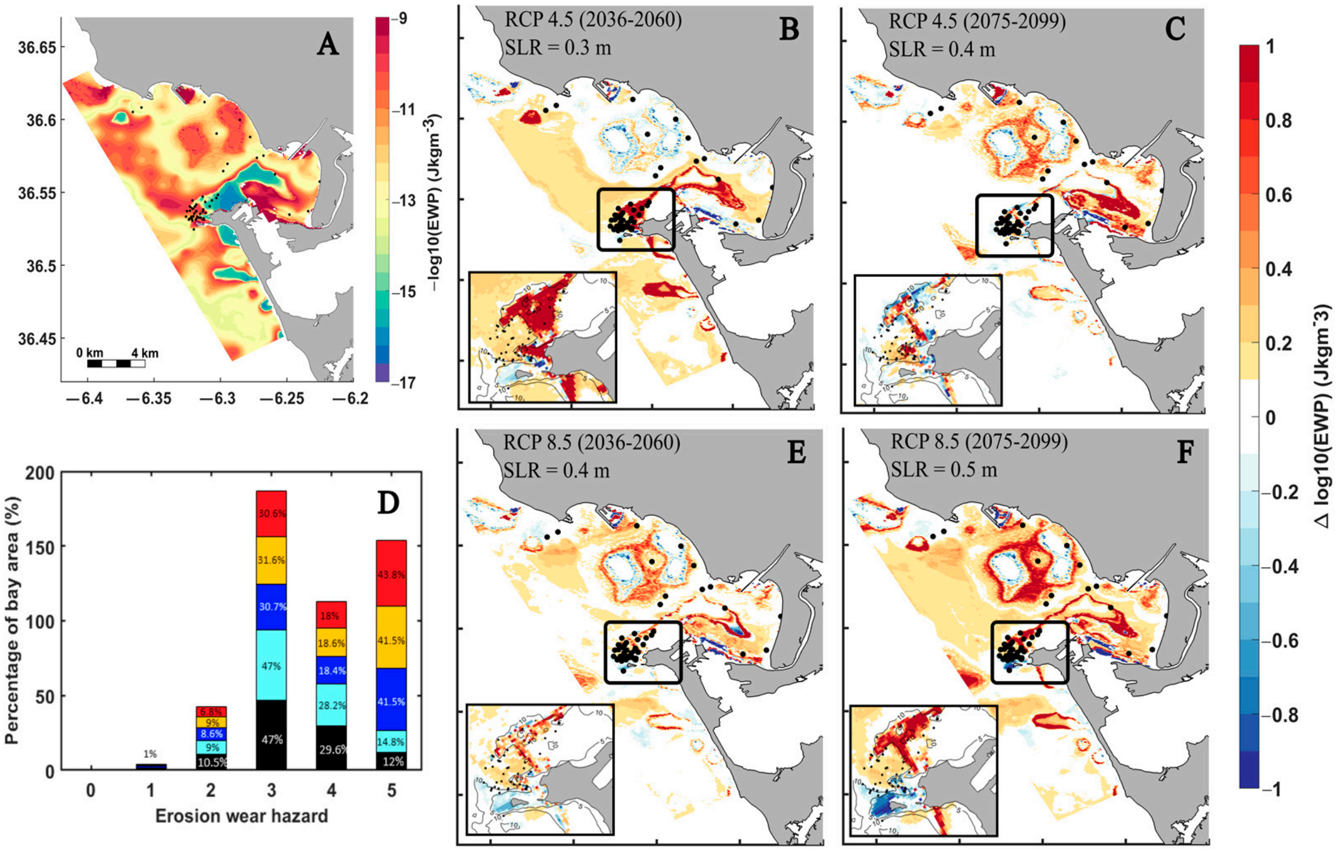


**Figure 8.** (**A**) A map of the erosive wear hazard (log of erosive wear potential) for the historical period. The absolute change in this hazard for (**B**) the 2036–2060 period of the RCP 4.5 scenario, (**C**) the 2075–2099 period of the RCP 4.5 scenario, (**E**) the 2036–2060 period of the RCP 8.5 scenario, and (**F**) the 2075–2099 period of the RCP 8.5 scenario compared with the historical period. The black points indicate the locations of UCH sites. (**D**) A histogram of the hazard at UCH sites and hazard classes. The sea level rise (SLR) for each period is shown in the bottom left corner and represents the average increase calculated from the five global models used.

### *3.4. UCH Risk Assessment*

Figure 9 shows the underwater cultural heritage risks (UCHRs) at the studied sites in the Bay of Cadiz. During the historical period, there are 7 UCH sites under decontextualization risk, 19 under scour risk, and 21 under wear erosion risk ($UCHR_{DE}$, $UCHR_{SC}$, and $UCHR_{EW} > 3.2$). The sites under risk are mainly located around the city of Cadiz, with the exception of two located by the eastern coast of the Bay of Cadiz (Valdelagrana). In general, the sites present lower risk values associated with decontextualization and larger risk values associated with erosion wear. In the historical period, the distribution of risks is skewed towards low values for $UCHR_{DE}$, centered near 3.2 for $UCH_{SC}$, and it presents a bimodal distribution with a narrow peak at 3.8 for $UCH_{WE}$. In the future scenarios, the number of UCH sites at risk (>3.2) remains unchanged for the risks of decontextualization and scouring. However, for wear erosion under the RCP 4.5 scenario, the number of sites at risk increases from 21 to 23 at the mid-century period and to 22 at the end of the century (Figure 10). The sites turning under risk are located at the rocky outcrops off the city of Cadiz and are related to strong and very local changes in erosion wear hazard (see Figure 8).

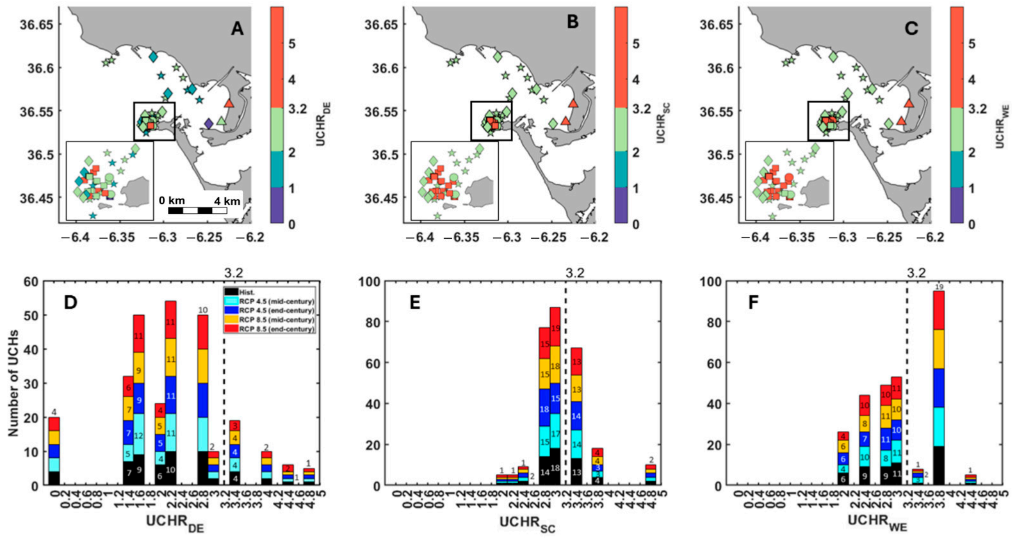

**Figure 9.** (**A**) The decontextualization risk ($UCHR_{DE}$) for UCH sites located in the Bay of Cadiz, (**B**) the scour risk ($UCHR_{SC}$) for UCH sites, and (**C**) the wear erosion risk ($UCHR_{EW}$) for UCH sites. Warm colors indicate a higher risk index, and different shapes refer to the prevalent material (diamonds, metallic material; squares, ceramic material; filled circles, stone; triangles, wood/organic material; pentagons, unknown material). Accumulated graphs of the classification of UCHs in terms of the risks of (**D**) decontextualization, (**E**) scour, and (**F**) wear erosion.

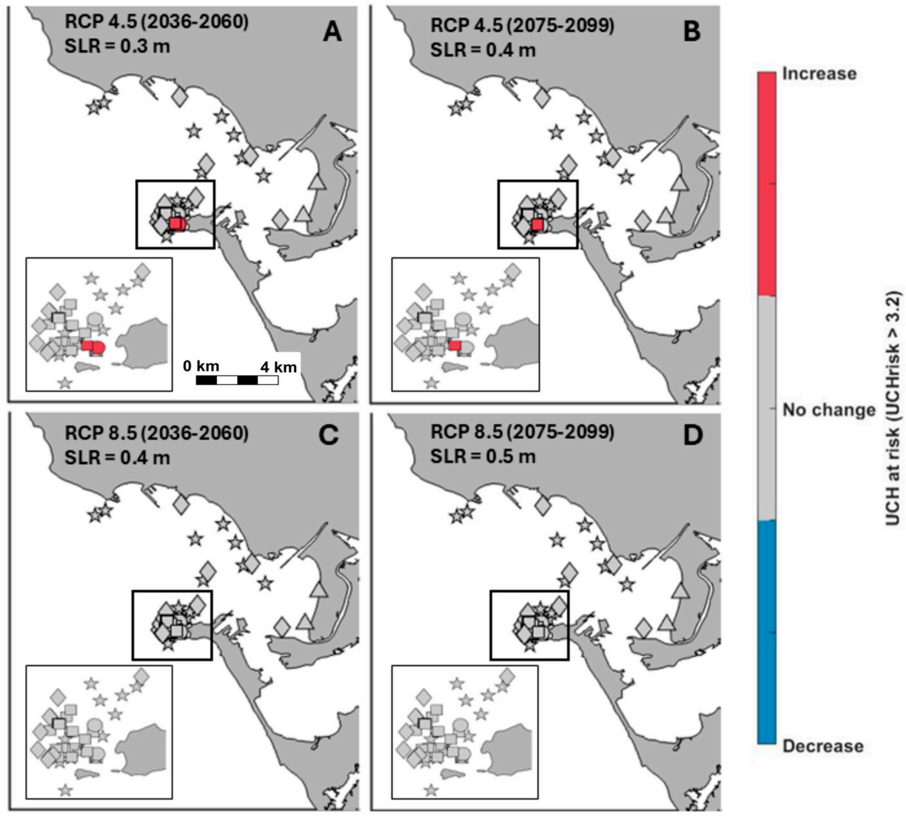


**Figure 10.** The erosive wear risk ($UCHR_{EW}$) for UCH sites located in the Bay of Cadiz. The absolute change for (**A**) the 2036–2060 period of the RCP 4.5 scenario, (**B**) the 2075–2099 period of the RCP 4.5 scenario, (**C**) the 2036–2060 period of the RCP 8.5 scenario, and (**D**) the 2075–2099 period of the RCP 8.5 scenario compared with the historical period. The sea level rise (SLR) for each period is shown in the bottom left corner and represents the average increase calculated from the five global models used.

## 4. Discussion

This study outlines a methodology to evaluate the impacts of climate change on UCH through wave-induced hazards. It is based on a hybrid downscaling [33] of the bias-corrected wave fields [31,32] corresponding to the CMIP5 RCP4.5 and RCP8.5 scenarios. Both scenarios show a robust reduction in significant wave height in the North Atlantic (see also Wang et al. [58] and Lemos et al. [59]). However, most UCH is placed in shallow coastal areas, where the wave fields will be affected by shallow water processes, coastline orientation and bathymetric relief, and by the concurrent SLR; therefore, downscaling the global wave fields is necessary. Our results show that the use of the EQM method and the directional adjustment improved the global wave model outputs (see Table S1). This correction is key for obtaining accurate high-resolution wave propagated fields. This is corroborated by the validation of the wave downscaled fields against SIMAR reanalysis points (Table 3). The validation presented very good results for both mean wave climate and for extreme P99 waves.

Changes in the future WEF are the result of the combination of changes in projected significant wave height, energy (~peak) period, and depth changes (Equation (2)). As changes in peak period are small, the resulting WEF changes result from the opposite contribution of significant wave height diminution and sea level rise. The result is a general reduction in the WEF in the Bay of Cadiz, with local increases in shallow rocky outcrops and coastal areas, where the depth increase by SLR allows for the higher waves to appear without breaking. These results are consistent with the findings of Aarns et al. [25] and Chaigneau et al. [28], who demonstrated that changes in depth induced by sea level rise can lead to higher wave amplitudes near the coast. The impact of sea level variations is substantially more important on extreme significant wave heights over the wide continental shelf where shallow water dynamics prevail, particularly in large tidal range areas [28]. However, our results show the important contribution of SLR to changes in the WEF in a mesotidal bay (see Figure 5). This demonstrates that accurate high-resolution wave propagation fields enable better capture of the nonlinear interactions between sea level and waves. Additionally, there is a shift in the direction of incident waves, increasing the wave exposure in certain areas of Cadiz and Rota. Along with these changes in the WEF, there is a reduction in wave orbital velocity (Figure S1; increased depth and decreased Hs), which is a fundamental parameter for UCH risk assessment, either by direct impact of orbital velocity on object decontextualization or scour and wear erosion impact.

Our assessment of the impact of wave climate changes on UCH hazards shows limited consequences. For decontextualization and scour hazard, the changes in the critical diameter of the moved object and in scour volume are, in general, small. There are considerable changes only in those locations (shallows and coastal areas), where the hazard indicators already had maximum values and had very high hazard levels (>0.16 m and > 0.4 $m^3$ for decontextualization and scour indicators, respectively (Table 3; Fernández-Montblanc et al. [7])). Therefore, it is not surprising that remarkable increases, such as the 0.2 m increase in the decontextualization hazard indicator, have no clear impact on the distribution of hazard levels within the bay. Indeed, there is a strong sensitivity of the hazard change assessment to the definition of the hazard level classes.

Hazard and vulnerability thresholds are mainly determined through the likelihood of exceeding certain predefined thresholds [60] and active participation from local users and stakeholders responsible for the management and conservation of cultural heritage [61,62]. The reliance on hazard categories based on historical data assumes that future conditions will follow probability distributions similar to those of the past. However, climate change is significantly altering these distributions, increasing the frequency and intensity of extreme events, which shifts hazard thresholds toward higher categories. This could explain why there are not important changes in UCH risk under the considered climate change scenarios; however, this does not imply that such changes are not occurring. The lack of quantitative data on observed and projected impacts under different climate scenarios limits the ability to establish acceptable risk thresholds and develop effective adaptation and mitigation strategies [63].

The proposed methodology represents the first attempt, to our knowledge, for addressing UCH risk assessment for wave-induced hazards under climate change projections, and it is not free of shortcomings and limitations. Some of the methodological limitations related to the simplifications applied to hazard quantification are exposed in [7]. Here, it is necessary to add the assumption used in the EQ bias correction that the wave parameter distributions (period, height, and direction) will remain unchanged in the future. Clearly, this may not be the case in real life, but it is the simplest and best choice we have. It is important to note that our study did not include the contribution of storm surge to the water level, as it was initially omitted due to the predominant influence of tides on the total water level in the study area. Additionally, the lack of consideration for possible changes in morphodynamic processes, such as those related to depth and the interaction between waves and currents, represents a significant limitation in our analysis. It is crucial to recognize that the relative rise in sea level could be mitigated by sediment accommodation depending on the sediment budget, which would have a substantial impact on coastal dynamics. Furthermore, the impact of waves on sea level was not included; if this factor was incorporated into the ocean model, it would result in a higher sea level, which, in turn, would have a greater effect on wave propagation and the hazards affecting underwater cultural heritage. For future research, it would be valuable to conduct a multiple-hazard analysis to assess whether risky events occur simultaneously in a cascading or cumulative manner over time. In risk assessment studies, multidisciplinary approaches and the use of precise data are of utmost importance for managing the impacts of climate change in coastal contexts [64]. Furthermore, the proposed methodology must be expanded to other environmental factors influencing UCH preservation (i.e., water temperature, salinity, and pH) to provide a holistic methodology to assess the evolution of the natural hazards affecting the in situ preservation of UCH in the context of CC.

## 5. Conclusions

Future changes in sea levels and wave climate in coastal areas represent one of the major threats to the preservation and conservation of underwater cultural heritage (UCH). However, understanding how these changes will unfold in the long term and the associated hazards remains a challenge due to the complexity and interaction between the processes involved. In this study, we propose an innovative methodology to assess the risk to UCH in shallow waters based on hybrid downscaling using an ensemble derived from CMIP5 wave projections. This methodology applies downscaling to bias-corrected wave fields corresponding to the RCP4.5 and RCP8.5 scenarios from CMIP5. The approach focuses on the primary wave-induced hazards, considering their impact on the long-term preservation of UCH: archeological decontextualization, scouring, and wear erosion. To evaluate the effects of climate change, we compare the historical period (1981–2005) with two future periods, the mid-century (2036–2060) and end-of-century (2075–2099) periods, for both scenarios.

First, we present and validate the methodology for wave correction and propagation. Our results show that the use of the EQM method and directional adjustment improved the global wave model outputs, which is essential for obtaining high-resolution and accurate propagated wave fields. Second, we assessed changes in wave climate, observing a general reduction in the wave energy flux in the Bay of Cadiz, with local increases in rocky outcrops and coastal areas, where the increased depth due to SLR allows higher waves to appear without breaking. This finding highlights the importance of high-resolution wave fields in capturing the nonlinear interactions between sea level and waves. Additionally, a shift in the direction of incident waves was identified, increasing wave exposure in certain areas of Cadiz and Rota.

In the bay, a general reduction in wave orbital velocity is observed due to increased depth and decreased significant wave height. This parameter is crucial for assessing UCH risk, as most UCH sites lie on the seafloor. However, in shallow areas, where the highest density of UCH is concentrated, significant changes in decontextualization and scouring hazards are observed. The only relevant changes in risk (UCHrisk > 3.2) are associated with wear erosion, particularly in the sites located on rocky outcrops off the city of Cadiz, where local changes in this hazard are marked. However, the strict definitions of hazard level classes, which shift thresholds toward higher categories, do not adequately reflect the changes in hazard classes. This factor could explain why significant changes in UCH risk are not observed under the considered climate change scenarios, although this does not imply that such changes are not occurring.

In conclusion, this study emphasizes the importance of conducting local-scale studies that incorporate the nonlinear interactions between sea level and waves in extreme wave studies, as these interactions could lead to local trends in wave energy that are different to those indicated in the global projections. This could result in variations in the impact on UCH risk in specific areas. It is also crucial to consider the high sensitivity in defining hazard level classes, as inadequate definitions may mask significant changes in UCH risk. The obtained results offer the possibility to iteratively redefine the hazard level and/or hazard classes accounting for future changes. The proposed methodology offers a tool to perform a quantitative analysis on the impact of CC on UCH rather than the existing state-of-the-art qualitative approach and method. The methodology developed in this study therefore represents a crucial step toward a more accurate understanding and more effective management of UCH risk in the face of climate change, an area that has been relatively overlooked until now. This tool provides innovative approaches for decision making in the protection and conservation of this invaluable heritage.

**Supplementary Materials:** The following supporting information can be downloaded at https://www.mdpi.com/article/10.3390/jmse13010136/s1.

**Author Contributions:** Conceptualization, C.F.-M., A.I. and T.F.-M.; methodology, C.F.-M., A.I. and T.F.-M.; software, C.F.-M., A.I. and T.F.-M.; validation, C.F.-M., A.I. and T.F.-M.; formal analysis, C.F.-M., A.I. and T.F.-M.; investigation, C.F.-M., A.I. and T.F.-M.; resources, C.F.-M., A.I., M.B. and T.F.-M.; data curation, C.F.-M., A.I. and T.F.-M.; writing—original draft preparation, C.F.-M.; writing—review and editing, C.F.-M., A.I., M.B. and T.F.-M.; visualization, C.F.-M.; supervision, A.I. and T.F.-M.; project administration, M.B. and T.F.-M.; funding acquisition, M.B. and T.F.-M. All authors have read and agreed to the published version of the manuscript.

**Funding:** This study was partially supported by the Ministry of Science and Innovation thorough the project "Vulnerability of littoral cultural heritage to environmental agents: impact of climate change (VOLICHE)" (PID2020-117812RB-I00/AEI/10.13039/501100011033).

**Institutional Review Board Statement:** Not applicable.

**Informed Consent Statement:** Not applicable.

**Data Availability Statement:** The raw data supporting the conclusions of this article will be made available by the authors, without undue reservation.

**Acknowledgments:** The authors acknowledge Lorenzo Mentaschi for his useful suggestions and for providing the global wave projection dataset used in this study.

**Conflicts of Interest:** The authors declare no conflicts of interest.

## References


1. Thiébot, J.; Idier, D.; Garnier, R.; Falqués, A.; Ruessink, B.G. The Influence of Wave Direction on the Morphological Response of a Double Sandbar System. *Cont. Shelf Res.* **2012**, *32*, 71–85. [CrossRef]
2. Pérez-Reverte Mañas, C.; Cerezo Andreo, F.; López Osorio, P.; González Gallero, R.; Mariscal Rico, L.; Arévalo González, A. Underwater Cultural Heritage as an Engine for Social, Economic and Cultural Development. State of Research at the University of Cadiz (Andalusia, Spain). *Heritage* **2021**, *4*, 2676–2690. [CrossRef]
3. Khakzad, S.; Pieters, M.; Van Balen, K. Coastal Cultural Heritage: A Resource to Be Included in Integrated Coastal Zone Management. *Ocean Coast. Manag.* **2015**, *118*, 110–128. [CrossRef]
4. Potts, A.L.A. *European Cultural Heritage Green Paper*; Europa Nostra: The Hague, The Netherlands; Brussels, Belgium, 2021.
5. Quinn, R. The Role of Scour in Shipwreck Site Formation Processes and the Preservation of Wreck-Associated Scour Signatures in the Sedimentary Record—Evidence from Seabed and Sub-Surface Data. *J. Archaeol. Sci.* **2006**, *33*, 1419–1432. [CrossRef]
6. Fernández-Montblanc, T.; Quinn, R.; Izquierdo, A.; Bethencourt, M. Evolution of a Shallow Water Wave-Dominated Shipwreck Site: Fougueux (1805), Gulf of Cadiz. *Geoarchaeology* **2016**, *31*, 487–505. [CrossRef]
7. Fernández-Montblanc, T.; Bethencourt, M.; Izquierdo, A. Underwater Cultural Heritage Risk Assessment Methodology for Wave-Induced Hazards: The Showcase of the Bay of Cadiz. *Front. Mar. Sci.* **2022**, *9*, 1005514. [CrossRef]
8. Fernández-Montblanc, T.; Izquierdo, A.; Quinn, R.; Bethencourt, M. Waves and Wrecks: A Computational Fluid Dynamic Study in an Underwater Archaeological Site. *Ocean Eng.* **2018**, *163*, 232–250. [CrossRef]
9. McNinch, J.E.; Wells, J.T.; Trembanis, A.C. Predicting the Fate of Artefacts in Energetic, Shallow Marine Environments: An Approach to Site Management. *Int. J. Naut. Archaeol.* **2006**, *35*, 290–309. [CrossRef]
10. Astley, A.J. The Taphonomy of Historic Shipwreck Sites. Ph.D. Thesis, University of Southampton, Southampton, UK, 2016.
11. Bates, C.R.; Lawrence, M.; Dean, M. Robertson Geophysical Methods for Wreck-Site Monitoring: The Rapid Archaeological Site Surveying and Evaluation (RASSE) Programme. *Int. J. Naut. Archaeol.* **2011**, *40*, 404–416. [CrossRef]
12. Quinn, R.; Smyth, T.A.G. Processes and Patterns of Flow, Erosion, and Deposition at Shipwreck Sites: A Computational Fluid Dynamic Simulation. *Archaeol. Anthropol. Sci.* **2018**, *10*, 1429–1442. [CrossRef]
13. Plets, R.; Quinn, R.; Forsythe, W.; Westley, K.; Bell, T.; Benetti, S.; McGrath, F.; Robinson, R. Robinson Using Multibeam Echo-Sounder Data to Identify Shipwreck Sites: Archaeological Assessment of the Joint Irish Bathymetric Survey Data. *Int. J. Naut. Archaeol.* **2011**, *40*, 87–98. [CrossRef]
14. Bethencourt, M.; Fernández-Montblanc, T.; Izquierdo, A.; González-Duarte, M.M.; Muñoz-Mas, C. Study of the Influence of Physical, Chemical and Biological Conditions That Influence the Deterioration and Protection of Underwater Cultural Heritage. *Sci. Total Environ.* **2018**, *613–614*, 98–114. [CrossRef] [PubMed]
15. Angelini, E.; Grassini, S.; Tusa, S. Underwater Corrosion of Metallic Heritage Artefacts. In *Corrosion and Conservation of Cultural Heritage Metallic Artefacts*; Woodhead Publishing: Cambridge, UK, 2013; pp. 236–259. [CrossRef]
16. Cámara, B.; De Buergo, M.Á.; Bethencourt, M.; Fernández-Montblanc, T.; La Russa, M.F.; Ricca, M.; Fort, R. Biodeterioration of Marble in an Underwater Environment. *Sci. Total Environ.* **2017**, *609*, 109–122. [CrossRef]
17. Björdal, C.G.; Nilsson, T. Reburial of Shipwrecks in Marine Sediments: A Long-Term Study on Wood Degradation. *J. Archaeol. Sci.* **2008**, *35*, 862–872. [CrossRef]
18. Alexandrakis, G.; Petrakis, S.; Kampanis, N. Preliminary Assessment of Wave Energy Hazards in a Shallow Underwater Cultural Heritage Site. In Proceedings of the 2023 IMEKO TC-4 International Conference on Metrology for Archaeology and Cultural Heritage, Rome, Italy, 19–21 October 2023.
19. Weisse, R.; von Storch, H. *Marine Climate and Climate Change, Storms, Wind Waves and Storm Surges*; Praxis Publishing: Chichester, UK, 2010.
20. Reguero, B.G.; Losada, I.J.; Méndez, F.J. A Recent Increase in Global Wave Power as a Consequence of Oceanic Warming. *Nat. Commun.* **2019**, *10*, 205. [CrossRef]
21. Casas-Prat, M.; Wang, X.L.; Swart, N. CMIP5-Based Global Wave Climate Projections Including the Entire Arctic Ocean. *Ocean Model.* **2018**, *123*, 66–85. [CrossRef]
22. Hemer, M.A.; Fan, Y.; Mori, N.; Semedo, A.; Wang, X.L. Projected Changes in Wave Climate from a Multi-Model Ensemble. *Nat. Clim. Change* **2013**, *3*, 471–476. [CrossRef]
23. Mentaschi, L.; Vousdoukas, M.I.; Voukouvalas, E.; Dosio, A.; Feyen, L. Global Changes of Extreme Coastal Wave Energy Fluxes Triggered by Intensified Teleconnection Patterns. *Geophys. Res. Lett.* **2017**, *44*, 2416–2426. [CrossRef]
24. Morim, J.; Hemer, M.; Wang, X.L.; Cartwright, N.; Trenham, C.; Semedo, A.; Young, I.; Bricheno, L.; Camus, P.; Casas-Prat, M.; et al. Robustness and Uncertainties in Global Multivariate Wind-Wave Climate Projections. *Nat. Clim. Change* **2019**, *9*, 711–718. [CrossRef]

25. Aarnes, O.J.; Reistad, M.; Breivik, Ø.; Bitner-Gregersen, E.; Ingolf Eide, L.; Gramstad, O.; Magnusson, A.K.; Natvig, B.; Vanem, E. Projected Changes in Significant Wave Height toward the End of the 21st Century: Northeast A Tlantic. *J. Geophys. Res. Ocean.* **2017**, *122*, 3394–3403. [CrossRef]
26. Morim, J.; Vitousek, S.; Hemer, M.; Reguero, B.; Erikson, L.; Casas-Prat, M.; Wang, X.L.; Semedo, A.; Mori, N.; Shimura, T.; et al. Global-Scale Changes to Extreme Ocean Wave Events Due to Anthropogenic Warming. *Environ. Res. Lett.* **2021**, *16*, 074056. [CrossRef]
27. Meucci, A.; Young, I.R.; Hemer, M.; Kirezci, E.; Ranasinghe, R. Projected 21st Century Changes in Extreme Wind-Wave Events. *Sci. Adv.* **2020**, *6*, eaaz7295. [CrossRef] [PubMed]
28. Chaigneau, A.A.; Law-Chune, S.; Melet, A.; Voldoire, A.; Reffray, G.; Aouf, L. Impact of Sea Level Changes on Future Wave Conditions along the Coasts of Western Europe. *Ocean Sci.* **2023**, *19*, 1123–1143. [CrossRef]
29. Alvarez, O.; Izquierdo, A.; Tejedor, B.; Mañanes, R.; Tejedor, L.; Kagan, B.A. The Influence of Sediment Load on Tidal Dynamics, a Case Study: Cádiz Bay. *Estuar. Coast. Shelf Sci.* **1999**, *48*, 439–450. [CrossRef]
30. Kagan, B.A.; Tejedor, L.; Álvarez, O.; Izquierdo, A.; Tejedor, B.; Mañanes, R. Weak Wave–Tide Interaction Formulation and Its Application to Cádiz Bay. *Cont. Shelf Res.* **2001**, *21*, 697–725. [CrossRef]
31. Meinshausen, M.; Smith, S.J.; Calvin, K.; Daniel, J.S.; Kainuma, M.L.T.; Lamarque, J.-F.; Matsumoto, K.; Montzka, S.A.; Raper, S.C.B.; Riahi, K.; et al. The RCP Greenhouse Gas Concentrations and Their Extensions from 1765 to 2300. *Clim. Change* **2011**, *109*, 213–241. [CrossRef]
32. Korres, G.; Ravdas, M.; Zacharioudaki, A. Mediterranean Sea Waves Hindcast (CMEMS MED-Waves) 2019. [Data Set]. [CrossRef]
33. Tolman, H.L. User Manual and System Documentation of WAVEWATCH III R Version 4.18. Available online: https://polar.ncep.noaa.gov/waves/wavewatch/manual.v4.18.pdf (accessed on 29 December 2024).
34. Perez, J.; Menendez, M.; Mendez, F.J.; Losada, I.J. Evaluating the Performance of CMIP3 and CMIP5 Global Climate Models over the North-East Atlantic Region. *Clim. Dyn.* **2014**, *43*, 2663–2680. [CrossRef]
35. De Winter, R.C.; Sterl, A.; Ruessink, B.G. Wind Extremes in the North Sea Basin under Climate Change: An Ensemble Study of 12 CMIP5 GCMs. *JGR Atmos.* **2013**, *118*, 1601–1612. [CrossRef]
36. Griffies, S.M.; Danabasoglu, G.; Durack, P.J.; Adcroft, A.J.; Balaji, V.; Böning, C.W.; Chassignet, E.P.; Curchitser, E.; Deshayes, J.; Drange, H.; et al. OMIP Contribution to CMIP6: Experimental and Diagnostic Protocol for the Physical Component of the Ocean Model Intercomparison Project. *Geosci. Model Dev.* **2016**, *9*, 3231–3296. [CrossRef]
37. Goward Brown, A.J.; Neill, S.P.; Lewis, M.J. The Influence of Wind Gustiness on Estimating the Wave Power Resource. *Int. J. Mar. Energy* **2013**, *3–4*, e1–e10. [CrossRef]
38. Lobeto, H.; Menendez, M.; Losada, I.J. Future Behavior of Wind Wave Extremes Due to Climate Change. *Sci. Rep.* **2021**, *11*, 7869. [CrossRef] [PubMed]
39. Fanti, V.; Ferreira, Ó.; Kümmerer, V.; Loureiro, C. Improved Estimates of Extreme Wave Conditions in Coastal Areas from Calibrated Global Reanalyses. *Commun. Earth Environ.* **2023**, *4*, 151. [CrossRef]
40. Camus, P.; Mendez, F.J.; Medina, R. A Hybrid Efficient Method to Downscale Wave Climate to Coastal Areas. *Coast. Eng.* **2011**, *58*, 851–862. [CrossRef]
41. Booij, N.; Ris, R.C.; Holthuijsen, L.H. A Third-Generation Wave Model for Coastal Regions: 1. Model Description and Validation. *J. Geophys. Res.* **1999**, *104*, 7649–7666. [CrossRef]
42. Battjes, J.A.; Janssen, J.P. Energy Loss and Set-up Due to Breaking of Random Waves. In Proceedings of the Sixteenth Conference on Coastal Engineering, Hamburg, Germany, 27 August–3 September 1978; pp. 569–587. [CrossRef]
43. Hanna, S.R.; Heinold, D.W. *Development and Application of a Simple Method for Evaluating Air Quality*; Technical Report; American Petroleum Institute, Health and Environmental Affairs Dept: Washington, DC, USA, 1985.
44. Mentaschi, L.; Besio, G.; Cassola, F.; Mazzino, A. Problems in RMSE-Based Wave Model Validations. *Ocean Model.* **2013**, *72*, 53–58. [CrossRef]
45. Mentaschi, L.; Besio, G.; Cassola, F.; Mazzino, A. Performance Evaluation of Wavewatch III in the Mediterranean Sea. *Ocean Model.* **2015**, *90*, 82–94. [CrossRef]
46. Spanish Ministry of Agriculture, Food and Environment. Data from: Plan de Ecocartografías del litoral Español. 2012. Available online: https://www.miteco.gob.es/es/costas/temas/proteccion-costa/ecocartografias/ecocartografia-cadiz.html (accessed on 29 December 2024).
47. Garrity, N.J.; Battalio, R.; Hawkes, P.J.; Roupe, D. Evaluation of Event and Response Approaches to Estimate the 100-Year Coastal Flood for Pacific Coast Sheltered Waters. In *Coastal Engineering 2006*; World Scientific Publishing Company: San Diego, CA, USA, 2007; pp. 1651–1663. [CrossRef]
48. Viavattene, C.; Jiménez, J.A.; Ferreira, O.; Priest, S.; Owen, D.; McCall, R. Selecting Coastal Hotspots to Storm Impacts at the Regional Scale: A Coastal Risk Assessment Framework. *Coast. Eng.* **2018**, *134*, 33–47. [CrossRef]
49. Ferreira, O.; Viavattene, C.; Jiménez, J.A.; Bolle, A.; Das Neves, L.; Plomaritis, T.A.; McCall, R.; Van Dongeren, A.R. Storm-Induced Risk Assessment: Evaluation of Two Tools at the Regional and Hotspot Scale. *Coast. Eng.* **2018**, *134*, 241–253. [CrossRef]

50. Mentaschi, L.; Vousdoukas, M.; Voukouvalas, E.; Sartini, L.; Feyen, L.; Besio, G.; Alfieri, L. The Transformed-Stationary Approach: A Generic and Simplified Methodology for Non-Stationary Extreme Value Analysis. *Hydrol. Earth Syst. Sci.* **2016**, *20*, 3527–3547. [CrossRef]
51. Gornitz, V. Vulnerability of the East Coast, U.S.A. to Future Sea Level Rise. *J. Coast. Res.* **1990**, *9*, 201–237.
52. Liang, B.; Shao, Z.; Wu, G.; Shao, M.; Sun, J. New Equations of Wave Energy Assessment Accounting for the Water Depth. *Appl. Energy* **2017**, *188*, 130–139. [CrossRef]
53. Alfieri, L.; Burek, P.; Feyen, L.; Forzieri, G. Global Warming Increases the Frequency of River Floods in Europe. *Hydrol. Earth Syst. Sci.* **2015**, *19*, 2247–2260. [CrossRef]
54. Knutti, R.; Sedláček, J. Robustness and Uncertainties in the New CMIP5 Climate Model Projections. *Nat. Clim. Change* **2013**, *3*, 369–373. [CrossRef]
55. Vousdoukas, M.I.; Voukouvalas, E.; Annunziato, A.; Giardino, A.; Feyen, L. Projections of Extreme Storm Surge Levels along Europe. *Clim. Dyn.* **2016**, *47*, 3171–3190. [CrossRef]
56. Del Río, L.; Plomaritis, T.A.; Benavente, J.; Valladares, M.; Ribera, P. Establishing Storm Thresholds for the Spanish Gulf of Cádiz Coast. *Geomorphology* **2012**, *143–144*, 13–23. [CrossRef]
57. Ribeiro, A.S.; deCastro, M.; Costoya, X.; Rusu, L.; Dias, J.M.; Gomez-Gesteira, M. A Delphi Method to Classify Wave Energy Resource for the 21st Century: Application to the NW Iberian Peninsula. *Energy* **2021**, *235*, 121396. [CrossRef]
58. Wang, X.L.; Feng, Y.; Swail, V.R. Changes in Global Ocean Wave Heights as Projected Using Multimodel CMIP5 Simulations. *Geophys. Res. Lett.* **2014**, *41*, 1026–1034. [CrossRef]
59. Lemos, G.; Semedo, A.; Dobrynin, M.; Behrens, A.; Staneva, J.; Bidlot, J.-R.; Miranda, P.M.A. Mid-Twenty-First Century Global Wave Climate Projections: Results from a Dynamic CMIP5 Based Ensemble. *Glob. Planet. Change* **2019**, *172*, 69–87. [CrossRef]
60. Raposeiro, P.D.; Fortes, C.J.; Reis, M.T.; Ferreira, J.C. Development of A Methodology to Evaluate the Flood Risk at the Coastal Zone. Available online: https://repositorio.lnec.pt/handle/123456789/1002230 (accessed on 29 December 2024).
61. Sevieri, G.; Galasso, C.; D'Ayala, D.; De Jesus, R.; Oreta, A.; Grio, M.E.D.A.; Ibabao, R. A Multi-Hazard Risk Prioritisation Framework for Cultural Heritage Assets. *Nat. Hazards Earth Syst. Sci.* **2020**, *20*, 1391–1414. [CrossRef]
62. Canesi, L.; Sardella, A.; Vogler, R.; Kaiser, A.; Vaccaro, C.; Bonazza, A. Hazard Analysis and Vulnerability Assessment of Cultural Landscapes Exposed to Climate Change-Related Extreme Events: A Case Study of Wachau (Austria). *Heritage* **2024**, *7*, 1917–1934. [CrossRef]
63. Bonazza, A.; Sardella, A. Climate Change and Cultural Heritage: Methods and Approaches for Damage and Risk Assessment Addressed to a Practical Application. *Heritage* **2023**, *6*, 3578–3589. [CrossRef]
64. Pica, A.; Lämmle, L.; Burnelli, M.; Del Monte, M.; Donadio, C.; Faccini, F.; Lazzari, M.; Mandarino, A.; Melelli, L.; Perez Filho, A.; et al. Urban Geomorphology Methods and Applications as a Guideline for Understanding the City Environment. *Land* **2024**, *13*, 907. [CrossRef]

# Participación en congresos

TechnoHeritage

RSEQ Real Sociedad Española de Química

GEQP

# TechnoHeritage2024

Sept 25-27th | SANTIAGO DE COMPOSTELA

# BOOK OF ABSTRACTS

https://technoheritage2024.com/

Edited by:
Massimo Lazzari
Maite Maguregui
José Santiago Pozo Antonio
Jorge Sanjurjo Sánchez
Patricia Sanmartín Sánchez



ISBN 978-84-1188-028-2
Depósito Legal: VG 487-2024

# Tests for the Efficacy of Three Consolidation Methods for the Organic Collection of Ses Fontanelles Shipwreck (Mallorca, Balearic Islands, Spain)

E. Fernández-Tudela (1), M. Goñalons Lapiedra(2), L. C. Zambrano Valdivia(3), D. Bernal-Casasola (2), M. Á. Cau-Ontiveros (4), E. García Riaza (5), J. Cardell Perelló (6) and M. Bethencourt Núñez (2)

(1) *Center for Underwater Archaeology, Andalusian Institute of Historical Heritage (IAPH), Spain*
(2) *University of Cadiz, Spain*
(3) *Department of Conservation and Restoration, Museum of Cadiz, Spain*
(4) *ICREA and ERAAUB-IAUB of the University of Barcelona (UB), Spain*
(5) *University of the Balearic Islands, Spain*
(6) *Council of Mallorca, Spain*

For decades, polyethylene glycol (PEG) has been the most widely used consolidation product, providing great advances and problems in the conservation of organic material. However, there are other products that for decades have been introduced or revised, focusing with a special interest on wood, and to a lesser extent in other materials such as leather, textile fibers or seeds. Some of them are the polyxylsilanes (plastination method) or the natural resins liked pine resin (acetone-colophony method).

This study delves into the conservation of organic materials recovered from the Ses Fontanelles Shipwreck (Mallorca, Balearic Islands, Spain) as part of the ARQUEOMALLORNAUTA project. The wreck site yields a diverse array of organic artifacts, ranging from cellulosic materials such as wood and plant fibers to protein-based elements like leather.

Three methods were selected for their suitability, availability, and ease of use: PEG 400 (saturation and air drying), plastination method (Biodur® S15+S3) and acetone-rosin method.

Samples of leather, vegetable fabrics (grass mats and ropes) and wood were treated to test the effectiveness of each of the products and materials to propose a protocol for the whole collection. The experiments were carried out at the Laboratory for Studies and Conservation of Historical Heritage (LEC-PH).

Scanning electron microscopy and digital microscopy were used to examine the surface and structural and dimensional changes. The Anti-Shrink Efficacy Index (ASE %) was used to evaluate the efficacy of the treatments.

All methods are effective in treating the materials studied. Attending on common aspects such as hygrometric stability or physical qualities (color, brightness, or elasticity), PEG and plastination result in relatively elastic materials, while rosin results in rigid and brittle materials. Color and gloss are also affected in all cases, with PEG being the treatment in which the materials darken the most, followed by rosin. In the case of plastination, no chromatic variation is observed but there is an increase in brightness. In all cases these parameters are acceptable.

# Assessment of the effectiveness of consolidants for the preservation of *Tituli Picti* on amphorae from the Late Roman Ses Fontanelles Wreck (Mallorca, Spain): An Analytical Approach

E. Fernández-Tudela(1), R. Zarzuela Sánchez(2), M. Goñalons Lapiedra(2), A. Gil (2), D. Bernal-Casasola (2), M. Á. Cau-Ontiveros(3), E. García Riaza (4), J. Cardell Perelló (5) and M. Bethencourt Núñez(2)

(1) *Center of Underwater Archaeology, Andalusian Institute of Historical Heritage (IAPH), Spain*
(2) *University of Cadiz (UCA), Spain*
(3) *ICREA and ERAAUB-IAUB of the University of Barcelona (UB), Spain*
(4) *University of Ballearic Islands (UIB), Spain*
(5) *Council of Mallorca, Spain*

During the archaeological works of 2021/2022 on the late Roman shipwreck of Ses Fontanelles (Mallorca, Balearic Islands, Spain), several amphorae and fragments with painted inscriptions made with *atramentum* were discovered. These *tituli picti* are exceptionally well-preserved and hold great historical and archaeological significance. They are one of the few examples in the world that provide novel information about the product, weight, and the merchants from the region of *Carthago Spartaria* (modern Cartagena) involved in maritime trade in the late 4th c. AD [1]. The preservation of the tituli is a priority, and to achieve this, the Laboratory for Studies and Conservation of Historical Heritage (LEC-PH) collaborated with the Nanomaterials Group (TEP-243) of the University of Cadiz (UCA) to research and establish a conservation methodology. This methodology can be applied to the entire collection of amphorae from the wreck.

The types of amphorae found with inscriptions were Almagro 51c, Ses Fontanelles I and wine flat-bottomed amphorae. Accordingly, specimens of various types of pottery were selected to check if there was a difference in behavior between the consolidating product and the type of support. After a literature review of the most used consolidants in ceramics, it was decided to carry out tests with two types of products: one based on water-based silica nanoparticles (Nanoestel®), and another based on ethyl-methacrylate dissolved in acetone (Paraloid B72®). Ten types of analysis were performed on these samples, including surface hardness, microindentation, SEM, spectrophotometer, glossometer, water-accessible porosity, peeling test, and pycnometer.

This methodology of applying numerous experimental analyses in order to ask for the penetration capacity, strength, gloss and effectiveness of the treatments is a novelty in the field of this type of material. Ultimately, one of the two products was selected based on the principles of reversibility and respect for the original surface.

References:

[1] A. Soler i Nicolau, A. Font, P. Berni, E. García, D. Bernal-Cassasola, M.A. Cau, J. Cardell & S. Munar, «El singular conjunto de tituli picti del pecio de Ses Fontanelles (Mallorca, islas Baleares) y su contribución a la epigrafía anfórica tardorromana hispánica», Cuadernos de Prehistoria y Arqueología de la Universidad Autónoma de Madrid, vol. 47, no.1, pp. 287-317, 2022.

# GOLDEN SPONSORS

# COLLABORATORS

TechnoHeritage

RSEQ Real Sociedad Española de Química

GEQP

https://technoheritage2024.com/

# 2024

# 3as Jornadas de
# Luso - Españolas de Hidrografía

## En Cádiz
## 9,10 y 11 de Octubre

hidrográfico marinha·portugal

IHM

UCA Universidad de Cádiz

cei·mar campus de excelencia internacional del mar

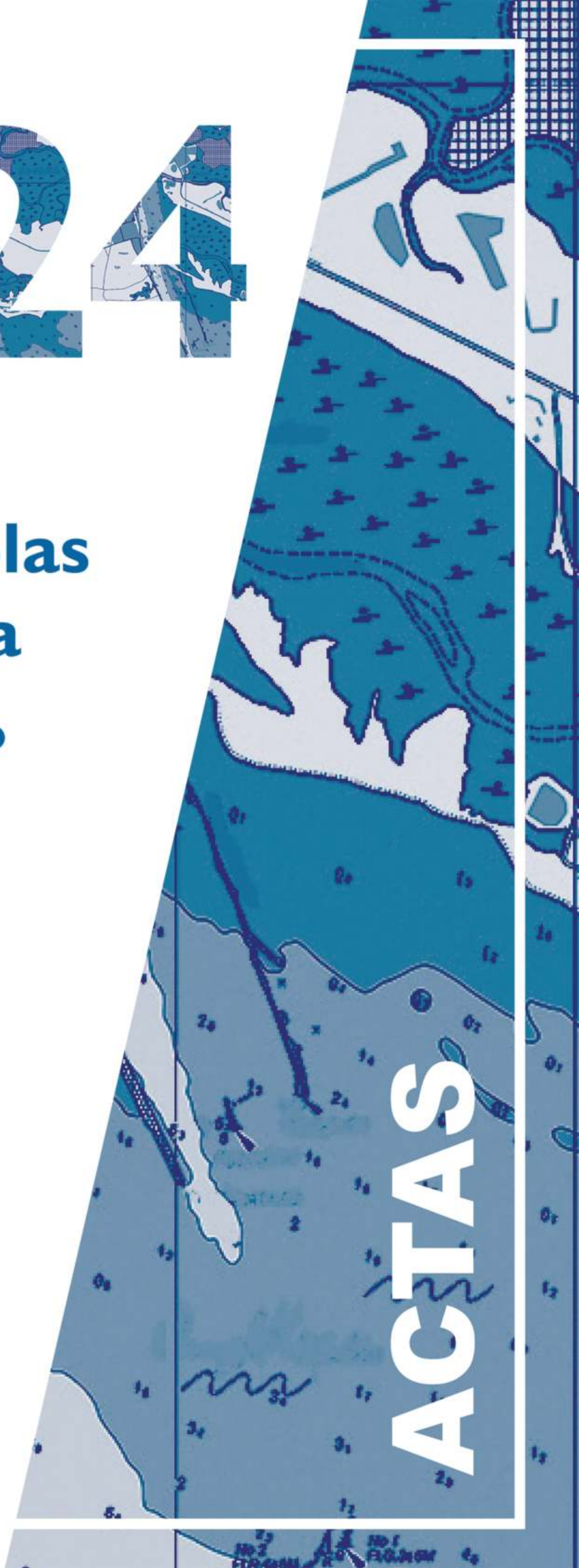

ACTAS

Edita:



ISBN 978-84-9828-998-5
Depósito legal 359-2024
Fecha de edición: octubre de 2024
Maqueta: Imprenta Instituto Hidrográfico de la Marina


ARQUEOLOGÍA
SUBACUÁTICA

# Desaparición del *Reina Regente*: Posibles causas y localización. Primeros datos obtenidos

**Ó. S. Ortega[1], M. Bethencourt[2], N. C. Ciarlo[3], T. Fernández-Montblanc[4]**

(1) Armada Española-Instituto Hidrográfico de la Marina, España, oortper@oc.mde.es

(2) Facultad de Ciencias del Mar y Ambientales, Universidad de Cádiz, Cádiz, España.

(3) Consejo Nacional de Investigaciones Científicas y Técnicas (CONICET) – Instituto de Arqueología de la Facultad de Filosofía y Letras de la Universidad de Buenos Aires (IA, FFyL-UBA), Ciudad Autónoma de Buenos Aires,

(4) Facultad de Ciencias del Mar y Ambientales, Universidad de Cádiz, Cádiz, España.

**Resumen:** El crucero *Reina Regente* de la Armada fue un buque moderno e innovador para la época. Sin embargo, desde un principio, existieron dudas de su diseño y comportamiento en la mar. El 10 de marzo de 1895, en medio de un temporal en el Estrecho de Gibraltar, desapareció con toda su dotación. A día de hoy aún se desconoce su ubicación precisa.

Para tratar de contribuir a la localización del *Reina Regente* se realizó un estudio integral de diferentes evidencias. Se analizó la documentación histórica de la construcción para determinar el estado operativo en su última singladura. Posteriormente, combinando información de los restos encontrados del naufragio y los datos meteorológicos del temporal, se desarrolló un modelo físico-matemático de dispersión lagrangiana para evaluar probabilísticamente su ubicación. Por último, se presentarán los primeros datos obtenidos en las exploraciones de la zona del plan de prospección propuesto, definido con base en los resultados de las investigaciones previas.

**Palabras Clave**: Crucero *Reina Regente*, Armada Española, modelo de dispersión lagrangiana, patrimonio cultural subacuático.

El crucero *Reina Regente* de la Armada, botado en 1887, fue un buque de guerra moderno e innovador para la época, de líneas elegantes y con capacidades teóricas de maniobra, autonomía y combate extraordinarias para un buque de su porte (figura 1).

En la mañana del día 10 de marzo de 1895, salió de la Bahía de Tánger e inició navegación en demanda del puerto de Cádiz. En esos momentos, arreciaba un temporal muy duro del suroeste y mar muy gruesa a arbolada. El *Reina Regente* nunca llegó a Cádiz, en medio de ese temporal desapareció junto con los 412 marinos de su dotación. A día de hoy aún se desconoce la localización de este pecio.

Prácticamente desde su entrada en servicio, comenzaron a plantearse dudas en cuanto al acierto de su diseño, condiciones de estabilidad, así como de su comportamiento en la mar, que se vieron acentuadas a partir de las importantes modificaciones realizadas en su diseño original. En esencia, estas consistieron en la sustitución de su artillería principal por otra de mayor calibre, lo que supuso un aumento en los pesos altos del buque. Al respecto, tras el estudio de la curva de estabilidad del *Reina Regente* (CF Villaamil, 1896) y comparando los resultados con criterios actuales (CEFLOT, 2018), se concluye que esta modificación afectó a su estabilidad y comportamiento marinero, aunque sin llegar a comprometer su seguridad en la navegación.

Por otra parte, las evidencias analizadas sugieren la existencia de deficiencias en el estado de alistamiento del buque el día de su última singladura. Principalmente, en la estanquidad de varios compartimentos, en los sistemas de achique, en la planta eléctrica y en las condiciones de habitabilidad (AGMAB, 1176/615; ACCGAR, 07/13)

A partir de todo lo anterior, de informes de la época y alegatos de testigos de las primeras maniobras a su salida de Tánger (AGMAB, 1176/614), se plantea la hipótesis de que el *Reina Regente* sufrió importantes inundaciones en sus compartimentos de más a proa, a las que tuvo que enfrentarse con medios de fortuna debido a sus ya citadas deficiencias de alistamiento. Ante esta situación, viendo peligrar el buque, su Comandante debió decidir abandonar la derrota original en demanda de Cádiz e invertir rumbo, tratando de capear el temporal y buscar resguardo.

Fig. 1 - Crucero *Reina Regente* (Museo Naval de Madrid. MN-92030)

Teniendo en cuenta que, navegando popa a la mar, una ola puede disminuir hasta un 70% las condiciones de estabilidad de un buque (CEFLOT, 2018), es probable que en algún momento el *Reina Regente* pudiera ser alcanzado por una ola de longitud de onda similar a su eslora, acabando con su ya mermada estabilidad, que le hizo zozobrar y hundirse prácticamente al instante.

Al analizar documentación de la época, se obtuvo información coherente con la hipótesis anterior. En este sentido, tienen especial importancia las investigaciones realizadas por el CF Aguirre en abril de 1895 (AGMAB 1176/614). Los resultados alcanzados entonces, junto con las hipótesis planteadas referentes a la derrota y causas del naufragio, permiten establecer de forma tentativa una primera aproximación a la zona donde ocurrió el naufragio. El polígono así establecido está ubicado entre los meridianos de Punta Camarinal y Cabo Trafalgar. Posteriormente, teniendo en cuenta los antecedentes de exploraciones en la zona, se consiguió definir un sector más reducido, que a los fines del estudio se denominó Área Inicial de Búsqueda (AIB) (figura 2).
En los días y semanas posteriores al naufragio, la mar arrojó diversos restos en distintos puntos de la costa. Partiendo de información inédita de estos restos (AGMAB, 1176/614), de la caracterización realizada del temporal del 10 de marzo de 1895, así como de datos oceanográficos y geofísicos de la zona, se ha implementado un modelo físico-matemático de dispersión lagrangiana con el objeto de simular las trayectorias de los restos del naufragio y determinar el


Fig. 2 - Croquis AIB (elaboración propia sobre visor IDE-IHM).

punto de partida de dichos objetos, es decir el lugar donde probablemente se hundió el *Reina Regente.* La metodología utilizada se basa en trabajos de investigación anteriores, relacionados con el pecio del *Fougueux* (1805) (Fernández-Montbanc et al, 2018). Los datos obtenidos representan zonas definidas en términos probabilísticos. Aunque en este caso tiene un carácter preliminar, los resultados son coherentes con la reducción de la primera aproximación de zona de naufragio a la AIB, como zona más probable de localización del pecio del *Reina Regente.*

Con base en todo lo anterior, en el marco del estudio desarrollado por el autor principal para completar el Máster en Arqueología Náutica y Subacuática de la Universidad de Cádiz (Ortega, O. 2020), se propuso un plan de prospección para la localización e identificación del *Reina Regente.* Este plan incluye la utilización de medios pertenecientes a la Armada, pero también contempla la necesaria coordinación y participación de otros organismos de las distintas administraciones del Estado con competencias en materia de patrimonio cultural sumergido, todo ello en cumplimiento de la normativa vigente (Armada Española, 2019; Ley 16/1985; Ley 14/2007).

A lo largo de los años, distintas unidades a flote del IHM efectuaron diversas exploraciones sistemáticas en el AIB, todo ello con el objetivo principal de llevar a cabo los cometidos y responsabilidades que legalmente tiene asignadas, en el cumplimiento de su misión principal de estado, consistente en la actualización permanente y el mantenimiento de la cartografía básica náutica. Lo anterior es parte imprescindible para contribuir a garantizar la seguridad en la navegación en las aguas de interés y de responsabilidad del País

De todas estas exploraciones, efectuadas, por su mayor proximidad temporal y por la utilización de tecnología más moderna, se destacan las efectuadas por el BH Tofiño en octubre de 2020 y marzo 2021. Los principales medios y sensores utilizados fueron sondador multihaz, sonar de barrido lateral, magnetómetro y perfilador de fondo.

Procesados y evaluados los primeros datos extraídos de estas exploraciones sistemáticas, se comprueba que en principio estos son coherentes con las hipótesis y los resultados obtenidos de las investigaciones y trabajos previos efectuados. Esto esencialmente consistió en la clasificación y priorización de las anomalías detectadas atendiendo a su probabilidad de correspondencia con el pecio del *Reina Regente*, según las características y datos obtenidos por el momento de cada una de ellas

Por lo tanto, y en caso de confirmarse estos resultados preliminares durante el desarrollo de fases posteriores del plan propuesto, los análisis efectuados podrían llegar tener una mayor relevancia, al poder ser considerados como un posible ejercicio metodológico cuya aplicabilidad puede extenderse a otros contextos de naufragios de época moderna y contemporánea.

**Agradecimientos:**

Al Coronel IM D. Miguel Aragón por su inestimable ayuda.

## REFERENCIAS

Archivo Central del Cuartel General de la Armada (ACCGAR). 007/13. Estado de vida y fuerza del Reina Regente del día 01 febrero de 1895.

Armada Española-Centro de Doctrina de la Flota (2018). *I-CP-03(B) Estabilidad del buque*. B.N Rota, Cádiz.

Armada Española (2019). Plan del Almirante de la Flota para la protección del Patrimonio Arqueológico Subacuático (Revisión 2).

Archivo General de Marina Álvaro de Bazán (AGMAB). B*uques, Reina Regente, Pérdida 1895*. 1176/614.

AGMAB. B*uques, Reina Regente, Hundimiento 1895*. 1176/615.

Fernández-Montblanc T., Izquierdo, A. y Bethencourt, M. (2018). Scattered shipwreck site prospection: the combined use of numerical modelling and documentary research (Fougueux, 1805). *Archaeological and Anthropological Sciences*, 10, pp. 141-156.

Ley 14/2007 del Patrimonio Histórico de Andalucía, 19 de diciembre 2007, núm 248, pp. 6-28.

Ley 16/1985 del Patrimonio Histórico Español, BOE, 29 junio de 1985, núm 155, pp. 59193-59311.

Ortega, O. (2020) *Desaparición del Reina Regente: Hipótesis de sus causas y localización. Propuesta de plan de prospección*. Trabajo de Fin de Master Oficial en Arqueología Náutica y Subacuática. Universidad de Cádiz

Villaamil, F. y Castellote, J. (1896). *Informe acerca de las causas probables de la pérdida del crucero Reina Regente. Madrid.*

SIMPOSIO INTERNACIONAL DE HISTORIA Y ARQUEOLOGÍA MARÍTIMAS

VIII

21 AL 25 OCTUBRE 2024

MÉRIDA, YUCATÁN, MÉXICO

Mar adentro, mar afuera: conexiones, percepciones y vestigios en el espacio marítimo litoral

Guadalupe Carrasco González, profesora titular de Historia Moderna de la Universidad de Cádiz (España), Diana Elizabeth Arana Recio, restauradora perito del Instituto Nacional de Antropología e Historia de Yucatán (México) y María Fernanda Valencia Suárez, investigadora del Centro Peninsular de Humanidades y Ciencias Sociales de la Universidad Nacional Autónoma de México, coordinadoras, **CERTIFICAN** que

| |
|---|
| Arano Diana, Ciarlo Nicolás, Carrasco Guadalupe, Barba-Meinecke Helena y Bethencourt Manuel |

ha participado en el VIII Simposio Internacional de Historia y Arqueología Marítima: *Mar adentro, mar afuera: conexiones, percepciones y vestigios en el espacio marítimo y litoral* que se ha celebrado en Mérida, Yucatán (México) entre los días 21 a 25 de octubre de 2024 presentando la ponencia

| |
|---|
| Historia y metalurgia de los revestimientos de cobre para el casco de embarcaciones de la Armada y Marina Mercante españolas (1780-1820) |

Y para que conste a los efectos oportunos, lo firmamos a 25 de octubre de 2024.

Guadalupe Carrasco González

Diana Elizabeth Arano

María Fernanda Valencia Suárez

Proyecto PID2021-126850NB-I00 financiado por:
MINISTERIO DE CIENCIA, INNOVACIÓN Y UNIVERSIDADES
Cofinanciado por la Unión Europea
AGENCIA ESTATAL DE INVESTIGACIÓN
CONNEXA MUNDI
Junta de Andalucía
Consejería de Universidad, Investigación e Innovación
PROA A LA MAR
uca. HUM-313
CULTURA
SECRETARÍA DE CULTURA
85 INAH
ARQUEOLOGÍA SUBACUÁTICA INAH
Museo Palacio Cantón
UCA Universidad de Cádiz
CEPHCIS
UNAM

# ANEXO II

## Algunas imágenes

Figura 1. Limpieza mecánica de taladro de carpintero (DSF392) del proyecto ARQUEOMALLORNAUTA. Fuente: Elaboración propia.

Figura 2. Digitalización de sandalia de cuero (DSF562) antes de su tratamiento (Proyecto ARQUEOMALLORNAUTA). Fuente: Elaboración propia.

Figura 3. Limpieza mecánica de fragmento de pipa de caolín (Proyecto Herakles) bajo lupa de aumento. Fuente: Elaboración propia.

Figura 4. Registro de palanqueta metálica tras su desconcreción parcial (Proyecto HERAKLES). Fuente: Elaboración propia.

Figura 5. Actividad de difusión del proyecto PORT-SUB dentro de las jornadas INNOVAZUL 2024. A la izquierda, M. Goñalons Lapiedra. Fuente: Alejandro Mañas.


Figura 6. Foto de equipo de la actividad de difusión en la Zona Expositiva III, 3as Jornadas Luso Españolas de Hidrografía. A la izquierda, M. Goñalons Lapiedra Fuente: Organización CEIMAR.


Figura 7. Actividad de difusión Blue Zone Forum - InnovAzul. En el centro, M. Goñalons Lapiedra Fuente: Habana Sánchez.

# ANEXO III

## Planes de prácticas

UCA Universidad de Cádiz

LEC-PH Laboratorio de Estudios y Conservación del Patrimonio Histórico
https://lec-ph.uca.es

Laboratorio de Conservación y Restauración
Aulario Simón Bolívar,
Avda. Duque de Nájera, 16- 11002 Cádiz
Laboratorio de Estudio de Materiales
Centro Andaluz Superior de Estudios Marinos
Avda. de la Universidad, s/n-11510 Puerto Real
Correo electrónico: **laboratorio.lecph@uca.es**

## PLAN DE PRÁCTICAS

### Prácticas de empresa y asignatura práctica - Máster en Arqueología Náutica y Subacuática

| | | | |
|---|---|---|---|
| Nombre alumno/a | Andrea Franco | | |
| Tutor/a | Marina Goñalons Lapiedra | | |
| Nº horas previstas | 225 | Nº horas programadas | 206'5 |

## CRONOGRAMA:

| **JUNIO** (8:30h a 16:30h) | | | | |
|---|---|---|---|---|
| 17 | 18 | 19 | 20 | 21 |
| 24 | 25 | 26 | 27 | 28 |
| **JULIO** (8:30h a 14h) | | | | |
| 1 | 2 | 3 | 4 | 5 |
| 8 | 9 | 10 | 11 | 12 |
| 15 | 16 | 17 | 18 | 19 |
| 22 | 23 | 24 | 25 | 26 |
| 29 | 30 | 31 | | |

Semana 1 → Mediciones y limpiezas

Semana 2 → Limpiezas

Semana 3 → Pieza completa

Semana 4 → Finalizar pieza y Proyectiles LB

Semana 5 → Finalizar proyectiles LB y prácticas con maderas LB

Semana 6 y 7 → Finalizar maderas y realizar embalajes

## TRABAJOS A EJECUTAR:

Mediciones y controles: Cambios de baños y mediciones de todos los materiales de ARQUEOSUB.

Limpiezas: Desconcreción y limpieza de algunas cerámicas de MANYS23 (ya secas pero con cascajos), concreciones de La Ballenera de años anteriores, almacenados en ALR02. Uso de métodos mecánicos como bisturí, escalpelo y ultrasonido.

Pieza completa: Documentación y limpieza de escudilla de peltre PMX23-001

Proyectiles LB: Tratamiento de inhibición, estabilización y secado de proyectiles de campañas anteriores de MANYS.

Prácticas con maderas: Se consolidarán las maderas de años anteriores del MANYS que se encuentran en la nevera, haciendo pruebas previas para determinar el método óptimo (PEG, colofonia o plastinación)*.

Figura 1. PMX23-001

Laboratorio de Conservación y Restauración
Aulario Simón Bolívar,
Avda. Duque de Nájera, 16- 11002 Cádiz
Laboratorio de Estudio de Materiales
Centro Andaluz Superior de Estudios Marinos
Avda. de la Universidad, s/n-11510 Puerto Real
Correo electrónico: **laboratorio.lecph@uca.es**

Realizar embalajes: Actividad de conservación preventiva. Se almacenarán todos los materiales intervenidos en cajas norma Europa, con su debida etiqueta, siglado si procede, y embalaje con espuma y/o bolsas de polietileno, gel de sílice.

Trabajos a realizar desde casa para completar las horas necesarias:

- Cumplimentar ficha modelo de cada una de las piezas intervenidas, previa toma de imágenes en el laboratorio.
- Ejecución de fotogrametría de la pieza de peltre
- Memoria de prácticas

*Esta práctica solo se realizará si se dispone del tiempo suficiente, ya que resulta prioritario finalizar los proyectiles y el almacenamiento de las piezas tratadas antes del periodo de agosto.

Universidad de Cádiz

LEC-PH
Laboratorio de Estudios y Conservación del Patrimonio Histórico
https://lec-ph.uca.es

Laboratorio de Conservación y Restauración
Aulario Simón Bolívar,
Avda. Duque de Nájera, 16- 11002 Cádiz
Laboratorio de Estudio de Materiales
Centro Andaluz Superior de Estudios Marinos
Avda. de la Universidad, s/n-11510 Puerto Real
Correo electrónico: **laboratorio.lecph@uca.es**

## PLAN DE PRÁCTICAS

## Prácticas de empresa - Máster en Arqueología Náutica y Subacuática

| | |
|---|---|
| Nombre alumno/a | Ilaria Vitiello |
| Tutor/a | Marina Goñalons Lapiedra |
| Nº horas previstas | 200 horas (8 CTS) |

Horario de 8:00 a 16:00 h.

## CRONOGRAMA:

| SEPTIEMBRE | | | | |
|---|---|---|---|---|
| 23 | 24 | 25 | 26 | 27 |
| 30 | | | | |
| **OCTUBRE** | | | | |
| | 1 | 2 | 3 | 4 |
| 7 | 8 | 9 | 10 | 11 |
| 14 | 15 | 16 | 17 | 18 |

Semana 1 → Toma de contacto y trabajo autónomo: Documentación fotográfica y registros.

Semana 2 → Mediciones y cambios de baño + Deshidratación material orgánico

Semana 3 y 4 → Tratamiento material orgánico + vítreo.

Semana 4 → Embalajes.

## TRABAJOS A EJECUTAR:

Documentación fotográfica y registros: Fotografiar y tomar medidas de materiales pendientes de ARQUEOSUB. Posteriormente se registrarán dichos datos en las fichas de registro.

Mediciones y cambios de baño: Cambios de baños y mediciones de todos los materiales de ARQUEOSUB.

Deshidratación de material orgánico: A lo largo de toda la semana se irán sumergiendo piezas orgánicas a plastinar en acetona para su deshidratación química, y se irán midiendo las densidades para controlar la eliminación de humedad.

Tratamiento de material orgánico: Tratamiento de consolidación por plastinación y/o mediante polietilenglicol (PEG) a distintas densidades.

Tratamiento de material vítreo: Se finalizarán tratamientos de limpieza, se consolidará (si procede) y secarán las piezas de vidrio pendientes de ARQUEOSUB (PMX23-00-003 y PMI23-S2-00).

Realizar embalajes: Actividad de conservación preventiva. Se almacenarán todos los materiales intervenidos en cajas norma Europa, con su debida etiqueta, siglado si procede, y embalaje con espuma y/o bolsas de polietileno, gel de sílice.

Laboratorio de Conservación y Restauración
Aulario Simón Bolívar,
Avda. Duque de Nájera, 16- 11002 Cádiz
Laboratorio de Estudio de Materiales
Centro Andaluz Superior de Estudios Marinos
Avda. de la Universidad, s/n-11510 Puerto Real
Correo electrónico: **laboratorio.lecph@uca.es**

## BIBLIOGRAFÍA RECOMENDADA DURANTE LAS PRÁCTICAS:

Si se desea saber más sobre los tratamientos a realizar, aquí se pueden encontrar algunos ejemplos:

ANASTASSIADES, A. y ELLIS, L. (2008) “The conservation of glass ingots from the Bronze Age Uluburun shipwreck”. *Studies in Conservation. The Journal of the International Institute of Conservarion of Historic and Artistic Works, 53 (4),* pp. 225-237

BRODA, M. y HILL, C.A.S. (2021) “Conservation of Waterlogged Wood—Past, Present and Future Perspectives”. Forests, vol. 12, no. 9.

CHRISTENSEN, M., KUTZKE, H. y HANSEN, F.K. (2012) “New materials used for the consolidation of archaeological wood–past attempts, present struggles, and future requirements”. *Journal of Cultural Heritage, vol. 13, no. 3*

HOCKER, E., ALMKVIST, G. y SAHLSTEDT, M. (2012) “The Vasa experience with polyethylene glycol: A conservator’s perspective”. *Journal of Cultural Heritage, vol. 13, no. 3*

MONTANA, G., RANDAZZO, L., CASTIGLIA, A., LA RUSSA, M.F., LA ROCCA, R. y BELLOMO, S. (2014) “Different methods for soluble salt removal tested on late-Roman cooking ware from a submarine excavation at the island of Pantelleria (Sicily, Italy)”. *Journal Cultural Heritage, vol. 15,* pp. 403-413

PIQUÉ, R., PALOMO, A., TERRADAS, X., AGUER, C., BOGDANOVIC, I., CHINCHILLA, J., GARCÍA, I., JOVER, A, LÓPEZ, O., MOITINHO, V., BUXÓ, R., BOSCH, À., TARRÚS, J., XAÑA, M. y VIVAR, G. (2013) “Registro, análisis y conservación de los objetos de madera del yacimiento neolítico de La Draga (Banyoles, Catalunya)”*. I Congreso de Arqueología Naútica y Subacuática Española, Cartagena, 14*, pp. 1136-1148

POURNOU, A. (2002) “A comparative study of conservation methods for waterlogged hazelnuts”. *Proceedings of the 8th ICOM Group on wet organic archaeological materials conference, Stockholm*, pp. 493-500

ZAMBRANO, L.C. (2014). “Estabilización del cuero húmedo mediante impregnación con polisiloxanos. Plastinación de un zapato militar del navío Fougueux, Cádiz, siglo XIX”. *I Congreso de Arqueología Naútica y Subacuática Española*, *Cartagena, 14,* pp. 403-412